# EXPERIMENTAL STUDY OF CREEP BEHAVIOUR OF TWO DIMENSIONAL KEVLAR BRAIDED COMPOSITES

By

Ahmed Samir Ead

A thesis submitted in partial fulfillment of the requirements for the degree of

Master of Science

Department of Mechanical Engineering

University of Alberta

# ABSTRACT

Creep is defined as the "progressive deformation of a material with time under constant load" and is of primary concern in structural design. This research sought to study the creep behaviour of braided composites. This information could be used to infer how fiber reinforced polymer (FRP) rebars, with a braided overwrap, would behave when used in structural design as an alternative to steel. To study the creep behaviour, braided composites were manufactured from Kevlar® 49 and Epon 826 epoxy resin at three braid angles, $35^{o}$, $45^{o}$ and $55^{o}$. To assess the creep behaviour, samples were loaded to three different percentages of their failure load, 40%, 50% and 60%. The strain-time curves produced from the strain data showed that the samples did exhibit creep behaviour. It was found that all samples loaded to 40% of the failure did not fail during the test time but maintained a steady creep rate. As the percentage loading increased, the strain experienced by the samples increased. $35^{o}$ braids at 40% were found to be the most durable with a projected endurance limit greater than 15 years. For the $45^{o}$ and $55^{o}$ braids, the endurance limit was lower. $45^{o}$ braided composites at 50% and 60% of the fracture load failed during the tests performed, exhibiting a lower endurance limit. This study is the first to assess creep of braided composites. Findings show that the braided overwrap in an FRP may be a limiting factor at higher loads, but judicious design choices in loading, braid geometry and core material should alleviate concerns.

# ACKNOWLEDGEMENTS

The completion of this thesis would have been impossible without the help, guidance and support of many. First, I would like to thank my supervisor Dr. Jason Carey for his continued support and mentorship. During my time as a Master student, not only has he made me a better student, but has always been there for solid advice on anything related to my work or not. I would like to also thank my co-supervisor Dr. Cagri Ayranci for his support and encouragement and the great ideas he offered that helped me get through tough patches.

I would also like to thank my lab colleagues for their support. Everyone in the lab has helped me get to this point. Whether that involved random laughs, walks for coffee or persuading me to go home and take a break, everyone in the lab has been extremely supportive.

I would like to thank my family, and in particular my mum and my dad, for their everlasting support. Seeing how proud I make them has helped overcome very difficult moments not only during my degree, but during my life as a whole. They've made me stronger, wiser and more motivated to try and always be a better version of myself every day. I'd like to thank my sisters for always being there for moral support and laughs even if they were drowning in work.

I apologize for the many people I have probably forgotten to mention, but you all have been paramount in me reaching this defining moment in my academic career and my life as a whole.

And before all, I'd like to thank God for His grace and mercy in making all this possible.

# TABLE OF CONTENTS

# LIST OF FIGURES

# LIST OF TABLES

# LIST OF ABBREVIATIONS

| | |
|---|---|
| 3D | Three Dimensional |
| FRP | Fiber Reinforced Polymer |
| ACI | American Concrete Institute |
| AFRP | Aramid Fiber Reinforced Polymer |
| GFRP | Glass Fiber Reinforced Polymer |
| CFRP | Carbon Fiber Reinforced Polymer |
| HM | High Modulus |
| ASTM | American Society for Testing Materials |
| QC | Quality Control |

# LIST OF SYMBOLS

| | |
|---|---|
| $\beta$ | Creep Rate Parameter |
| $\varepsilon$ | Strain |
| $\Delta\varepsilon$ | Change in Strain |
| $\theta$ | Braid Angle |
| $\sigma$ | Stress on braided samples |
| $\omega$ | Rotational speed of carriers |
| $d_i$ | Inner diameter of braid |
| $d_o$ | Outer diameter of braid |
| $e$ | Euler's Number |
| $E$ | Longitudinal Elastic Modulus |
| $f$ | Percentage Failure load |
| $F_{load}$ | Applied Load |
| $l$ | Lengths |
| $t$ | Time |
| $t_f$ | Endurance Limit (time to failure) |

# CHAPTER 1 INTRODUCTION

## 1.1 Motivation

Concrete is the most widely used structural material in the construction industry [1]. Traditionally, steel has been used to reinforce concrete; however, it poses serious challenges due to corrosion when exposed to harsh environments [2]–[4] . Polymeric composites have been proposed as an alternative to reinforce concrete in the form of Fiber Reinforced Polymer (FRP) rebars [5]. A particular hybrid FRP rebar designed by Ivey *et al.* uses a braided composite to surround a carbon core which functions as a strong, light alternative to steel [6].

According to the American Concrete Institute (ACI), before a material can be used to reinforce structures, there are a number of criteria that need to be tested to ensure safety in application. Such criteria include mechanical strength, fatigue strength, environmental resistance and creep strength [7, 8]. To validate the use of the hybrid FRP rebar, further testing was needed to ensure that these criteria were met. This work focuses on the creep behaviour aspect of durability.

Creep is defined as the "progressive deformation of a material with time under constant load" (in actual testing, load is sustained but not constant) [9]. The field-specific literature available on creep studies have looked at the effect of creep on pultruded composites and on fibers, however, no work was found that characterizes the creep behaviour of braided FRP rebars or braided composites.

Accordingly, this research sought to study the creep behaviour of braided composites. This could be used to infer how different FRP rebars could behave when used in structural design as an alternative to steel. In the previous work done in our group on FRP rebars, carbon was used as

the core of a tubular Kevlar® braid. Currently, most commercially available FRP composite rebars in structural design use glass fibres. The lack of research in using braided Kevlar® fibres as a component in hybrid FRP rebars has encouraged this research as a critical step towards advancing the use of hybrid FRP rebars in structural design.

## 1.2 Thesis Scope

The creep behaviour of tubular braided Kevlar® composites was considered for this work. To justify the use of tubular braided composites in structural applications, the ability of the tubular braids to sustain constant loads for long periods of time needs to be studied. Kevlar® composites were studied due to previous work characterizing the mechanical behaviour of the braided composites [10]. This work attempts to generally characterize the creep behaviour of the composites. Furthermore, the relationship between the braid angle and the loading percentage and the creep behaviour is investigated. This work will not extrapolate to the general behaviour of braid overwrapped FRP rebars, but will provide some possible insight in future use of braided overwrap in FRP rebars.

## 1.3 Thesis Outline

In the second chapter, a literature review is performed on the existing research. The traditional reinforcement of concrete with steel is described. The disadvantages with using steel are then presented as motivation to use composite materials as an alternative. The properties of composites and manufacturing techniques are reviewed. The use of composites is then discussed

in the framework of structural design. Mechanical characterization of pultruded rebars is explained along with the existing literature on the use of braided hybrid Kevlar® FRP composites. The literature available on the durability of these rebars is finally presented, showing how current research lacks creep studies on braided composites.

The manufacturing process for Kevlar® braided composites and experimental methods to assess creep behaviour are explained in the third chapter. The different steps involved in manufacturing the tubular braided composites are detailed as well as steps involved in sample quality control. The experimental methods include the setup used to take the images of the tubular braids during the creep test, calculate strain from the images and post process the image to produce plots.

In the fourth chapter, the experimental results are presented. The general creep behaviour of the braided composites is explained. Additionally, the influence of different independent variables on the creep behaviour of the tubular braided composites is discussed.

Finally, conclusions made from this work are presented in chapter five along with limitations. The thesis is concluded with recommendations for future work in continuation of this first study on the creep behaviour of braided composites.

Appendix A includes the MATLAB® scripts used to plot the various curves presented in this work. It also includes the scripts used to calculate the variables highlighted in chapter four.

## 1.4 References


[1] N. Subramanian, "Introduction to Reinforced Concrete," in *Design of Concrete Reinforced Structures*, Oxford University Press, 2013, pp. 1–44.

[2] D. D. L. Chung and X. Fu, "Effects of Corrosion on the Bond Between Concrete and Steel Rebar," *Cem. Concr. Res.*, vol. 27, no. 12, pp. 1811–1815, 1997.

[3] B Vidya, D Manasa, and C Prasad, "Corrosion of steel in concrete with and without silica fume," *IUP J. Struct. Eng.*, pp. 16–25.

[4] ISIS Canada, "ISIS Educational Module 2: An Introduction to FRP Composites for Construction," 2006.

[5] ISIS Canada, "ISIS Educational Module 3: An Introduction to FRP-Reinforced Concrete," 2006.

[6] Marcus Ivey, "Towards the Development of Pseudoductile FRP Rebar," University of Alberta, 2015.

[7] ISIS Canada, "ISIS Educational Module 6: Application and Handling of FRP Reinforcements for Concrete," 2006.

[8] ISIS Canada, "ISIS Educational Module 8: Durability of FRP Composites for Construction," 2006.

[9] International Federation for Structural Concrete, "FRP Reinforcement in RC structures."

[10] Garrett William Melenka and Jason P. Carey, "Experimental analysis of diamond and regular tubular braided composites using three-dimensional digital image correlation," *J. Compos. Mater.*, vol. 0, no. 0, pp. 1–21, 2017.

# CHAPTER 2 BACKGROUND

## 2.1 Concrete Use in Traditional Structural Members

Concrete is the most common material used in construction [1]. The annual consumption of concrete as of 2012 was approximately 18,000 million tonnes [1]. Concrete traditionally consists of a mixture of water, cement and aggregates [1]. Although aggregates form the majority of the concrete, the cement serves as a 'matrix' which binds the constituents of the concrete together [1]. Concrete has several advantages that make it desirable in structural design. Concrete can be easily moulded into any shape and is economically advantageous [1].

Despite these advantages, there are a few disadvantages to using concrete in structural design. There is a significant difference in the tensile and compressive strength in concrete. Although concrete has a good compressive strength, it is much weaker in tension [2]. According to the E2 American Concrete Institute (ACI) report, the tensile strength of concrete is only 10% of its compressive strength [2]. These extremes in the mechanical properties of concrete can be explained with reference to the microstructure of concrete. Concrete consists of a region which is known as the transition zone [3]. The transition zone is the interface between the cement and the aggregates in the concrete. This region is considered the weakest region of the concrete and hence determines the behaviour of concrete under different loads [3]. When loaded, cracks begin to form in this region and propagate to cause failure [3]. Significantly higher loads are needed for crack formation and propagation in compression than in tension [3]. This very low tensile strength often means that concrete is often "disregarded in design of most concrete structures"

[2]. To compensate for the low tensile strength of the concrete, these concrete structures are often reinforced with steel [2]. This reinforcement is often in the form of steel girders [4].

Steel is an excellent alloy which can be used for reinforcing the concrete structural elements. It compensates for the very low tensile strength of the concrete with its high tensile strength. Structural reinforcing steel has excellent stiffness as well. Such properties have encouraged traditionally reinforcing concrete with steel. An important element of reinforcing concrete with steel is considering the placement of steel in the concrete [2]. Correct reinforcement of concrete with steel can improve the overall tensile and compressive properties of the reinforced concrete.

Different types of steels are used to reinforce the concrete structural members [5]. These different types of steels vary mainly in their chemical composition, which ultimately reflects on the mechanical properties of the steel. The main types of steels used to reinforce concrete are carbon steel and alloy steel [5]. Carbon steel contains iron along with other elements including carbon, silicon and manganese [5]. Increasing the carbon content (up to 1.4%) increases the strength and hardness of the steel [5]. However, as the carbon content increases, the ductility of the reinforcing steel bars decreases. A lower ductility steel fails at lower strains [5]. In alloy steel, the iron is alloyed with one or several other metallic elements, such as titanium, chromium and vanadium, to improve the properties of the steel [5]. By alloying these elements with iron, the properties of the iron can be improved significantly to make it more suitable for applications where tailored properties of steel are required.

In addition to the chemical composition of the steel, considerations must be made to the type of loads the structural member is subject to. Accordingly, the steel is placed in the member at locations which minimize crack propagation. Figure 2-1 shows a beam supported at its midpoint.

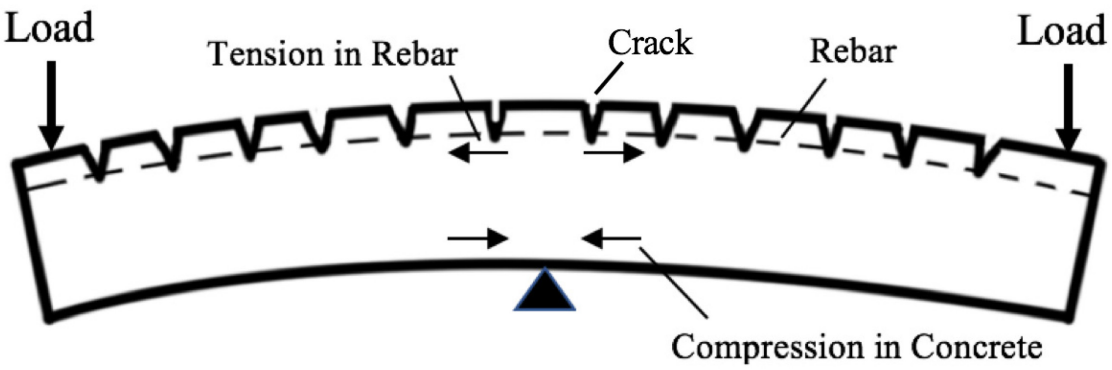


**Figure 2-1: Due to the high tensile stresses applied on the top of the beam, reinforcing the concrete with steel at the upper half prevents crack propagation through the beam at failure reproduced from [2]**

Steel reinforced concrete members may also be classified according to the behaviour exhibited by the members at failure [6]. An *over-reinforced* beam tends to fail in a brittle manner when exposed to high compressive stresses [6]. Failure in these types of members corresponds to a failure in the concrete region of the beam [6]. An *under-reinforced* beam tends to fail in a ductile manner through the reinforcing steel rebars when exposed to high tensile loads [6]. The failure in this case begins with the yielding of the steel. Finally, a reinforced structural member may be classified as a *balanced section* if both the steel and concrete fail simultaneously [6, 7].

## 2.2 Disadvantages of Steel Reinforcement in Concrete

Despite the advantages attributed with reinforcing concrete with steel, there are several disadvantages. The main disadvantage cited with using steel reinforced concrete is the eventual degradation which occurs to these members when exposed to harsh environments [8]. When exposed to such harsh environments, steel suffers from chemical pitting corrosion [9]. Corrosion

involves the chemical attack on the steel reinforcements in the concrete. This corrosion has adverse effects on the steel reinforced concrete. According to Chung [10], this corrosion is one of the major contributing factors to the limited lifespan of steel reinforced concrete structures. Prolonged exposure to harsh environments weakens the bond between the steel rebars and the concrete [10].

Chung found that beyond five weeks of corrosion, the bond strength between steel and concrete decreased as the time left for corrosion increased [10]. Furthermore, Koutsoukos *et al.* [11] showed that corrosion causes a decrease in the cross-sectional area of the steel rebars reinforcing concrete. This ultimately reduces the structural integrity of the steel reinforced concrete structures [11]. Figure 2-2 shows a heavily corroded concrete column.

**Figure 2-2: Concrete column with corrosion resulting in exposure of steel reinforcement**

These disadvantages have created a movement towards finding alternatives to steel that can be used to reinforce concrete. Fiber Reinforced Polymer (FRP) rebars are one of the alternatives that are frequently considered.

## 2.3 FRP Rebars for Concrete Reinforcement

Composite materials are those materials that are composed of two or more constituents combined to create a material that has superior properties than the raw materials combined [12]. Traditionally, the constituents of composite materials are composed of a matrix and one (or more) reinforcement(s). The matrix is a continuous phase and in most applications is the constituent with the higher volume fraction within the composite [12]. The reinforcement represents the phase that is often added to the matrix to tailor properties of the composite depending on the application in which the composite is to be used [12].

There are many methods in which a reinforcement can be added to a matrix. The different methods are used according to the specific requirements of the application in which the composite is being used. There are two configurations of fibres in a matrix [12]. *Continuous fibres* consist of long fibre reinforcement running through the matrix [12]. Such fibres are used commonly when directional properties are required of the composite. These composites are of high strength and elastic modulus [12]. However, they are also relatively expensive to manufacture [12]. *Discontinuous fibres* consist of shorter fibre strands which are uniformly distributed through the matrix at random orientations [12]. Discontinuous fibres offer much lower strength and modulus but are also significantly cheaper to manufacture [12]. This work used continuous fibres.

FRP rebars are composite materials which have gained popularity in structural applications over the past few decades [13]. Applications of such FRP rebars include reinforcement of concrete as

well as external plates used to reinforce concrete structures [13]. The FRP rebars consist of continuous fibres which run through the polymer matrix [13], making these continuous fibre composites.

By combining materials in this manner, the resulting FRP rebars can have diverse properties depending on the selected matrix and the selected reinforcement [13]. The role of the matrix and the reinforcement in the composite often defines the class of materials from which they are selected for manufacturing a composite [13]. The role of the matrix is to provide the general shape of the composite and to bind the fibres together. It also serves to protect the fibres. Furthermore, it is common to assume that the matrix does not contribute to the load bearing capacity of the composite in the longitudinal direction along the fibres. On the other hand, the role of the fibres is predominantly to provide the load bearing component of the selected composite. Accordingly, the matrix is often selected to be either a thermoset or a thermoplastic [13]. In structural applications, thermosets are more commonly used [13]. The fibres are often selected to have a high stiffness and a high tensile strength [13]. Furthermore, the fibres reinforcements are of small diameters [13] to minimize the inherent flaws in the fibres, increase the surface area to volume ratio, and to decreases potential stress concentrations within the composite. For structural applications, the fibres are often Carbon or Aramid (Kevlar®) and the matrix is an epoxy [14]. By combining these materials, the resulting stress-strain curve for FRP rebars is between the stiff fibres and the soft, ductile polymer matrix, but with the same failure strain as the fiber [14]. Figure 2-3 shows a representative stress-strain curve for an FRP composite produced with a thermoplastic resin compared to its constituent fibres and matrix.

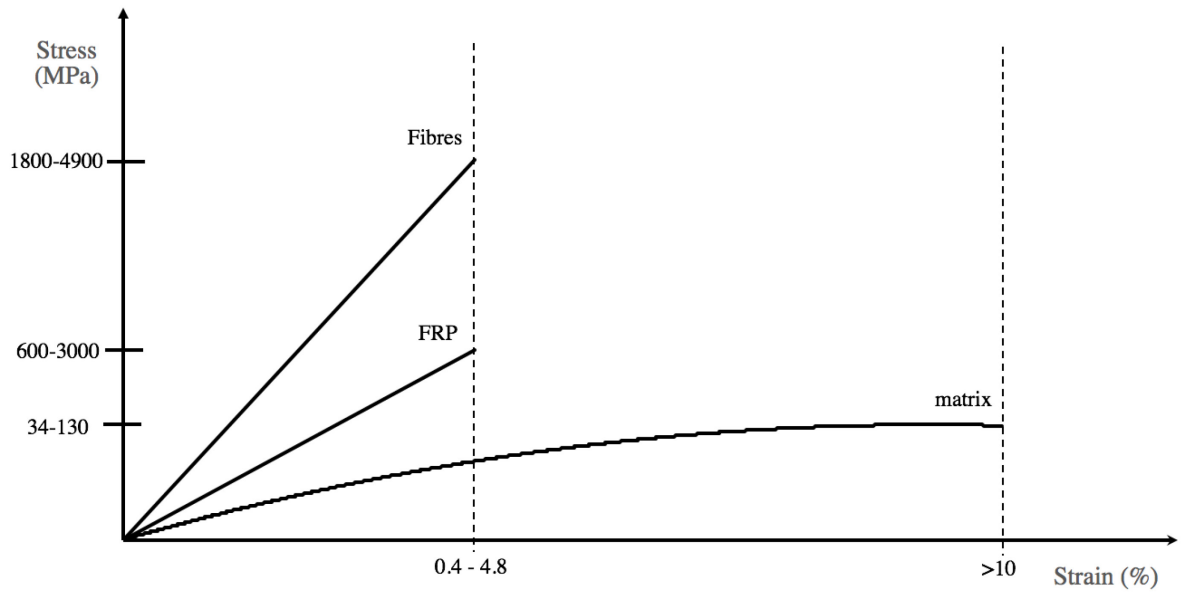


**Figure 2-3: The combined stress-strain curve for a fibre reinforced thermoplastic composites. Despite the ultimate tensile strength being higher than the matrix, the fibres determine the strain at failure reproduced from [14]**

Although Figure 2-3 shows the typical stress-strain curve for an FRP composite, the mechanical properties of the FRP rebars vary significantly depending on the materials used to manufacture the rebars. Although carbon and Kevlar® are most common as stated previously, glass is another material which is also used in manufacturing FRP rebars [15]. Figure 2-4 shows a comparative stress-strain graph for a number of different FRP rebars by different manufacturers. Table 2-1 also shows the typical values for several mechanical properties for different reinforcing bars compared to steel as presented in [16].

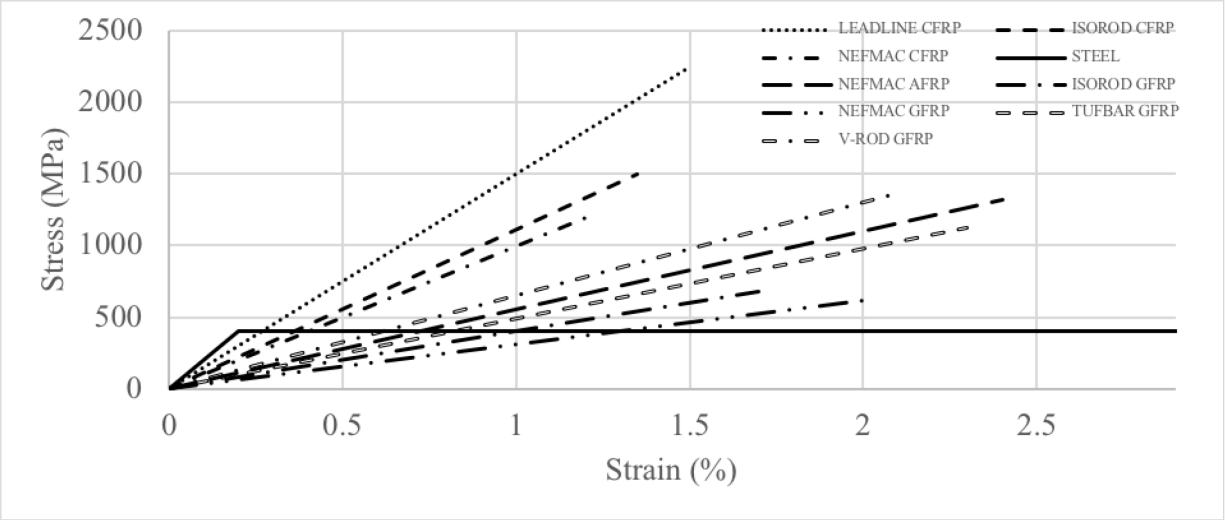


**Figure 2-4: Comparative stress-strain curve for different composite materials include Carbon FRP (CFRP), Glass FRP (GFRP) and Aramid (Kevlar®) FRP (AFRP) reproduced from [15], [17], [18]**

**Table 2-1: Typical mechanical properties for FRP reinforcing bars compared to steel as presented in [16] and [19]**

| | Steel | GFRP | CFRP | AFRP |
|---|---|---|---|---|
| Tensile Strength, MPa | 483 to 690 | 483 to 1600 | 600 to 3690 | 1720 to 2540 |
| Elastic Modulus, GPa | 200 | 35 to 51 | 120 to 580 | 41 to 125 |
| Rupture Strain, % | 6.0 to 12.0 | 1.2 to 3.1 | 0.5 to 1.7 | 1.9 to 4.4 |
| Yield Strain, % | 0.14 to 0.25 | N/A | N/A | N/A |
| Relative Cost | 1 | 2.16 | 4.16 | 4.16 |

With comparable stiffness to steel and higher ultimate tensile strength, the disadvantages of using steel have created a push towards FRP rebars as a substitute reinforcement in concrete. According to SIMTReC (Structural Innovation and Monitoring Technologies Resource Centre) Canada, the cited advantages of using FRP rebars includes their "resistance to electrochemical corrosion [and] high strength-to-weight ratio" [15]. Although corrosion in FRP composite rebars can be severely amplified under high temperatures and loads, they remain preferable than steel in harsh corrosive environments [20]. The high specific strength of the FRP composites represents a significant advantage when installing the FRP rebars in concrete structures [15]. Placement of the FRP rebars in applications becomes much less time consuming due to the significantly lower density of the rebars [15]. These advantages, coupled with the comparable mechanical properties shown in Table 2-1, have encouraged further studies aimed at identifying the feasibility of replacing steel with these FRP rebars.

## 2.4 Manufacture of FRP Rebars

There are many methods to manufacture composite materials [12]. The manufacturing methods used mainly depend on the type of composite that will be manufactured [12]. FRP composites are polymer matrix composites and for these specific manufacturing methods are preferred [12]. These manufacturing methods are shown in Figure 2-5.

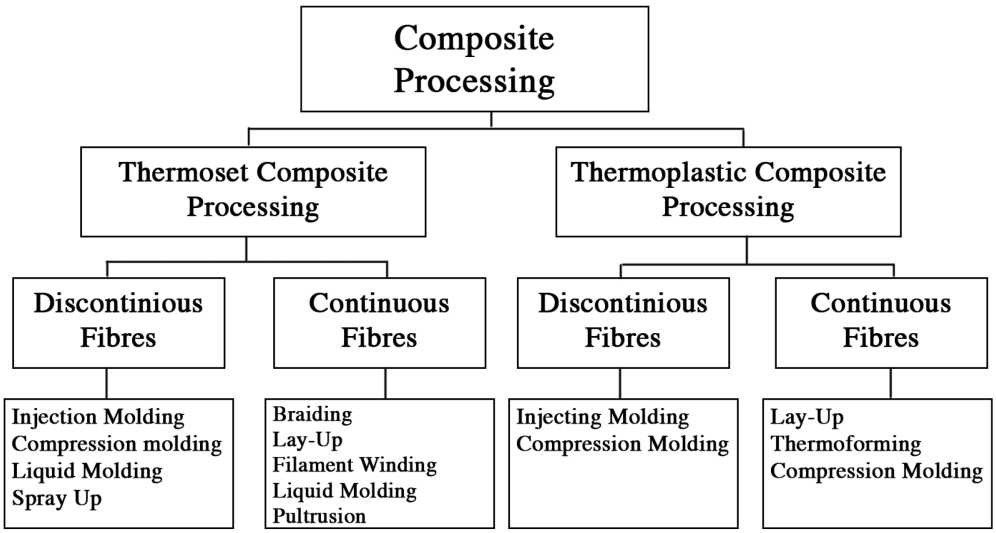


**Figure 2-5: Manufacturing methods for polymer matrix composites. [12]**

The hierarchal chart in Figure 2-5 can be used to identify the most suitable method to produce the FRP rebars [12]. As identified earlier, for FRP rebars it is often common to use thermosets and continuous fibres for directional properties [13]. That would mean that one of the following techniques would be suitable: braiding, lay-up, filament winding, liquid molding or pultrusion [12]. For manufacturing FRP rebars, pultrusion and braiding are used extensively [14].

The technology of braiding has been firmly established by Ko [21]. In braiding, three or more yarns are intertwined to form a pattern [21]. When compared to filament winding, braiding has a number of differences. In chapter 3 of the book, *Handbook of Advances in Braided Composite Materials,* the authors describe the differences between the two processes [22]. In terms of manufacturing, filament winding involves deposition of fibres along the length of the desired part with a traversing carriage. In braiding, several fibres are intertwined on a mandrel moving in the axial direction of the part [22]. This means that the created parts are often different in terms

of performance. The crossovers in both techniques result in similar strength reductions, however, the crossovers result in a much higher reduction in elastic modulus in braids [22]. Braiding is not a recent manufacturing method [21]. The use of braids in several applications has existed in the textile industry, including the use of braids to manufacture heavy duty ropes [21]. The production of braided FRP composites can be broken into two main steps, braiding and pultrusion.

Research performed in the area of braidtruded FRP rebars has shown that braiding can positively influence the mechanical properties of the FRP including avoiding the brittle failure mechanism discussed earlier [23]–[25]. As mentioned, braiding involves intertwining two or more yarns to create a braided pattern similar to that shown in Figure 2-6 [26]. The highly attractive element of braiding is the simplicity involved in the manufacturing process [26]. In braiding, carriers are attached to a braiding machine, which may be horizontal or vertical [26]. The carriers are loaded with the material which will be braided. When the machine is started, the carriers follow a maypole dance pattern as presented in [26]. This allows the braid to be formed on a tubular cross section such as a mandrel [26]. The result of the rotation of the carriers combined with the movement of the mandrel along the axis of the braiding machine is that the yarns do not intertwine and that sets of the same yarn are all moved together [26]. This helps maintain the properties of the braid such as the braid angle throughout the entire braiding process [26]. Another braiding system is called the rotary braider, however, these braiding systems cannot produce flat braids in spite of their higher production rates [26]. Herein, we will be more focused on the maypole braider.

**Figure 2-6:Schematic of a regular (2/2) braid pattern as reproduced from [26]**

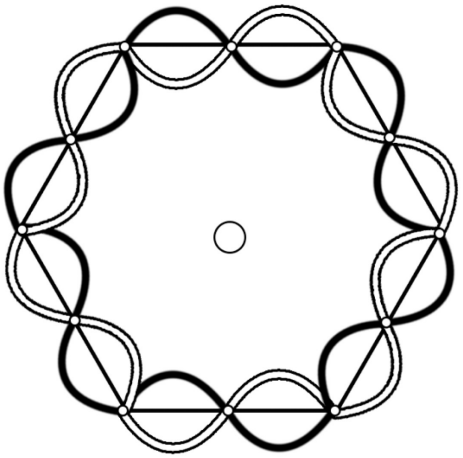

**Figure 2-7: Maypole dance pattern followed by the carriers in a maypole rotary system as reproduced from [26]**

The result of using a maypole braiding system to manufacture the braids is shown in Figure 2-8. As the machine operates, the carriers move along the path shown in Figure 2-7 resulting in the yarns being wrapped over one another [26]. This creates a braid with a nearly constant braid angle [26].

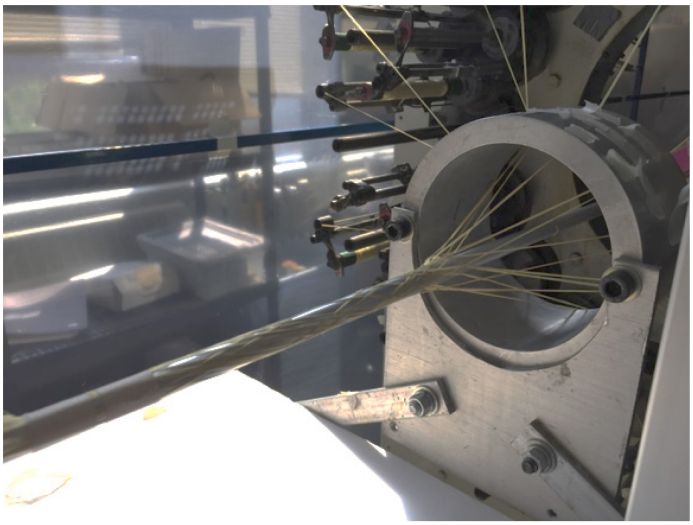

**Figure 2-8: Picture showing zoomed in view on braid during braidtrusion process [23]**

Carey and Ayranci indicated that using braiding as a step in the fabrication of the FRP composite bars allows improvement of properties by altering the braiding parameters [27]. Pheonix showed through experiments that increasing the braid angle decreased the tensile strength of the composites [28]. Smith and Swanson also performed several experiments to identify the factors that contribute to the stiffness and the strength of braided composites [29]. The research set out to study the effects of factors such as the braid angle and the fibre volume fraction [27], [29]. Melenka also performed an analytical and experimental study on tubular braided composites. In his work, he demonstrated how the volume averaging method can be used to model the braided composites [30].

Pultrusion is extensively used in the manufacture of FRP rebars and has been cited in a number of sources [14], [23]–[25]. Pultrusion essentially involves pulling strands of fibres from spools [14]. The fibres are then passed through a resin bath which soaks the fibres in the matrix of the composite [14]. The fibres are finally pulled through to an oven where curing occurs [14].

Using the two manufacturing processes (braiding and pultrusion) together results in a combined process called braidtrusion. This fabrication method is seen quite often in research relating to manufacture and characterization of the braided FRP composite rebars [23]–[25]. A schematic representation of the production line of the braidtrusion process is shown in Figure 2-9 as presented in [31]. Most research involving braided FRP composite rebars have used braidtrusion as the manufacturing method and so this paper will be following the same fabrication techniques as presented in [23]–[26].

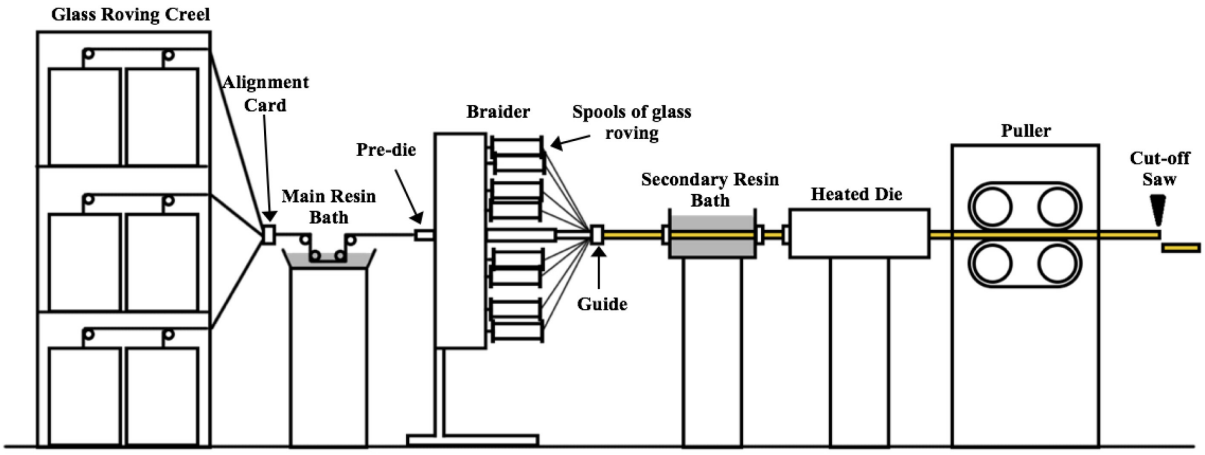


**Figure 2-9: Schematic of braidtrusion process adapted from [31]**

## 2.5 Characterization of FRP Rebars

Despite the comparable stiffness, one of the major problems of FRP rebars is that they are linearly elastic until failure [14]. As can be seen in Figure 2-4, the stress-strain curves for the FRP rebars indicate no plastic behaviour before failure [15], [24]. This means that if failure occurs, this failure is often catastrophic and sudden [14]. In a balanced beam, the failure of the

entire structure occurs at the ultimate strain of the FRP rebars, accompanied by a significant deflection [14]. A number of studies have attempted to improve on the properties of the FRP rebars and the literature regarding this aspect is discussed below.

Ahmadi *et al*. showed that using a braidtrusion process to manufacture the FRP rebars significantly improved the shear modulus of the FRP composites [31]. Figure 2-10 shows a schematic of the braided FRP rebars used in the research. GFRP rebars of different braid angles were produced and compared to unidirectional pultruded composites of the same fibre and matrix volume fractions [31]. Results from the study indicated that braiding resulted in a 56.4% improvement in the shear modulus of a 45-degree braided GFRP composite [31]. Ahmadi *et al.* reported that braidtrusion resulted in a 1.5 times improvement in the shear modulus of lowest fibre weight ratio tested [31].

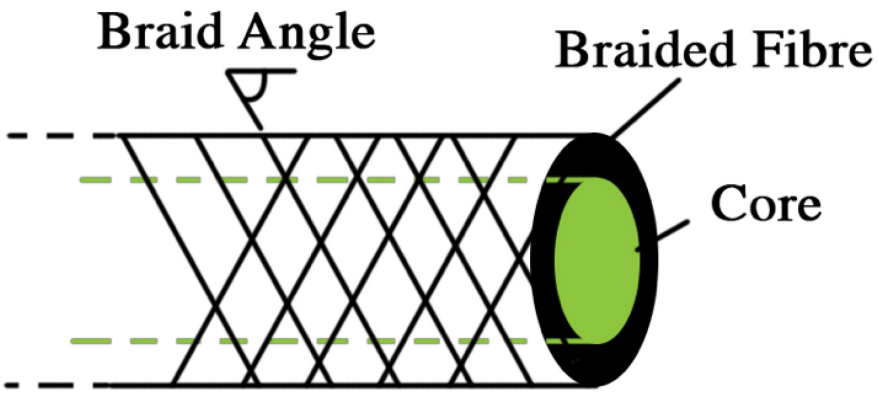


**Figure 2-10: Model of GFRP braidtruded composites used by Ahmadi *et al.* [31]**

Many studies have relied on using braidtrusion to manufacture rebars which are then characterized [23]–[25]. Fangueiro *et al.* compared the performance of braidtruded GFRP and steel when used to reinforce a concrete beam [32]. A bending test was performed on prepared

concrete beams reinforced with GFRP rebars against a similar bending test on steel reinforced concrete beams [32]. Despite the comparative mechanical properties presented in Table 2-1, Fangueiro *et al.* found that the steel reinforced concrete beam was able to bear almost double the load of the composite reinforced concrete beam [32]. The strain before failure, however, was larger in the composite reinforced concrete beam [32].

Research to improve the tensile strength of the FRP composites has also been conducted. An extensive study was performed by Park *et al.* to improve on the tensile strength of the braidtruded GFRP rebar. They attempted to enhance the tensile strength by enhancing several factors including the selection of the resin and filler used as well as improving the fibre volume fraction. Authors concluded that proper selection of the resin is important but does not contribute to the tensile strength of the composite rebar and concluded that proper selection of a filler, particularly a polyvinyl alcohol filler, resulted in improved mechanical properties for the composite rebar. Finally, their research also found that core fibre tensioning increased the fibre volume fraction and ultimately improved the ultimate tensile strength of the GFRP rebars [33].

Despite the improvements that have been suggested through research, the failure mechanism in FRP rebars remains highly problematic [24]. As presented earlier in Figure 2-4, FRP rebars are considered to be elastic until failure [15], [24]. This means that at the failure strain, the FRP rebar fails catastrophically [15], [17], [21]. Naani *et al.* performed studies on a braided hybrid composite rod and obtained a stress-strain curve that was bilinear [34]. Bakis *et al.* also performed experiments on hybrid FRP composite rebars in attempts to improve ductility [25]. By combining high and low elongation fibres, an improvement in pseudo-ductility is observed [25]. This means that failure is not sudden and possible measurements to prevent catastrophic failure

may be taken [25]. Ko *et al.* also attempted to improve the ductility of the braided FRP rebars [24]. The research involved manufacturing 5-mm diameter hybrid composite rebars consisting of a core of high modulus (HM) carbon and braids of aramid (Kevlar® 49) fibres [24]. A schematic of the cross section of the prepared samples is shown in Figure 2-11. A total of 6 samples were prepared and mechanically tested [24]. Mechanical characterization of the hybrid rebars was performed in a Universal Testing machine. The specimens were 424-mm in length and were tested under a strain rate of 0.02 mm/min [24]. Extensometers were attached to the specimens to measure the strain until failure [24]. The testing of the six samples resulted in 6 stress-strain curves as shown in [24]. Ko *et al.* showed in [24] that the hybrid of HM carbon and aramid was not strictly linear in the stress-strain response.

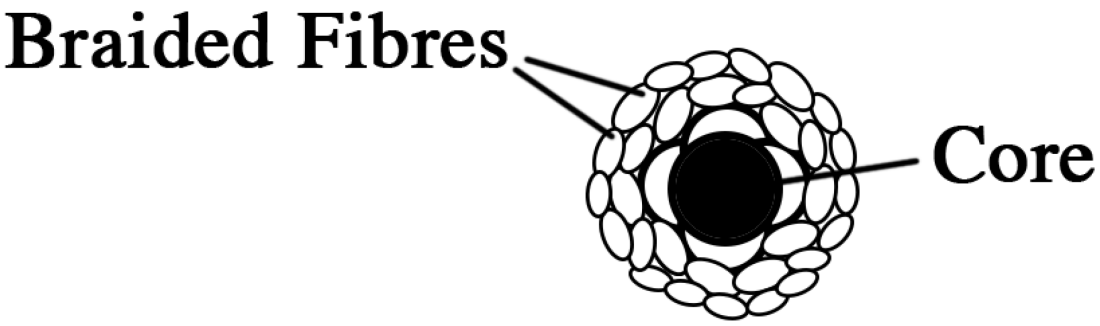


**Figure 2-11: Schematic representing the cross-section of the hybrid rebar used in [24]**

The hybrid used by Ko *et al.* in [24] was able to achieve a pseudo-ductile failure mode rather than the brittle failure mode expected. A maximum ultimate strain of 2.5% was also achievable with these hybrid FRP rebars [24]. The previously noted catastrophic failure mechanism of FRP

rebars can be avoided with these improvements in ductility. This would mean higher longevity of structures reinforced with the proposed FRP rebars.

Similarly, Ivey *et al.* attempted to improve the pseudo-ductility of the FRP rebars by developing a manufacturing method which ensured more consistent results for the produced FRP rebars [23]. Through the research conducted, Ivey *et al.* developed a manufacturing method which produced specimens with a nominal outer diameter of 6.5mm and a braid angle of 20.7° [23]. Tensile tests performed on the specimens resulted in a pseudo-ductile failure [23]. However, the method developed by Ivey produced braided FRP rebars with a mean elastic modulus of 84.2 GPa which is significantly less than the stiffness of steel which is around 200 GPa, but higher than available glass FRP rebars [23]. Even though this might seem problematic, the difference in moduli might not be an issue depending to the method of reinforcement discussed earlier. Over-reinforced concrete structures are designed such that the concrete fails before the failure of the reinforcement rebars. Despite the lower elastic modulus, the FRP will not fail before the concrete if used in an over-reinforced design. Over-reinforced concrete structures will compensate for the premature failure of the braided FRP composite rebars.

The research presented in this section shows how several studies have attempted to tackle the linearly elastic and brittle behaviour of FRP rebars [20], [23]–[25]. A major disadvantage of using these FRP rebars is that the failure mechanism is brittle, which means that failure is sudden and catastrophic in nature [14], [24]. Improvements suggested through research include tensioning the core fibres and using braiding as a manufacturing technique for these FRP rebars [23]–[25]. The manufacturing process naturally contributes to the properties of the produced rebars.

## 2.6 Durability of FRP Rebars

FRP are usually seen as advantageous to steel due to their resistance to the chemical corrosion attributed to steel reinforced structures [14]. However, the issue of durability of FRP rebars is much more complex than assumed [35]. Degradation in the case of a composite material depends on the two phases, the matrix and the reinforcement [35]. Failure of FRP can be due to the failure of either or the failure of the interface between the matrix and the reinforcement [35]. Katz performed a study to investigate the effect of cyclic loading on the bond strength between FRP rebars and concrete [36]. Results of the research done by Katz showed that cyclic loading was accompanied with a reduction of up to 70% in the bond strength [36]. Several explanations were offered for this behaviour, including abrasion of the FRP rod surface and delamination of the resin on the surface of the rod [36]. Micelli and Naani showed that the resin properties contribute significantly to the durability of the FRP rebars and that environmental effects are insignificant for conditioned specimens [37]. Porter and Barnes performed tests on GFRP samples to test the strength of the composite rebars when exposed to alkaline environments for periods of 2-3 months [38], [39]. As a result of these accelerated tests, the tensile strength of the GFRP composites dropped to up to 34% residual strength [38], [39]. Another important study by Sen *et al*. showed that in an alkaline environment, the strength of the GFRP samples decreased by 75% after 25 days of exposure [39], [40]. It is important to note that these durability tests were conducted on composite rebars with thermoset matrices including vinyl ester and polyester [35], [37], [39], [40].

Although significantly more expensive, CFRP rebars offer higher stiffness for reinforcement. Attempts to improve the ductility of FRP composites have therefore often cited CFRP composites as the tested samples [23]–[25]. Dawood and Rizkalla showed that adding a silane agent to CFRP composites used to support steel structures significantly enhanced the durability of the bond between the CFRP and the steel [41]. Wan *et al.* also attempted to show the effect of water on the durability of CFRP rebars in concrete [42]. The experiments performed by Wan *et al.* showed that the presence of water resulted in a significant decrease in the bond strength between the CFRP rebars and the concrete [42].

Due to the higher diversity of properties attainable, hybrid FRP composites are often used as mentioned previously in Ivey *et al*., Harrison *et al.* and Naani *et al.* and the research conducted on the ductility of FRP rebars [23]–[25]. The research regarding the durability of braided Kevlar® composites, however, is very limited. Aboelseoud and Myers studied the durability of a hybrid sandwich composite exposed to various environmental conditions [43]. The conditions tested by the research included an alkaline environment as well as a saline environment [43]. Aboelseoud and Myers reported that both environmental conditions caused de-bonding between the matrix and the fibre [43]. Cao *et al.* performed a number of tests to study the effect of temperature elevation on the tensile properties of hybrid composites [44]. The research concluded that elevated temperature reduces the tensile strength of hybrid FRP composites [44]. Furthermore, the research also pointed out that elevated temperature plays an important role in failure mechanisms. At 16 $^{o}$C, delamination of the hybrid FRP composite occurred. [44]

Studying the durability of braided composites also involves the study of the fatigue behaviour of these composites. Fatigue represents the resistance of the material to cyclic loading. Tate *et al.*

studied the influence of braid angle on the fatigue behaviour of the braided composites [45]. In the study, the endurance limit was defined as the stress that results in a million fatigue cycles for the composite. The study concluded that the endurance limit was 40% of the ultimate tensile strength for the $25^o$ and $30^o$ and 45% for the $45^o$ braided composites. The study also found that matrix cracks and delamination were insignificant during 90% of the fatigue life [45]. Tate and Kelkar also attempted to create a degradation model for biaxial braided composites under fatigue loading [46]. This model was also meant to represent the decrease in stiffness during the experiment. After experimentation, the researchers deduced that S-N curves could be made for the various braid angles that were tested [46]. Attempts to study the fatigue behaviour of a carbon fibre reinforced polymer composite using infrared thermography have been performed by Montesano *et al.* [47] . They found that the results obtained using this technique closely matched the experimental results.

Another important element to consider in the long-term durability of the concrete reinforcement is the creep behaviour of the reinforcement. Creep is the term used to describe the deformation of a material with time under constant load [48]. A typical creep curve for a composite material is shown in Figure 2-12. In a creep test, the material is loaded instantaneously to the maintained load (within 5 minutes of the beginning of the test). This creates an initial strain in the sample, $\varepsilon_o$. The material is then kept at this load for the duration of the test. Strain is measured during the test and the resulting stress-time graph is used to describe the three stages of creep. The primary stage involves the initial balancing of the load applied. During this stage, strain rate (defined as $\frac{d\epsilon}{dt}$) gradually decreases until it reaches a near constant value in the secondary stage. The

secondary stage continues until the material reaches the tertiary stage at which the strain rate increases rapidly before the material fails.

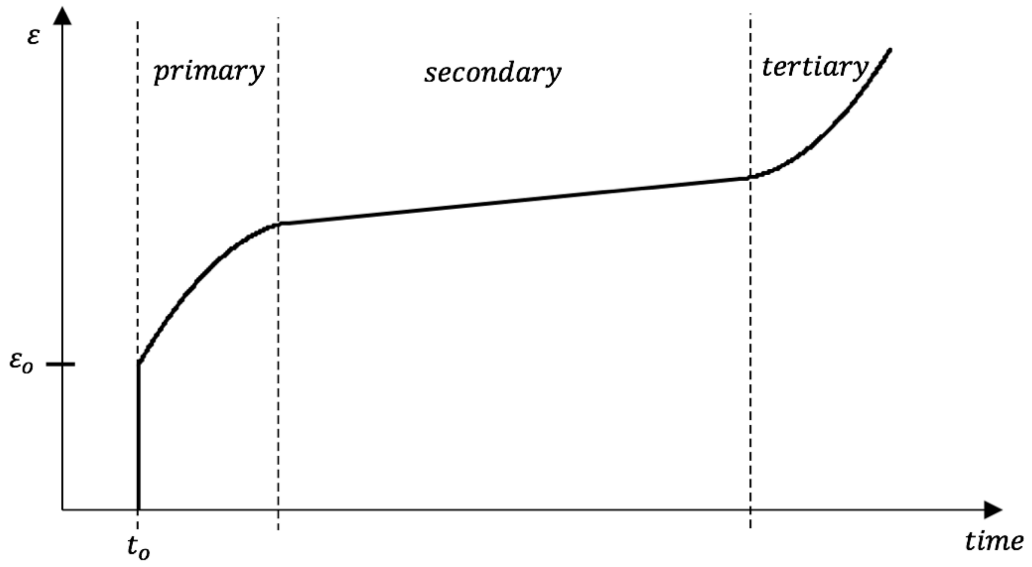


**Figure 2-12: A graph of strain against time for a material tested in creep showing primary, secondary and tertiary stages**

The behaviour shown in Figure 2-12 can be described using a mathematical equation relating strain to time. A material which is loaded under creep experiences strain as described by equation (2-1).

$$\varepsilon(t) = \varepsilon_o + \beta \log(t) \qquad \textbf{(2-1)}$$

where, $\varepsilon$ is the strain as a function of time, $\varepsilon_o$ is the initial strain experienced by the sample after being loaded to a percentage of failure load and $\beta$ is the creep parameter, which is equal to $\frac{d\varepsilon}{dlogt}$ and t is the time (usually in hours) of the test.

When a composite material is exposed to a sustained load for a long period of time it may fail after a period of time known as the "endurance limit" [48]. This endurance limit can often be used to quantify and compare the performance of composites in creep.

In creep of composites, a distinction needs to be made between the creep of the resin matrix and creep of the fibre reinforcements. Each can result in failure when exposed to creep. In terms of creep of thermoset resins, research has focused on the dynamic viscoelastic properties of the resin in creep tests [49], [50]. According to a report by the International Federation for Structural Concrete (FIB), thermosetting resins are resistant to creep at room temperatures and show little degradation within 100°C increases in temperature [48].

For the creep behaviour of the individual fibres, a wealth of literature is available. Walton and Majumdar studied the creep behaviour of Kevlar® 49 fibre at room temperature. The results of the study showed that the creep strain was low when compared to other similar polymers [51]. A more extensive study conducted by Ericksen studied the creep behaviour of Kevlar® 49/epoxy composites. Ericksen additionally performed individual creep tests on the epoxy and the fibres before studying creep in the composites. Results of the experimental study indicated that no steady state creep was observed, only an initial transient stage [52]. Another study conducted by Hanson attempted to study the effect of temperature on the creep characteristics of Kevlar® 49/epoxy composites. The results agreed well with the results obtained by Ericksen. In creep, the composites exhibited an accelerated primary creep phase and slow secondary creep phase [53]. Finally, a study conducted by Goertzen and Kessler researched the creep behaviour of carbon fiber/epoxy matrix composites. They concluded that no creep rupture failures occur at room

temperature in the short term for loads up to 77% of the ultimate tensile strength of the composites. [54]. Creep testing of braided composites is not absent from literature. Jing *et al.* studied the creep behaviour of three-dimensional braided SiC composites at elevated temperatures [55]. The creep behaviour of the braided composites was studied at 1100$^{o}$C and 1300 $^{o}$C. The composites showed a steady second stage creep behaviour and rupture time was similar. Explanations for the different fracture surfaces was also offered in the research. Yamaguchi *et al.* showed that the level of the stress ratios after extrapolation of the data for 57 years was 47% in the aramid fiber reinforced polymer composite rebars. It should be noted, however, that samples used in this study were not braided composites, making it difficult to relate these results to braided composites [56]. No other research on the creep behaviour of braided composites or any research braidtruded rebars was found.

SIMTReC Canada and the Canadian Standards Association (CSA) report has pointed out the requirements for FRP composite materials to be used in structural applications as reinforcement to concrete [20, 57]. The report provided by SIMTReC Canada presents further insight in the different durability elements that should be considered if FRP composite materials are to be used in structural applications [20]. Implications of using the FRP composites in moist and saline environments are broadly discussed to give a general expectation of the FRP composites which are to be used in structural concrete [20]. Despite this general description, very little research is cited with regards to FRP composite rebar durability.

## 2.7 Conclusion

Reinforcing concrete with steel has been a method commonly used to improve the tensile properties of concrete. One of the main problems with using steel as a reinforcement to concrete is corrosion. FRP rebars can be used as a replacement with their high specific strength and comparable stiffness to steel. There are many elements that need to be considered before replacing the steel reinforcement with composite reinforcement.

The assumed linear elastic behaviour of the FRP composite materials is a significant problem as it results in a sudden catastrophic failure of the entire beam at the fracture strain. Attempts have been made to improve on the pseudo-ductility of these FRP rebars using a variation of fabrication methods and proper selection of matrix and reinforcement for the composites. Further research, however is necessary to show how altering fabrication parameters might influence the pseudo-ductile behaviour of the FRP composite rebars.

Durability of hybrid FRP rebars remains mostly unknown. Although a few studies have attempted to study their durability, the durability behaviour of hybrid FRP composites is still a relatively new area of research. Details of the method of failure under harsh conditions are seldom found in literature. This represents an obstacle in the gradual introduction of FRP composites in structural applications.

Two of the main areas where there is a lack of research is the cyclic and creep behaviour of braided composites. Although some research is available for the fatigue behaviour of braided composites, very little literature exists on the creep behaviour. Existing literature is exclusive to composites manufactured using moulding techniques with very few studies on creep of Kevlar®

composites. This is an obvious setback in the introduction of braided FRP composites as a viable alternative to steel. This research will attempt to further study the creep behaviour of Kevlar® braided composites at room temperature. These results will then be used to draw conclusions on the projected life expectancy of these Kevlar® braided composites and how different manufacturing and testing parameters influence creep behaviour. The overall creep behaviour will be investigated to contribute to existing literature to advance the market of FRP composite rebars which may serve as an alternative to steel in reinforced concrete.

## 2.8 References


[1] N. Subramanian, "Introduction to Reinforced Concrete," in *Design of Concrete Reinforced Structures*, Oxford University Press, 2013, pp. 1–44.
[2] ACI Education Bulletin, "Reinforcement for Concrete— Materials and Applications."
[3] P. Kumar Mehta and Paulo J.M. Monteiro, *Concrete Microstructure, Properties and Materials*, 4th ed. McGraw-Hill Education, 2001.
[4] "Adaptive Components | Håvard Vasshaug." .
[5] X. Gu, "Mechanical Properties of Concrete and Steel Reinforcement," in *Basic Principles of Concrete Structures,* Springer, 2016, pp. 21–58.
[6] N. Subramanian, "Flexural Analysis and Design of Beams," in *Design of Concrete Reinforced Structures*, Oxford University Press, 2013, pp. 142–213.
[7] T.J. MacGinley and B.S. Choo, Reinforced Concrete Design Theory and Examples, 2nd ed. .
[8] ISIS Canada, "ISIS Educational Module 2: An Introduction to FRP Composites for Construction," 2006.
[9] B Vidya, D Manasa, and C Prasad, "Corrosion of steel in concrete with and without silica fume," *IUP J. Struct. Eng.*, pp. 16–25.
[10] D. D. L. Chung and X. Fu, "Effects of Corrosion on the Bond Between Concrete and Steel Rebar," *Cem. Concr. Res.*, vol. 27, no. 12, pp. 1811–1815, 1997.
[11] P. Koutsoukos, D. Michalopoulos, and C. A. Apostolopoulos, "The Corrosion Effects on the Structural Integrity of Reinforcing Steel," *J. Mater. Eng. Perofrmance*, vol. 17, no. 4, pp. 506–516, 2008.
[12] F. C. Campell, "Introduction to Composite Materials," in *Structural Composite Materials*, ASM International, 2010.
[13] ISIS Canada, "An Introduction to FRP Composites for Construction."
[14] ISIS Canada, "ISIS Educational Module 3: An Introduction to FRP-Reinforced Concrete," 2006.

[15] ISIS Canada, “ISIS Educational Module 6: Application and Handling of FRP Reinforcements for Concrete,” 2006.
[16] ACI Committee 440, “Guide for the Design and Construction of Structural Concrete Reinforced with FRP Bars,” 2006.
[17] V-ROD, “V-ROD HM.” .
[18] TUFBAR, “TUFBAR Fiberglass Rebar (40 GPA).” .
[19] Chris Burgoyne and Ioannis Balafas, “Why is FRP not a financial success?”
[20] ISIS Canada, “ISIS Educational Module 8: Durability of FRP Composites for Construction,” 2006.
[21] Frank Ko, “Braiding,” *ASM Handb.*, vol. 21, pp. 69–77.
[22] Jason P. Carey, Handbook of Advances in Braided Composite Materials - Theory, Production, Testing and Applications. .
[23] Marcus Ivey, “Towards the Development of Pseudoductile FRP Rebar,” University of Alberta, 2015.
[24] Frank K. Ko, Win Soomboonsong, and Harry G. Harris, “New Ductile Hybrid FRP Reinforcing Bar for Concrete Structures,” *J. Compos. Constr.*, pp. 28–37, 1998.
[25] A. Nanni, C. Bakis, J. Terosky, and S. Koehler, “Self-monitoring, pseudo-ductile, hybrid FRP reinforcement rods for concrete applications,” *Compos. Sci. Technol.*, vol. 61, pp. 815–823, 2001.
[26] Frank Ko, Andrew Head, and Christopher Pastore, *Handbook of Industrial Braiding*. Atkins and Pearce.
[27] Jason Carey and Cagri Ayranci, “2D braided composites: A review for stiffness critical applications,” *Compos. Struct.*, vol. 85, pp. 43–58, 2008.
[28] S. Pheonix, “Mechanical Response of a Tubular Braided Cable with an Elastic Core,” *Text. Res. J.*, vol. 48, no. 2, 1978.
[29] L. Smith and S. Swanson, “Selection of Carbon Fiber 2D Braid Preform Parameters for Biaxial Loading,” *Compos. Des. Manuf. Cost Eff.*, vol. 48, pp. 33–44, 1994.
[30] Garrett William Melenka, “Analytical and Experimental Analysis of Tubular Braided Composites,” University of Alberta, 2016.
[31] M.S. Ahmadi, M.S. Johari, M. Sadighi, and M. Esfandeh, “An experimental study on mechanical properties of GFRP braid-pultruded composite rods,” *EXPRESS Polym. Lett.*, vol. 3, no. 9, pp. 560–568, 2009.
[32] R. Fangueiro, G. Sousa, F. Soutinho, S. Jalali, and M. de Araujo, “Application of Braided Fibre Reinforced Composite Rods in Concrete Reinforcement,” *Mater. Sci. Forum*, vol. 514–516, pp. 1556–1560, 2006.
[33] Young-Hwan Park, Young-Jun You, Jang-Ho Jay Kim, and Sung-Jae Kim, “Methods to enhance the guaranteed tensile strength of GFRP rebar to 900 MPa with general fiber volume fraction,” *Constr. Build. Mater.*, vol. 75, pp. 54–62, 2015.
[34] Antonio Naani, Marcus Henneke, and Tadashi Okamoto, “Tensile properties of hybrid rods for concrete reinforcement,” *Constr. Build. Mater.*, vol. 8, no. 1, pp. 27–34, 1994.
[35] Francesca Ceroni, Edoardo Cosenza, Manfredi Gaetano, and Marisa Pecce, “Durability issues of FRP rebars in reinforced concrete members,” *Cem. Concr. Compos.*, vol. 28, pp. 857–868, 2006.

[36] Amnon Katz, "Bond to Concrete of FRP Rebars After Cyclic Loading," *J. Compos. Constr.*, vol. 4, no. 3, pp. 137–144, Aug. 2000.
[37] Francesco Micelli and Antonio Naani, "Durability of FRP rods for concrete structures," *Durab. FRP Rods Concr. Struct.*, vol. 18, pp. 491–503, 2004.
[38] M. Porter and B. Barnes, "Accelerated durability of FRP reinforcement for concrete structures," *Proc. 1st Int. Conf. Durab. Fiber Reinf. Polym. FRP Compos. Constr.*, vol. 98, pp. 191–202, 1998.
[39] Gilbert Nkurunziza, Ahmed Debaiky, Patrice Cousin, and Brahim Benmokrane, "Durability of GFRP bars: A critical review of the literature," *Prog Struct Engng Mater*, vol. 7, pp. 194–209, 2005.
[40] Rajan Sen, Gray Mullins, and Tom Salem, "Durability of E-glass/Vinylester Reinforcement in Alkaline Solutions," *ACI Struct. Jounal*, pp. 369–375, 2002.
[41] Mina Dawood and Sami Rizkalla, "Environmental durability of a CFRP system for strengthening steel structures," *Constr. Build. Mater.*, vol. 24, no. 9, pp. 1682–1689, 2010.
[42] Baolin Wan, Michael Petrou, and Kent Harries, "The Effect of the Presence of Water on the Durability of Bond between CFRP and Concrete," *J. Reinf. Plast. Compos.*, vol. 25, no. 8, pp. 875–890.
[43] Mohamed A. Aboelseoud and John J. Myers, "Durability of Hybrid Composite Beam Bridges Subjected to Various Environmental Conditioning," *J. Compos. Constr.*, vol. 20, no. 6, 2016.
[44] Shenghu Cao, Xin Wang, and Zhis WU, "Tensile Properties of CFRP and Hybrid FRP Composites at Elevated Temperatures," *J. Compos. Mater.*, vol. 43, no. 4, 2009.
[45] Jitendra Tate, Ajit Kelkar, and John Whitcomb, "Effect of braid angle on fatigue performance of biaxial braided composites," *Int. J. Fatigue*, vol. 28, no. 10, pp. 1239–1247, 2006.
[46] Jitendra Tate and Ajit Kelkar, "Stiffness degrafation model for biaxial braided composites under fatigue loading," *Compos. Part B Eng.*, vol. 39, no. 3, pp. 548–555, 2008.
[47] John Montesano, Zouheir Fawaz, and Habiba Bougherara, "Use of infrared thermography to investigate the fatigue behavior of a carbon fiber reinforced polymer composite," *Compos. Struct.*, vol. 97, pp. 76–83, 2013.
[48] International Federation for Structural Concrete, "FRP Reinforcement in RC structures."
[49] Pericles Theocaris, "Viscoelastic Properties of Epoxy Resins Derived from Creep and Relaxation Tests at Different Temperatures," *Rhelogica Acta*, vol. 2, no. 2, pp. 92–96, 1962.
[50] D. Katz, Y. Smooha, and A. I. Isayev, "Dynamic Properties of an unfilled and filled epoxy resin subjected to extensional creep," *J. Mater. Sci.*, vol. 15, no. 1980, pp. 1167–1174, 1980.
[51] P. L. Walton and A. J. Majumdar, "Creep of Kevlar® 49 fibre and a Kevlar® 49-cement composite," *J. Mater. Sci.*, vol. 18, no. 1983, pp. 2939–2946, 1983.
[52] R. H. Ericksen, "Room temperature creep of Kevlar® 49/epoxy composites," *Composites*, no. July 1976, pp. 189–194, 1976.
[53] Morgan P. Hanson, "Effect of Temperature on Tensile and Creep Characteristics of PRD49 Fiber/Epoxy Composites," NASA, Washington, D. C., 1972.

[54] W. K. Goertzen and M. R. Kessler, “Creep Behaviour of carbon fiber/epoxy matrix composites,” *Mater. Sci. Eng.*, vol. A 421, no. 2006, pp. 217–225, 2006.
[55] Xin Jing, Xiaoguang Yang, Duoqi Shi, and Hongwei Niu, “Tensile creep behavior of three-dimensional four-step braided SiC/SiC composite at elevated temperature,” *Ceram. Int.*, vol. 43, no. 9, pp. 6721–6729, 2017.
[56] T. Yamaguichi, Y. Kato, T. Nishimura, and I. Uomoto, “Creep Rupture of FRP rods made of Aramid, Glass and Carbon Fibers.” Proceedings on the Third International Symposium on Non-metallic (FRP) Reinforcement for Concrete Structures, 1997.
[57] CSA, “Canadian Highway Bridge Design Code,” 11th Edition, Jan. 2014.

# CHAPTER 3 EXPERIMENTAL METHODS

## 3.1 Introduction

According to the American Concrete Institute report [1], an important element for Fiber Reinforced Polymer (FRP) composites to be used to reinforce concrete is their durability under sustained loads for long periods of time. To study the creep behaviour of the FRP composite rebars, it was first important to study the creep behaviour of the composite braids. Studies on carbon fiber based composites have shown that carbon fiber composites are resistant to creep rupture under ambient conditions [2]. Most current FRP composite rebars use glass fiber, with little research studying using Kevlar® fiber in structural design [3]. To advance the available market for FRP composites, studying the creep durability of the Kevlar® braided composites used in the proposed hybrid FRP composites is important.

In this chapter, the manufacturing process for composite braids, the sources of error in the manufacturing process and sample quality control is detailed. The experimental design for data acquisition is presented with methods of post-processing and analysis explained.

## 3.2 Manufacturing Methods

### 3.2.1 Braidtrusion

The manufacturing process followed the work of Melenka *et al.* [4]. Preforms were produced using a Maypole braiding machine (Steeger Hs140/36-91, Steeger GmbH and Co., Wuppertal, West Germany) shown in Figure 3-1. The 36 carriers of the machine were loaded with Kevlar® 49 (1420 Denier) and used to produce regular braid preforms (2x2) on an aluminum mandrel

(7/16-inch diameter). A sample preform is shown in Figure 3-2. In addition to using the Maypole braiding machine, a caterpillar puller was used to move the mandrel during the braiding process. This puller is shown in Figure 3-3.

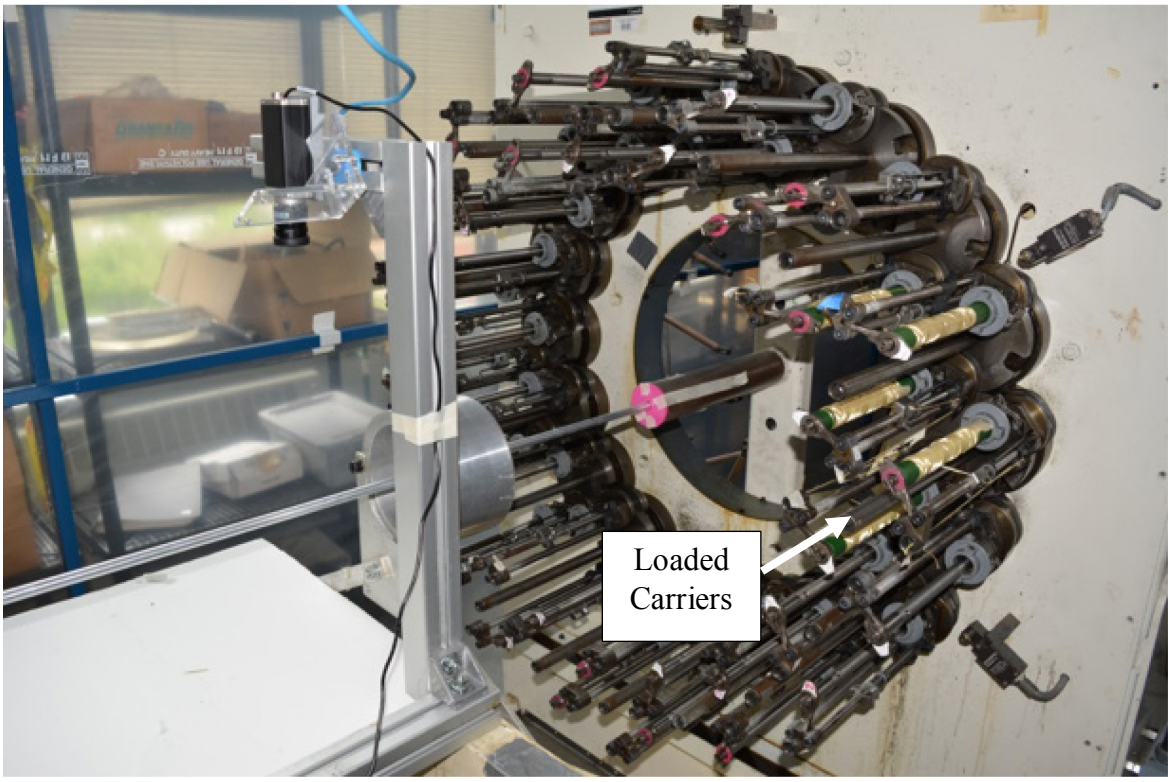


**Figure 3-1: Image of Maypole Braider with a few sample bobbins loaded on the right-side carriers.**

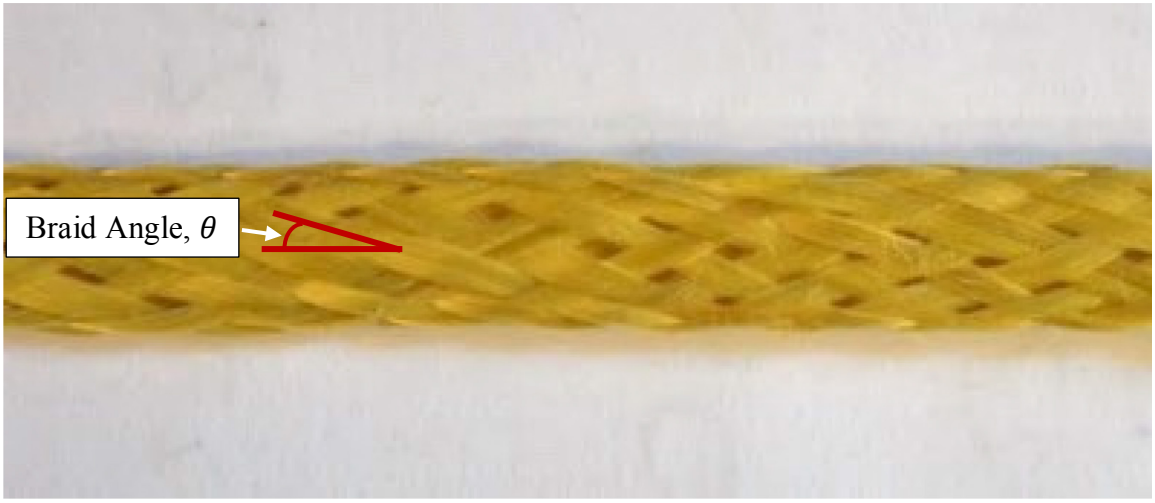


**Figure 3-2 Image of sample preform ($35^{o}$) obtained from the braidtrusion process**

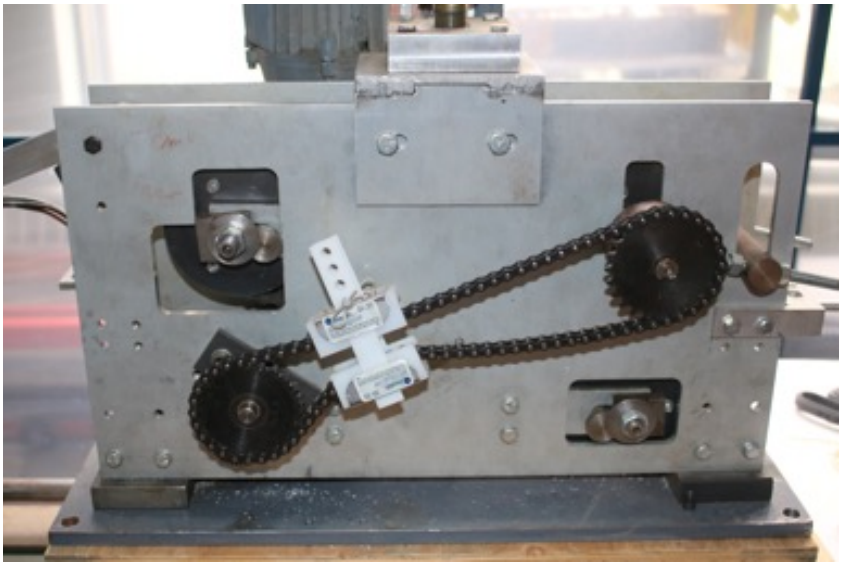

**Figure 3-3 Image of caterpillar puller that moves the mandrel through as the preform is braided on it**

### 3.2.2 Braid Angle Manufacturing Parameters

A program in LabVIEW$^{TM}$ software was created to control the input voltages to the braider and puller that controlled their speed. By altering the speeds of the braider and the puller, the different braid angles were manufactured. The relationship between the speeds of the braider and puller are related to the braid angle by equation 3-1 [5].

$$\theta = \arctan(\frac{\omega R}{v}) \quad \textbf{(3-1)}$$

where, $\omega$ is the rotational speed of the carriers (rad/s), $R$ is the radius of the mandrel (m) and $v$ is the take-up speed of the puller (m/s)

The program was designed to use this relationship to produce different braid angles by controlling the values of the rotational speed of the carriers and the take-up speed of the puller. Input in the software was in the form of voltages. A calibration function to convert the input voltages to the speeds was used to identify the values needed to theoretically produce the braided composites at the different braid angles.

### 3.2.3 Braid Angle Quality Control

Quality Control (QC) of the manufactured preforms was performed to ensure that the final braid angles were consistent and close to required specifications. Accordingly, a camera was set up above the mandrel between the braider and the puller. This recorded the formation of the braid on the mandrel as the braiding process occurred. The camera setup is shown in Figure 3-4.

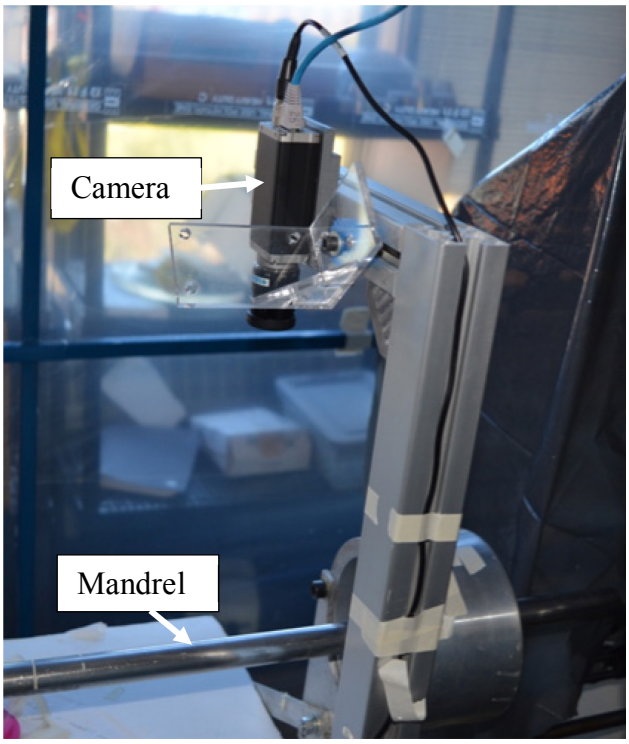


**Figure 3-4 Image of camera setup used to take footage of braid formation during manufacturing**

The videos obtained from the camera were analyzed and used to obtain images (from the frames of the video) of the braid during manufacture. These frames were exported to ImageJ (Image Processing and Analysis in Java, National Institutes of Health, Maryland, USA). The braid angles were measured by constructing solid angle lines along the axis of the mandrel and along the braids on the mandrel. The angle between these two constructed lines represented the braid angle. An example of a measurement of the angle on a 55˚ braid is shown in Figure 3-5.

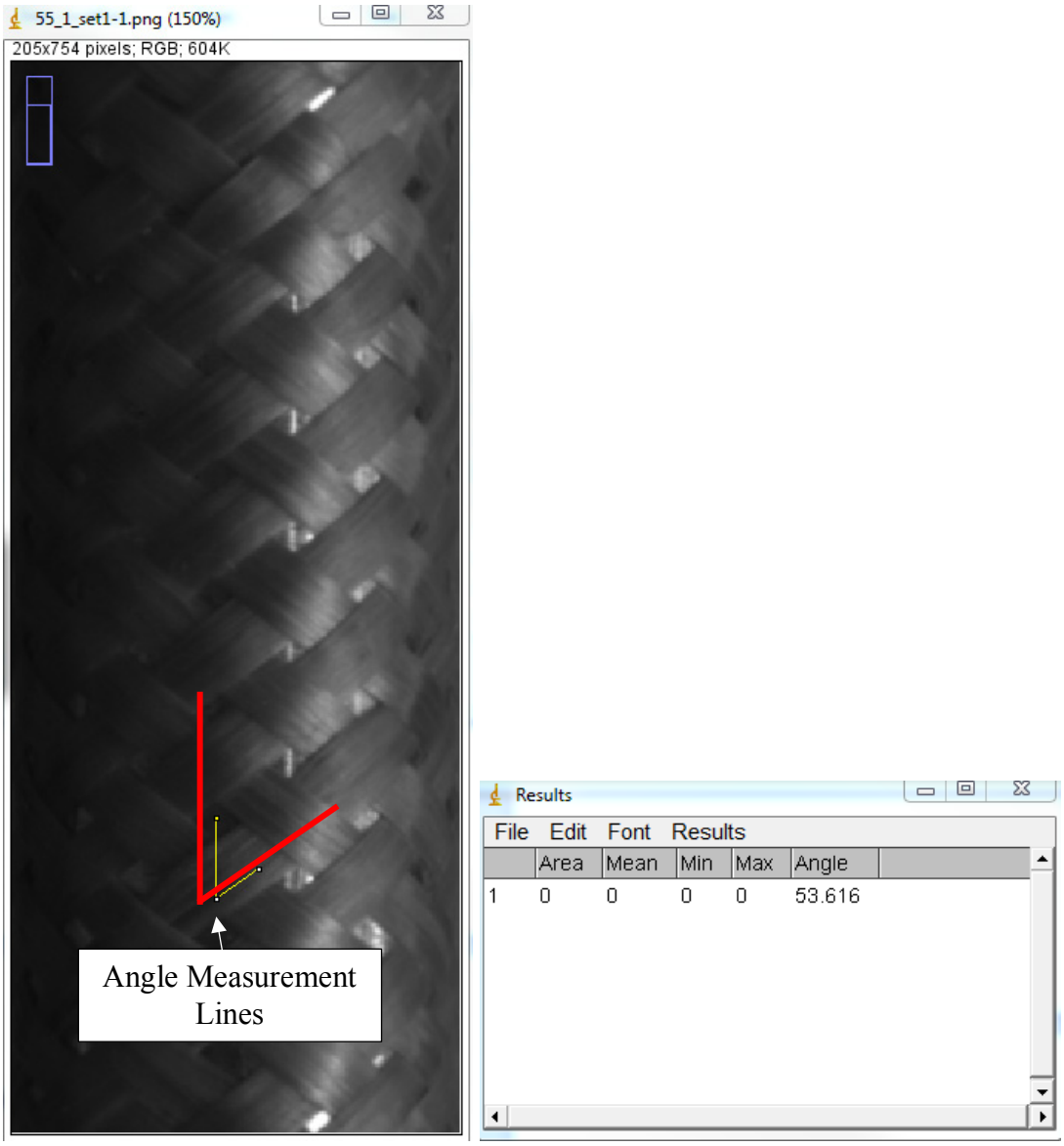


**Figure 3-5: A screenshot of a sample measurement of angles (for a 55˚ braid) obtained from the frames of the video from the camera setup in Figure 3-4**

### 3.2.4 Impregnation and Curing

Once the preforms were pulled off the mandrels, the fibers were impregnated with the resin and hardener mix. The resin used was Epon 826 (Hexion Inc., Ohio, USA) and the hardener used was

Lindau LS-81k (Lindau Chemicals Inc., South Carolina, USA). The resin and hardener mix are recommended for composites designed using pultrusion, making them a reasonable choice for this work [6]. Furthermore, the previous work which attempted to quantify the mechanical properties of tubular braids and of rebars used these same materials for the matrix of the composites [4]. In the combined system, resin and hardener are combined in a weight ratio of 1:1. The typical physical properties of the resin and hardener are presented in Table 3-1. The mechanical properties of the combined resin-hardener system is presented in Table 3-2 [7].

**Table 3-1 Physical Properties of Epon 826 Resin and Lindau LS-81k Hardener**

| Material | Viscosity at 25°C | Density at 25°C | Specific Gravity |
|---|---|---|---|
| Epon 826 | 6,500-9,500 cP | 1162.32 kg/m$^3$ | 1.16 |
| Lindau LS-81k | 200-300 cP | 1174.3 - 1198.26 kg/m$^3$ | 1.16-11.20 |

**Table 3-2 Mechanical Properties of Epon 826 Resin and Lindau LS-81k Hardener combined system**

| Glass Transition Temperature | Tensile Strength, at Break | Tensile Elongation, at Break | Tensile Modulus |
|---|---|---|---|
| 136 °C | 73.8 MPa | 5 % | 2730.32 MPa |

The method of impregnation was a two-step process. The preforms were carefully 'socked on' to curing mandrels in a caterpillar fashion. The preforms placed on the Teflon curing mandrels is shown in Figure 3-6.

**Figure 3-6 Image of a preform socked onto the clamped Teflon-shell/steel-core curing mandrels**

Using a syringe, the resin-hardener mix was applied on top of the preforms on the mandrels. To ensure complete impregnation of the resin and hardener, the resin-hardener mix was massaged thoroughly for approximately 5 minutes. Following this, the impregnated preforms were placed in a vertical tray for curing. The cure cycle followed was identical to the one specified in the data sheet [7]. The composites were cured at 66˚C for 1.5 hours (step 1), followed by curing at 85˚ for 1 hour (step 2) and finally curing at 150˚ for 3 hours (step 3). Once the samples cooled down to room temperature they were removed from the oven and cut into the sample size of around 150 mm in a 3D printed fixture. To ensure that the edges of the tubular braided composites were level, a file was used to sand the edges down. Inspection of the braids interior showed that resin-

hardener mixed had reached the interior and was fully impregnated. Three sample tubular braids are shown in Figure 3-7(a) and a picture of a sample interior is shown in Figure 3-7(b).


(a) (b)

**Figure 3-7: (a) Image of three sample fully cured braided composites produced angles of 35°, 45° and 55° (b) Image showing sample impregnation of the exterior and interior of the manufactured braids**

Once the final samples were obtained, they were labelled in accordance to the angle and the sample number. The manufactured samples were cut to the designated sample size in a 3D printed mould. Dimensions of produced samples are presented in the next chapter.

### 3.2.5 Sample Preparation

To apply the required tensile loads to the samples, tabs were to be attached to the ends of the samples using a high-strength two-part Loctite epoxy (Henkel AG & Company, KGaA, Düsseldorf, Germany). The two-part epoxy was allowed 24 hours to dry for full adhesion of braids to the end tabs. To maintain the alignment of the curing braid, the braid was placed on a

rail. Hose clamps were used to ensure that the end tabs were held firmly in place. A prepared sample for tensile testing is shown in Figure 3-8. A flowchart summarizing the different steps involved in the manufacture of the Kevlar® composite samples is presented in Figure 3-9.

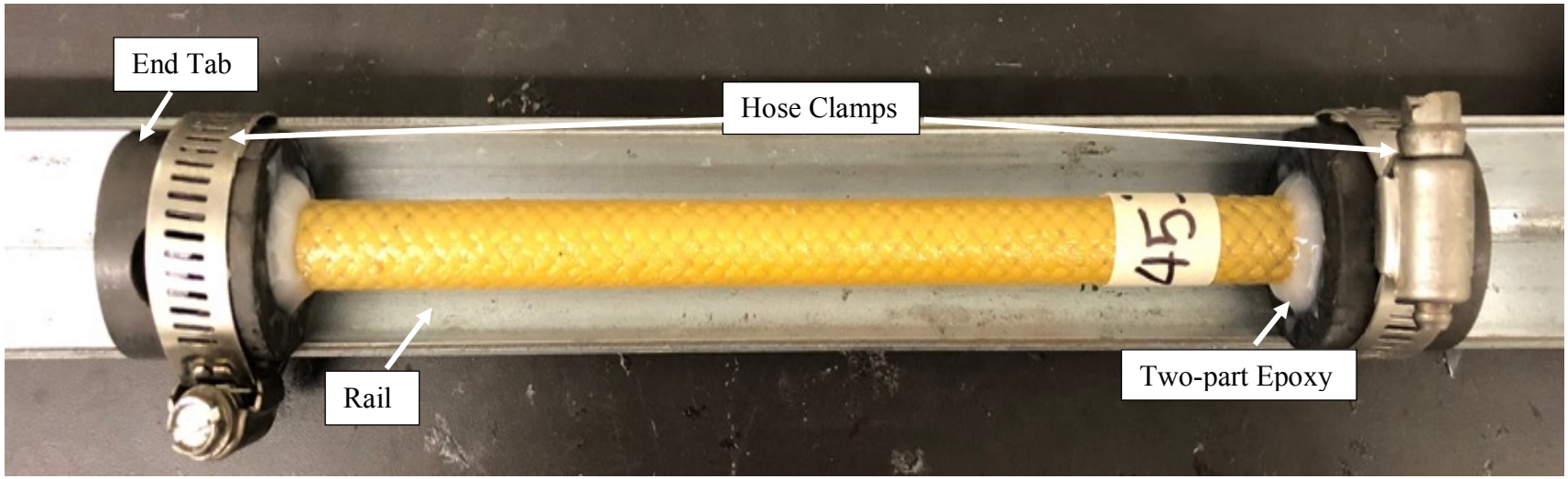


**Figure 3-8: Image of clamped tubular braid attached to MTS end tabs using Loctite Adhesive and aligned by rail and hose clamps.**

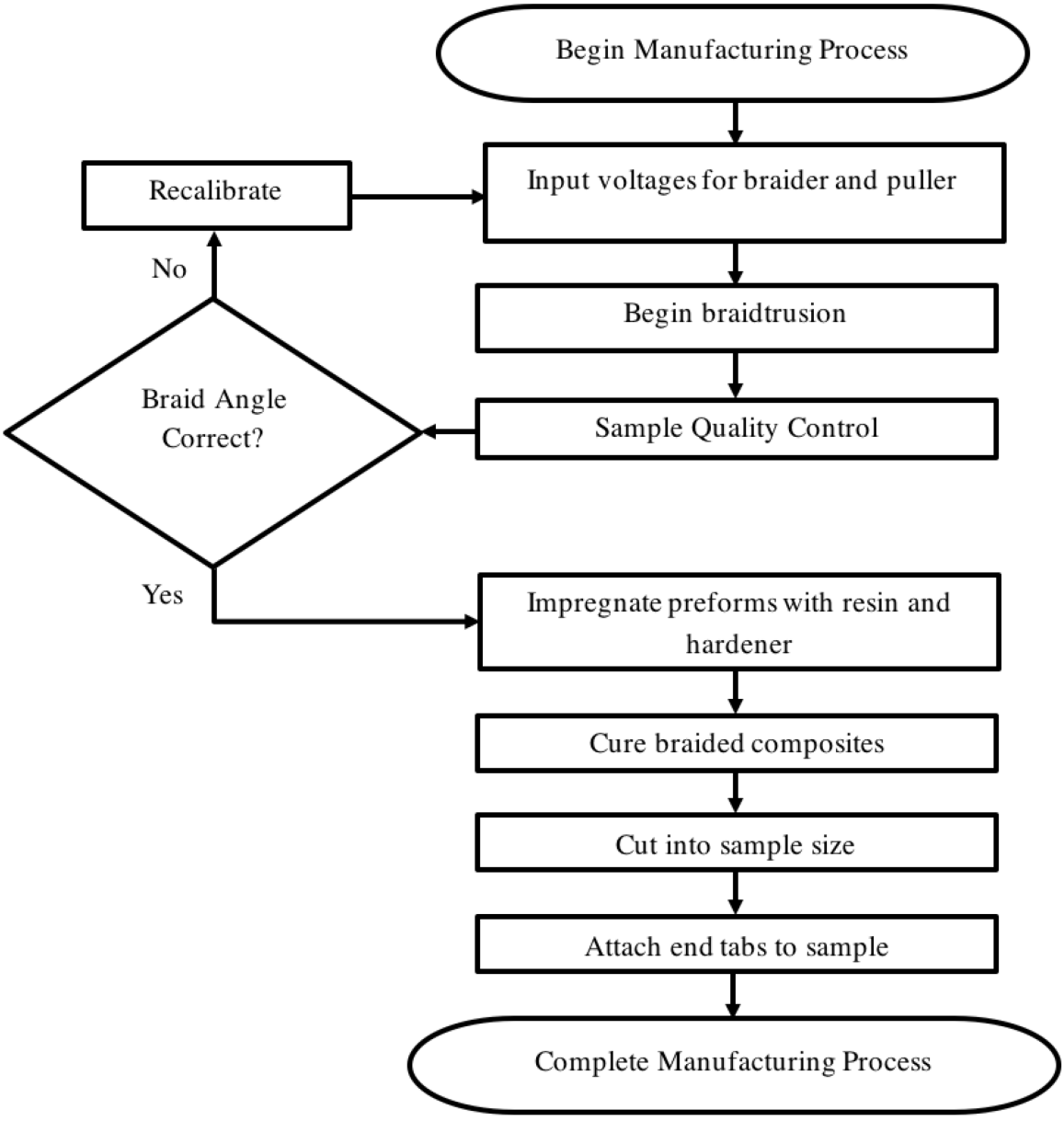


**Figure 3-9: Flowchart describing the manufacturing process**

## 3.3 Errors in Manufacturing Process

Identifying the errors resulting from the manufacturing process were essential to gain some insight on the accuracy of the process and quantify the errors that could influence the creep results obtained from the experimental work. The most significant source of error in the experiment was the errors in the braid angles measured. Although the calibration function for the puller and braider speed is theoretically correct, the tensioned yarns pulled on the mandrel as the braid preform was being created. When replaced with a larger, heavier mandrel (1" in diameter) the variation in the angles was noticeably less. It was concluded that this is a result of the difference in the rigidity of the mandrels. The results for the measured angles on the different mandrels are presented in Figure 3-10. As can be seen from the box and whisker plots, the larger mandrel resulted in a smaller standard deviation from the theoretical angle and a smaller range of values for the braid angles. The errors in the manufacturing process can be seen in the deviation from the theoretical angle which is more significant in the smaller diameter mandrel. An additional source of error in the manufacturing process lied in the many steps involved in the creation of the final polymer composite. Removing the preforms from the mandrel, placing them on the curing mandrels and massaging the resin-hardener mix are steps that may influence the final braid angle. The relationship between these errors and the final experimental results are presented in the next chapter.

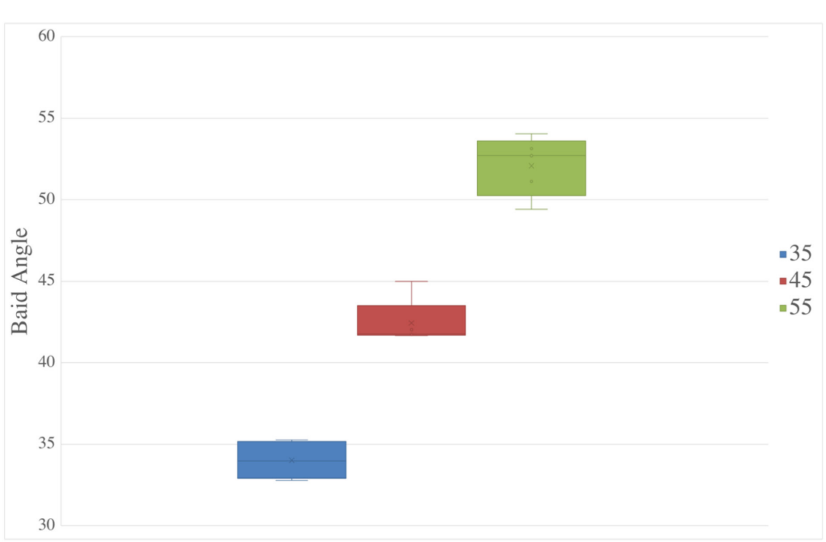


(a)

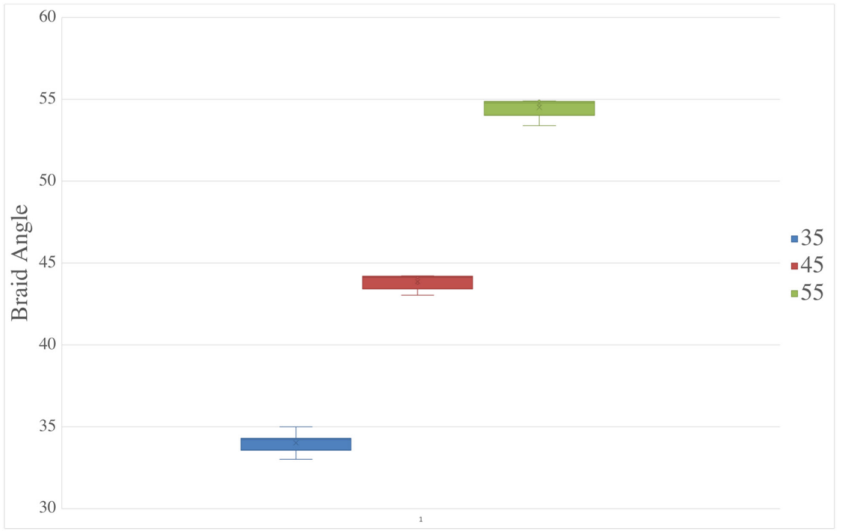


(b)

**Figure 3-10: Box and Whisker plots for the braid angles measured for preforms on (a) 7/16'' diameter mandrel and (b) 1'' diameter mandrel**

## 3.4 Creep Test Experimental Design

To study the behaviour of the Kevlar® composites in creep, an experimental setup was designed to apply a constant force to the tubular braided samples. End tabs on the sample were fit in the grips of a hydrauloc MTS machine and pinned to ensure that the end of the sample translated with the grips to create a load on the sample. A 4400 N load cell was used to apply the necessary load on the samples. Figure 3-11 shows a labelled diagram of the machine used in this work to perform the creep tests on the Kevlar® samples with a clarifying schematic.

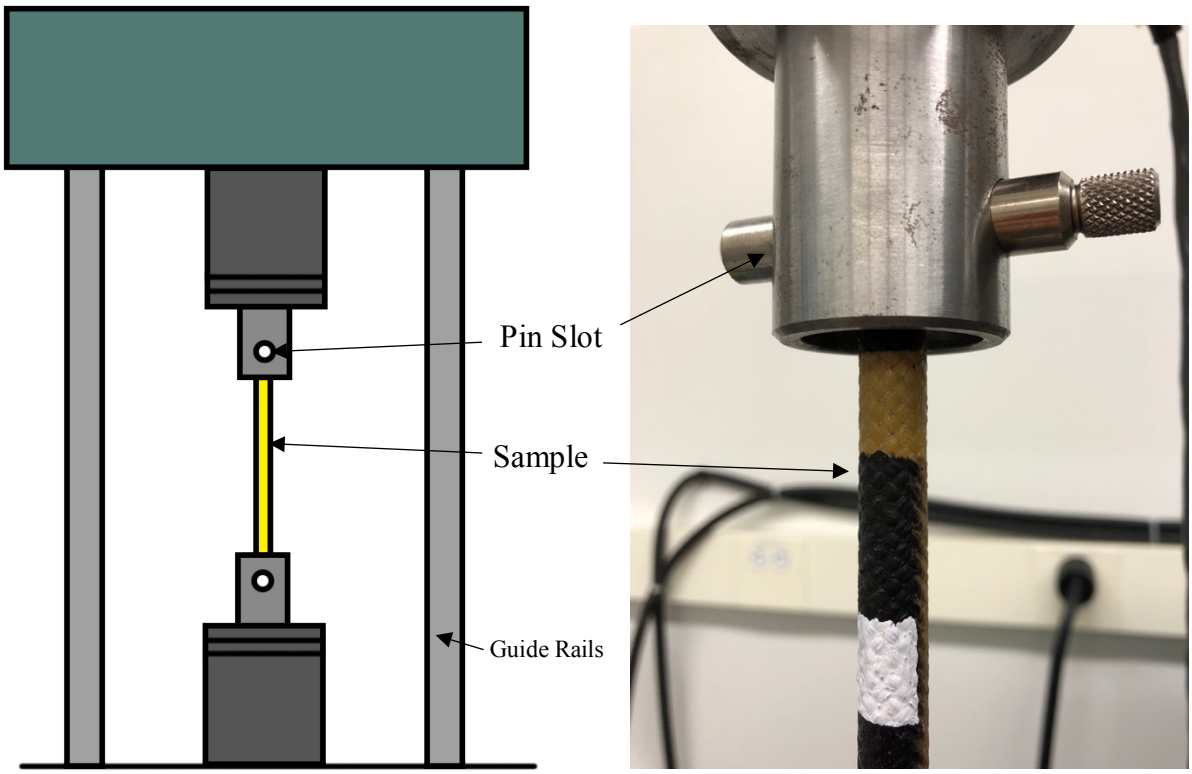


(a) (b)

**Figure 3-11 : Image showing (a) schematic of the experimental setup and (b) zoomed in image of fixation method used to perform creep tests on Kevlar® samples**

According to the ASTM D7337 standard for tensile creep testing of Fiber Reinforced Polymer Matrix composites, the load applied on the sample must remain within ±1% of the desired load during the test. Pilot tests on the MTS machine showed that this was achieved with the experimental setup for the loads used in this work. The machine allowed the user to control the voltage which translated into a load on the sample. Initial pilot tests allowed the user to create a conversion function from machine input to load. This was used to convert the calculated loads into machine input for testing. This plot is shown in Figure 3-12. The resolution of the MTS machine was approximately 9 N of force.

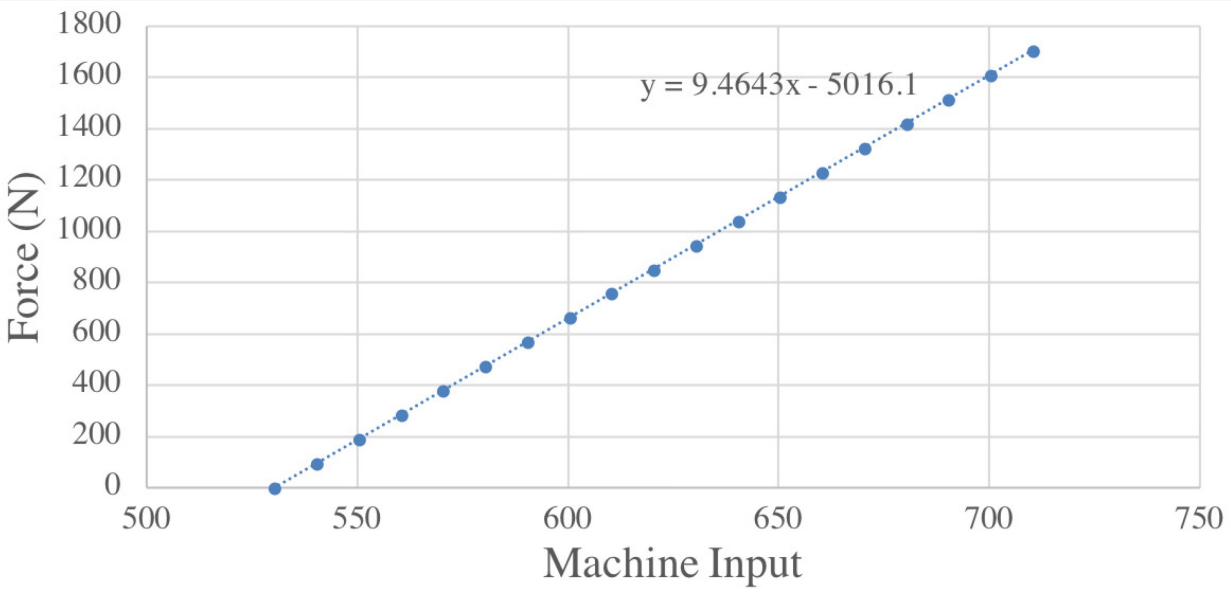


**Figure 3-12: Conversion plot for MTS machine used to set the load for creep tests in the experimental setup**

## 3.5 Creep Test Parameters

### 3.5.1 Load

As mentioned earlier, this research sought to study the creep behaviour of tubular braided composites. Upon pilot testing of the tubular braided composites, the mechanical behaviour of the braided composites was found to behave similar to previous work by Melenka *et al.* [4]. In these pilot tests, the tubular braids were loaded to a percentage of the fracture loads and the strain observed for the loads. Strain at the loads was measured and used to confirm that the Elastic Moduli of the tubular braids was similar to the braid samples used by Melenka *et al.* . They had studied the tensile behaviour of the braids and compared the mechanical behaviour of braids at the three braid angles used in this study [4]. Using equation 3.1 below fracture loads were determined.

$$F_{load} = f * \frac{\pi}{4} * \left({d_o}^2 - {d_i}^2\right) * \sigma_{UTS} \quad \textbf{(3.1)}$$

where, f is fractional percentage of the total load, $d_o$, $d_i$ are the outer and inner diameters of the braid and $\sigma_{UTS}$ is the ultimate tensile strength of the braids as calculated by Melenka et. al. [4] expecting similar behaviour from samples produced by the same methods and using the same materials.

Samples were placed inside the MTS machine and loaded to the appropriate forces as calculated from equation 3.1. According to the ASTM D7337 standard for tensile creep testing of Fiber Reinforced Polymer Matrix, for creep testing, the creep load should be applied to the specimen within a time of 20 seconds to 5 minutes from the time the experiment is initiated [8]. Once the

sample was inserted, the load on the specimen was brought up to the required load within 30 seconds, meeting the ASTM standards.

### 3.5.2 Test Duration

The overall duration of the creep tests was also determined through pilot tests. In these pilot tests, sample braids were loaded to the maximum percentage loads tested in this study (60% of fracture load) and monitored over the course of 4 days, with images being taken every 5 minutes. From these pilot creep tests, sample braids were shown to be in the secondary stage of creep (and maintain a constant slope of strain rate) after 24 hours of testing. Due to strain values being quite far from the fracture strain, it was unrealistic to wait until the samples entered the tertiary phase. To standardize testing time between the different experiments, testing was performed for 48 hours on all samples, with images being taken every 5 minutes. This resulted in a total of 576 images per test.

Before recording any data, the $35^{o}$ tubular braids were tested at 60% of the fracture loaded and were found to not break after four days of being sustained at a constant load. $35^{o}$ are known to perform better in tensile applications and by testing at the highest percentage of failure load, an idea of the behaviour of the composites could be inferred. After four days, the sample was still within the secondary stage of creep. All samples were therefore tested for 48 hours. This ensured that samples reached the secondary stage of the creep test and also provided sufficient time to ensure that samples did not break during the tests. To ensure that samples had reached the secondary stage of the test, the numerical difference between successive values was plotted for the duration of the test using a specifically-developed MATLAB® function.

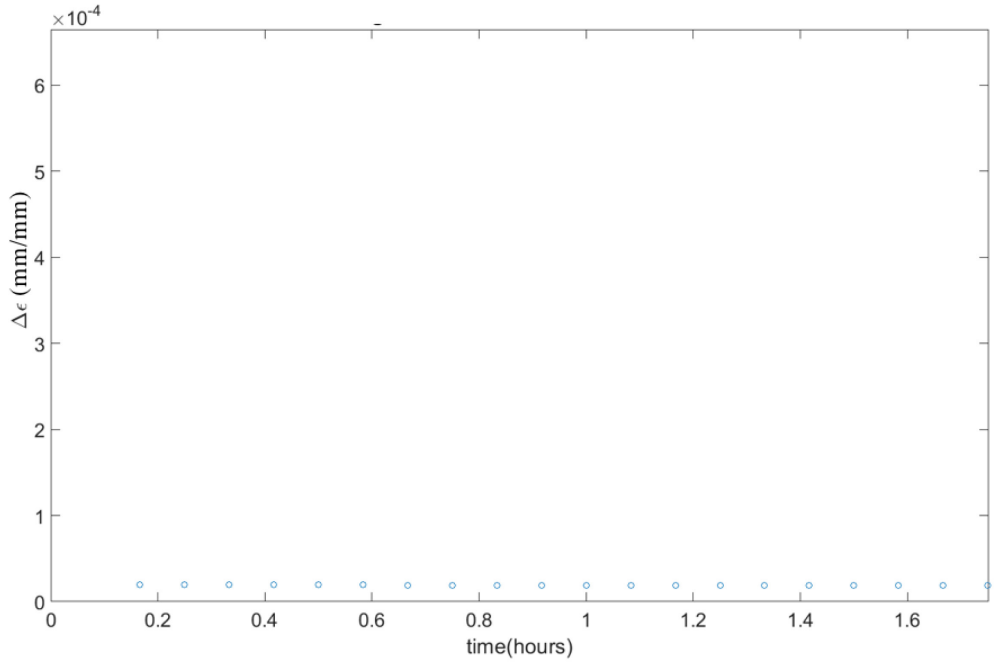


**Figure 3-13: Plot showing the change in the strain values post initial loading phase. Y-axis is extended to compare values to initial strain difference value of 0.0132.**

The strain difference plots in Figure 3-13 were sufficient evidence that samples reached a steady strain rate early in the test. Values of the $\Delta\varepsilon$ almost immediately plateaued to values less than $5x10^{-5}$ and continued to decrease until the end of the test. This confirmed that the selected time was sufficient for the creep tests. The total number of tests for the different samples with the times the tests were performed for are shown in the sample experiment matrix shown in Table 3-3. Samples which performed as expected were tested only once.

**Table 3-3: Braided composite test sample experiment matrix**

| Angle | Percentage of Failure Load (%) | Number of Samples Evaluated |
|---|---|---|
| 35° | 40 | 2 |
| | 50 | 4 |
| | 60 | 1 |
| 45° | 40 | 1 |
| | 50 | 4 |
| | 60 | 3 |
| 55° | 40 | 1 |
| | 50 | 1 |
| | 60 | 2 |

## 3.6 Strain Data Acquisition

In creep testing, strain data is collected over extended periods of time. Unlike tensile tests to failure, data points in a creep test consist of periodic measurements of strain over a duration of time. This section will focus more on the setup for collection of strain data from the creep tests.

### 3.6.1 Virtual Extensometer Setup

To measure the strain of the composite braids a "virtual extensometer" was used. This is a non-contact optical technique of strain measurement. The setup for the virtual extensometer is shown in Figure 3-14.

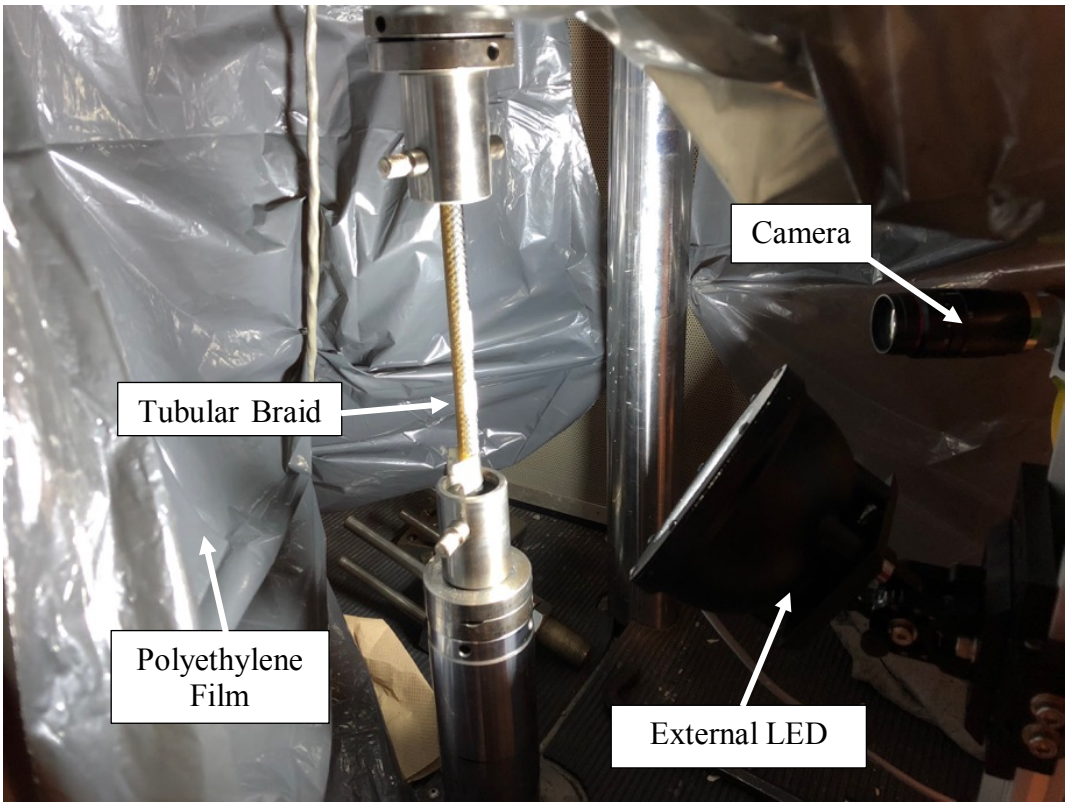


**Figure 3-14: Image of Virtual Extensometer setup used for strain measurement**

The method of measurement of the strain relied on a simple error fitting code which has been developed by Aldrich *et al*. [9]. A scientific camera (Basler acA3800-10gm, Basler AG, Ahrensburg, Germany) is used to take images of the sample during the creep test. The first step involves spray painting the sample in a matte black color. This spray paint allows covers the yellow color of the Kevlar® and provides better contrast for the virtual extensometer. Once the spray paint is applied, two white marks are placed on the sample at the ends of the area of interest. These white marks contrast with the black matte color of the braid. The program developed by Aldrich *et al.* works so that an error function is fitted to match the change in the

colouration to the picture. This error function is used to track the movement of the marks placed on the braid. The separation of the marks relative to the first image is used to calculate strain.

An external LED was used to control the illumination of the sample during the setup so as not to oversaturate the picture of the braid but provide adequate illumination for the optical strain measurement technique to accurately measure strain. The external LED was set to be slanted upwards at an angle of approximately $45^{o}$. This ensured that none of the light was reflected back into the camera lens that would create glare on the images. In order to ensure that no background light affected the images taken of the sample, a black polyethylene film was wrapped around the setup.

The first image in the test was taken at 0 N load and the second image was taken five minutes later, after the entire load had been applied to the sample. This created a shift in the white markings that was used to calculate strain by the virtual extensometer. This is shown in Figure 3-15.

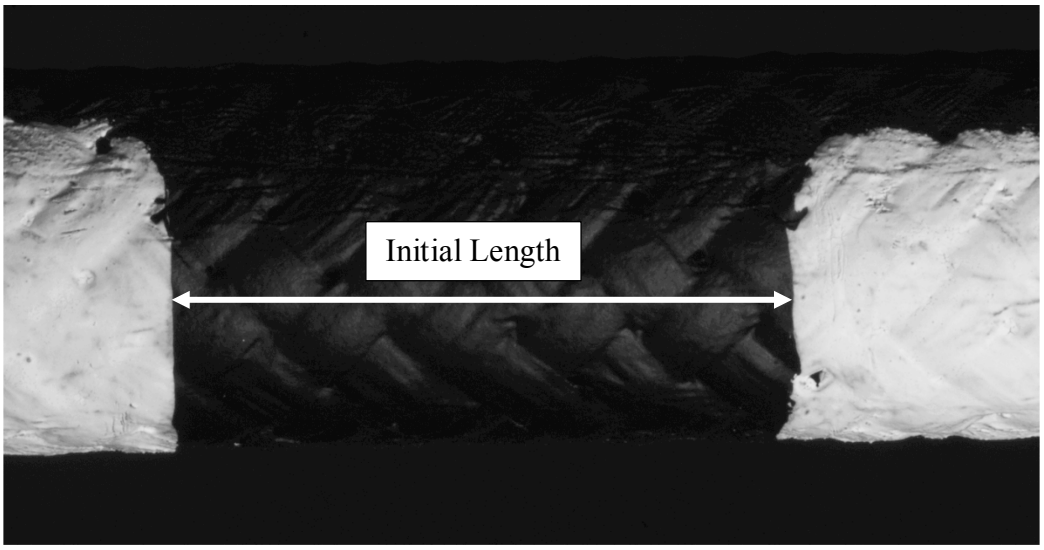


(a)

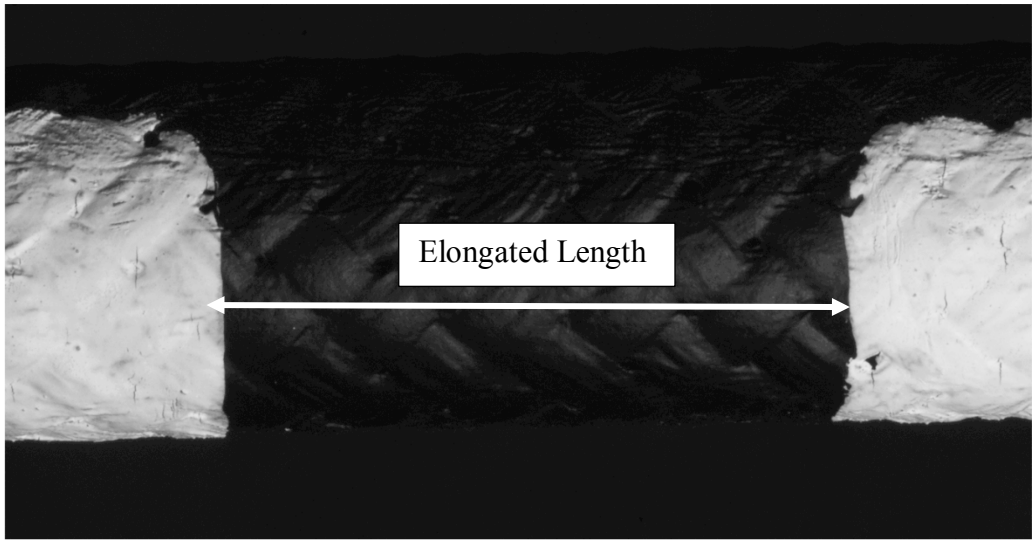


(b)

**Figure 3-15: Images showing how the initial strain was calculated between the (a) Image 1 and (b) Image 2 in a sample set of images**

### 3.6.2 Conversion of Strain Data to Creep Curves

Once the images were processed, the MATLAB® code produced a graph of strain vs the number of images taken. Since the image number was representative of time, plots were modified in MATLAB® to produced strain vs time plots. A sample plot for the 35° tubular braid loaded to 40% of the fracture load is shown in Figure 3-16.

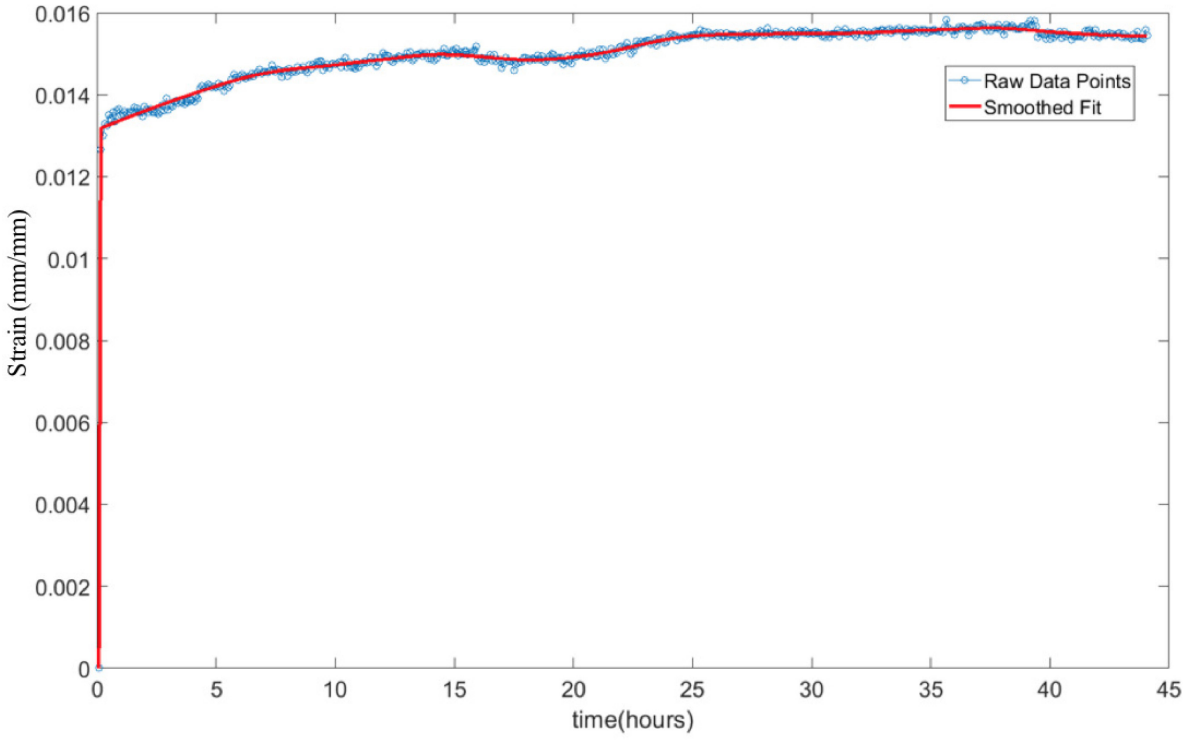


**Figure 3-16: Creep curve for a 35° braid loaded to 40% of the fracture load**

The virtual extensometer software developed by Aldrich *et al.* [9] uses the initial length as a reference and calculates the strain based on this initial length. Since the second image in a set was taken five minutes after the first image (when the load was applied, and sample was allowed

to stabilize), the initial strain could be checked using ImageJ. Using equation 3-2, the initial strain was calculated using ImageJ to measure lengths and compared to the values reported by the virtual extensometer software. This confirmed the viability of the technique in measuring the strain experienced by the samples during the creep test.

$$\varepsilon_o = \frac{l_2 - l_1}{l_1} \quad \textbf{(3-2)}$$

where, $l_2$ is the length between two fixed points in the second image, $l_1$ is the length between the same two points in the initial (unloaded) image.

In addition to calculating the initial strain $\varepsilon_o$ using the images from the test, another technique involved using the Elastic Moduli of the tubular braids. Elastic modulus values for Kevlar®-Epoxy tubular composites are available in previous work by Melenka *et al.* [4]. During the initial loading of the samples, the behaviour of the tubular braids was assumed to be linearly elastic. Accordingly, Hooke's law can be applied to the initial strain to work out the expected value for the initial strain using equation 3-3.

$$\varepsilon_o = \frac{\sigma_{app}}{E} \quad \textbf{(3-3)}$$

where, $\sigma_{app}$ is the stress applied on the samples and $E$ is the longitudinal elastic modulus of the braided composite.

Depending on the lighting conditions of the sample, the raw data was often dispersed. A local regression function in MATLAB® was used to smooth the data by assigning lower weights to outliers. The MATLAB® script can be found in Appendix A.

### 3.6.3 Endurance Limit

According to the American Concrete Institute report, an important element to study in the testing of Fiber Reinforced Polymer (FRP) composite is the endurance limit. This is defined as "the time to rupture for FRP's under a given level of sustained load" [1]. If hybrid braided FRP rebars are to be used in structural design, reporting the endurance limit of the tubular braided composites is essential to make an argument for or against their use.

According to the general creep formula after the initial straining of the sample, the only factor that influences strain is time. Endurance limit represents the time taken to reach the strain at which the tested material will fracture. Accordingly, the general creep equation can be written for the specific case of failure as equation 3-4.

$$\varepsilon_f = \varepsilon_o + \beta \log(t_f) \quad \textbf{(3-4)}$$

where, $\varepsilon_f$ is the failure strain of the sample and $t_f$ is the time for the sample to fail (endurance limit).

The tubular braided composites used in this research followed the manufacturing method used by Melenka *et al.* [4]. The data presented by their work identified the strain at which the tubular braided composites would fail, or $\varepsilon_f$ presented in equation 3-4. The $\varepsilon_f$ values for the 35°, 45° and 55° were 2.4%, 1.75% and 1.5% respectively. To calculate the value of $t_f$, equation 3-4 can be rearranged as equation 3-5.

$$t_f = e^{\frac{\varepsilon_f - \varepsilon_o}{\beta}} \quad \textbf{(3-5)}$$

where $e$ is Euler's number.

Using equation 3-5, the rupture time could be calculated. Values for the failure strain ($\varepsilon_f$) could be obtained from static tensile tests done on the composites and the value of the initial strain ($\varepsilon_o$) could be obtained from the first point in the strain data.

$\beta$, the creep rate parameter, is defined as the slope of the creep curve when strain is plotted against the logarithmic of time. This plot is called an isostress creep curve [3]. From this plot, the intercept with the y-axis represents the initial strain ($\varepsilon_o$) and the slope of the line represents the creep rate parameter. A labelled example of a typical isostress curve is shown in Figure 3-17.

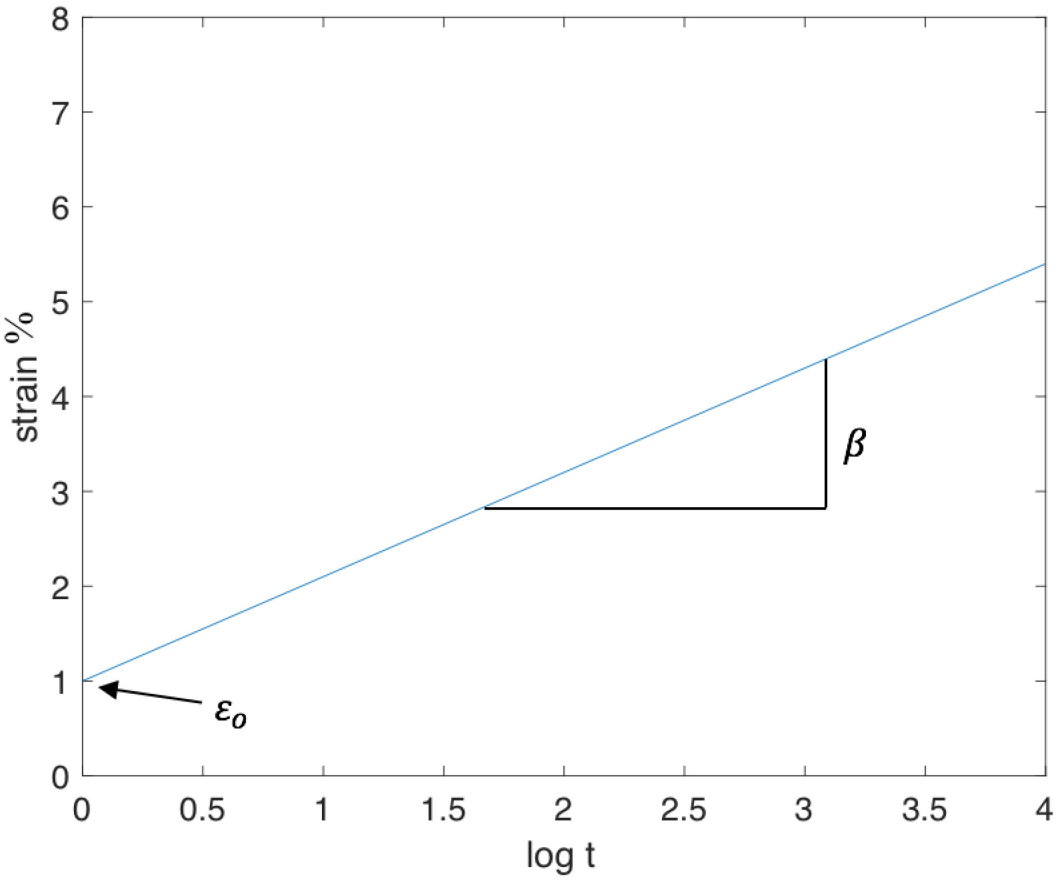


**Figure 3-17: Plot of a typical isostress creep curve showing the initial strain ($\varepsilon_o$) and the creep rate parameter ($\beta$)**

From the isostress curve, the value of the creep rate parameter can be calculated and input back into equation 3-5 with the initial strain ($\varepsilon_o$) and fracture strain ($\varepsilon_f$) values to work out the endurance limit. Conversion of the strain vs time graphs was done in MATLAB®.

To calculate the value of $\beta$, a MATLAB® script was developed. The script was written to calculate the difference between the strain values for each two points. This difference was then compared to an error value of $10^{-5}$. If the value of the difference was less, this point was marked and every point following this used to calculate the slope by dividing the difference in strain values by the difference in the logarithmic values of time. These slope values were then averaged to work out the average value of the slope, which represents $\beta$.

## 3.7 References


[1] ACI Committee 440, "Guide for the Design and Construction of Structural Concrete Reinforced with FRP Bars," 2006.

[2] W. K. Goertzen and M. R. Kessler, "Creep Behaviour of carbon fiber/epoxy matrix composites," *Mater. Sci. Eng.*, vol. A 421, no. 2006, pp. 217–225, 2006.

[3] Marcus Ivey, "Towards the Development of Pseudoductile FRP Rebar," University of Alberta, 2015.

[4] Garrett William Melenka and Jason P. Carey, "Experimental analysis of diamond and regular tubular braided composites using three-dimensional digital image correlation," *J. Compos. Mater.*, vol. 0, no. 0, pp. 1–21, 2017.

[5] Jason P. Carey, Handbook of Advances in Braided Composite Materials - Theory, Production, Testing and Applications. .

[6] Hexion Inc., "Technical Data Sheet (Epon Resin 826)." 2005.

[7] "Epoxy Resin System for Pultrusion or Filament Winding." Hexion, Jul-2007.

[8] ASTM, "Standard Test Method for Tensile Creep Rupture of Fiber Reinforced Polymer Matrix Composite Bars - D7337."

[9] D. Aldrich, C. Ayranci, and D.S. Nobes, "OSM-Classic : An optical imaging technique for accurately determining strain," *SoftwareX*, no. 6, pp. 225–230.

# CHAPTER 4 RESULTS AND ANALYSIS

## 4.1 Introduction

This research sought out to find the performance of braided tubular composites when exposed to a maintained load for a period of time following standardized creep tests. In this chapter, the results obtained from the experiment and the analysis performed on the results are presented. For the tests performed, creep curves were produced for samples manufactured with different parameters and tested at different loads. These were then compared to each other to identify trends in the data and variables which influenced the creep behaviour of the braided composites. In this chapter, all results from this work are presented and analyzed. At the end of the chapter, a full discussion of these results is presented.

## 4.2 Sample Dimensions

An important step in the analysis of the results was to measure the dimensions of the produced samples. Using representative samples from the three different braid angles, a micrometer was used to measure the inner and outer diameters of the braided composites. Calipers were used to measure the length of the samples. The results obtained from the samples are presented in Table 4-1.

**Table 4-1: Measured sample dimensions for manufactured braids**

| Sample Number | Inner Diameter (mm) | Outer Diameter (mm) | Measured Braid Angle (deg) |
|---|---|---|---|
| | 11.57 | 12.49 | 35.13 |
| 35_1 | 11.63 | 12.28 | 34.88 |
| | 11.63 | 12.42 | 34.03 |
| | 11.54 | 12.11 | 34.76 |
| 35_2 | 11.47 | 12.09 | 34.24 |
| | 11.54 | 12.13 | 34.56 |
| | 11.53 | 12.30 | 44.78 |
| 45_1 | 11.55 | 12.33 | 44.31 |
| | 11.59 | 12.38 | 44.00 |
| | 11.56 | 12.13 | 43.53 |
| 45_2 | 11.61 | 12.19 | 42.847 |
| | 11.58 | 12.20 | 42.95 |
| | 11.54 | 12.40 | 54.16 |
| 55_1 | 11.5 | 12.51 | 54.46 |
| | 11.57 | 12.54 | 54.32 |
| | 11.53 | 12.44 | 53.32 |
| 55_2 | 11.57 | 12.27 | 55.01 |
| | 11.57 | 12.43 | 54.03 |

## 4.3 Strain Data

By fitting an error function to the markings on the samples, the strain was calculated for each image taken during the duration of the test. The virtual extensometer was sensitive to strains to the sixth decimal place. Figure 4-1 shows a set of images taken for the $35^{o}$ braid with strain values obtained from the virtual extensometer software reported. The time at which the images were taken in the test is also reported in hours.

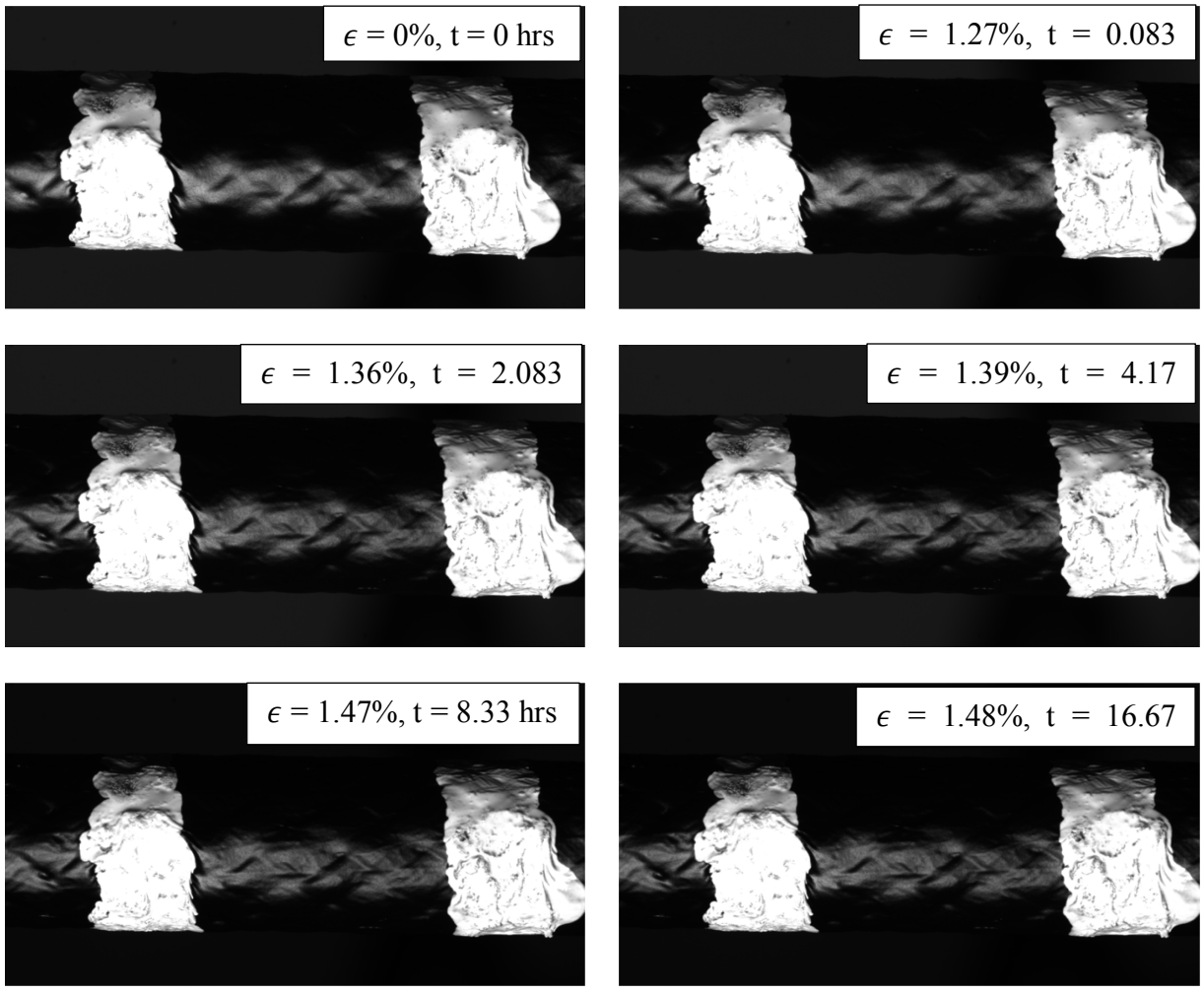

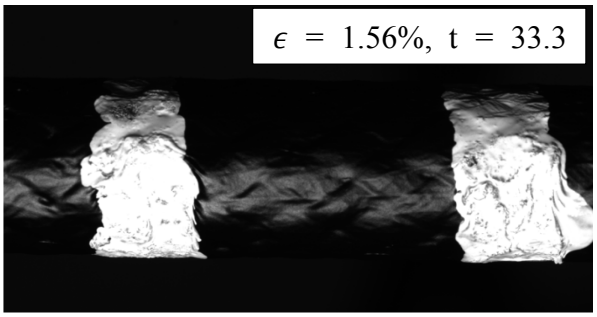


**Figure 4-1: Set of images taken at different times for the 35$^o$ braid loaded at 40% with strain values from the virtual extensometer reported for each image**

The range of the strain values reported by the virtual extensometer were well within the expected values reported in previous work by Melenka *et al.* [1]. In their work, strain values for 35$^o$ braids linearly increased until failing at values around 2.4%. Although the range of values was correct, the virtual extensometer was found to be very sensitive to light. Fluctuations in the lighting would result in changes in strain that did not fit with the general behaviour of the composite. This is shown in Figure 4-2.

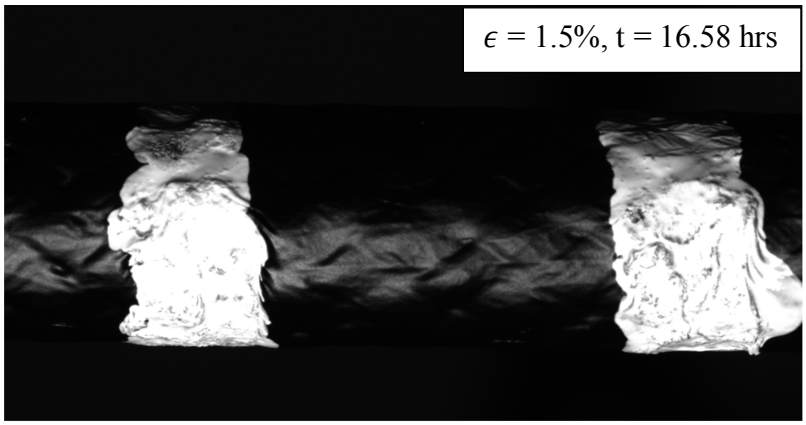


(a)

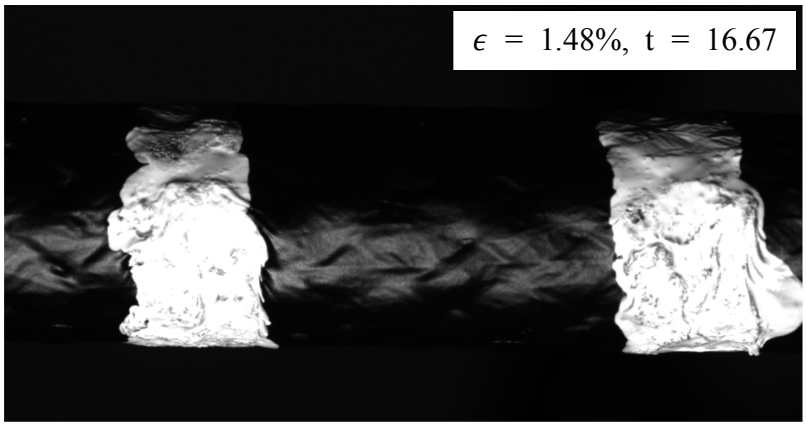


(b)

**Figure 4-2: Image (a) #199 and (b) #200 (5 minutes apart) in the creep test for the 35$^{o}$ braid loaded at 40% of failure load and the strain values from the virtual extensometer**

Even though the load was maintained at a constant value (within ±1 of the set load), a drop in the values of strain was difficult to explain. As the sample was being loaded in tension, the reported strain as measured by the distance between the two marks should not decrease for the duration of the test. However, close observation of the two images in Figure 4-2 shows that the lighting changed slightly between the two images. Although the polyethylene film was taped around the machine, it was very difficult to cover all the openings, particularly where the camera was

placed. Since the virtual extensometer works by isolating the white marks from the black background of the sample, this could possibly explain how strain decreased in a few images before returning to the expected behaviour.

Out-of-plane strain was also taken into account in this work. Typically, using two cameras to take images and using the set of images to calculate the three-dimensional strain is how 3D digital image correlation is performed. However, it was found that out-of-plane strain caused the images to become out of focus, which resulted in very large errors in the virtual extensometer. This method of self-correction was sufficient for this work.

For the $45^{o}$ braids, although strain data was collected for the samples loaded at 40% of the failure load, samples failed when loaded at 50% and 60%. Immediately after setting the load, cracks began to form on the paint as the sample began to exhibit a non-linear strain behaviour. Although the three tested samples did not fail immediately, the progression of cracks in the images predicted the failure of the samples, which was confirmed when the samples failed. These initial cracks can be seen in the two images presented in Figure 4-3. These were taken to be warning signs of samples failing earlier than the expected duration of the test.

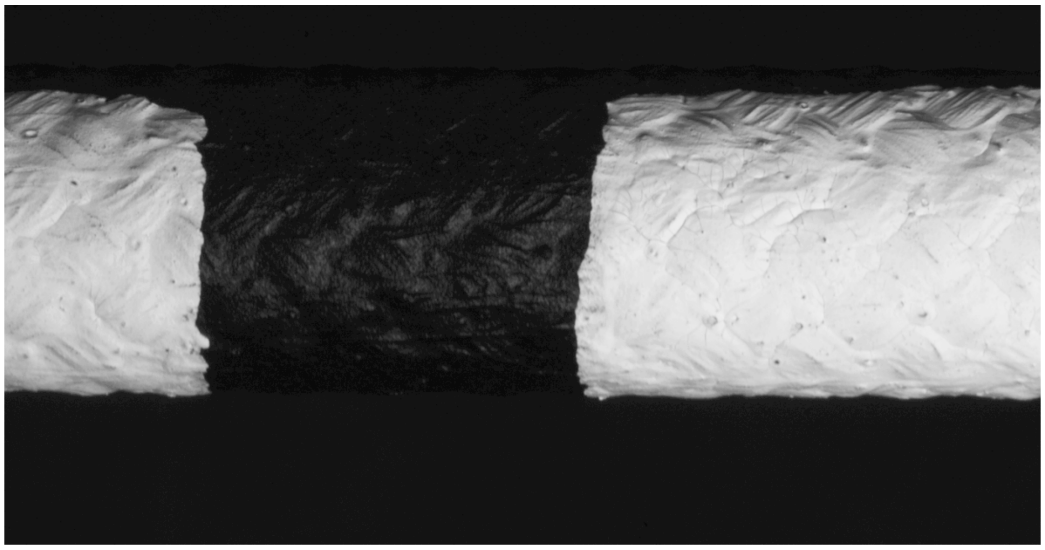

(a)

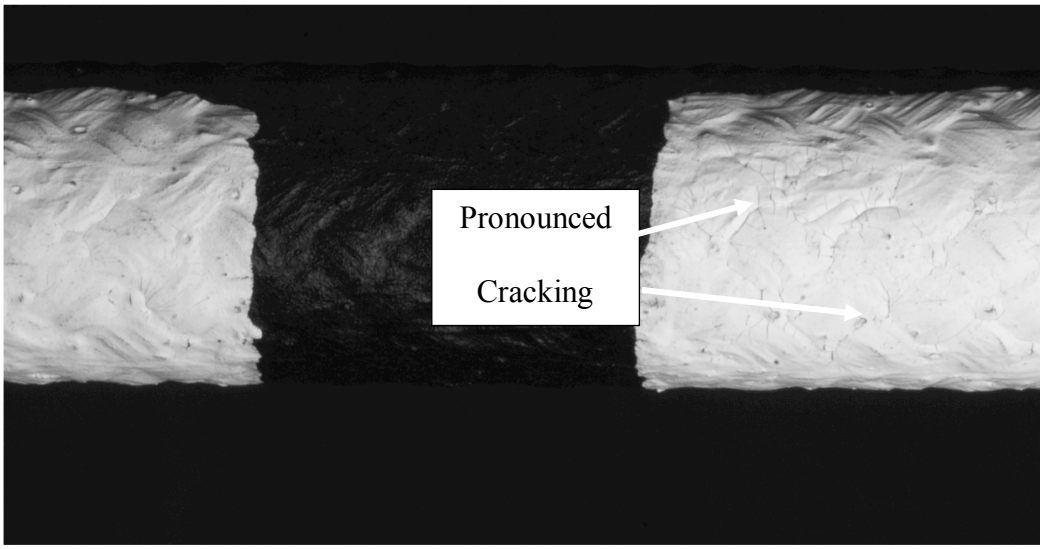


(b)

**Figure 4-3: Image (a) #1 and (b) #2 from a 45$^{o}$ sample loaded at 60% of failure load**

## 4.4 Creep Behaviour of the Braided Composites

In describing the creep curve of a material, three important regions are of concern, the primary, secondary and tertiary stage. A labelled version of the strain-time creep curve obtained from the $35^{o}$ braid loaded at 40% is in Figure 4-4. By comparing the experimental creep curves to the expected creep curve, a number of conclusions on the behaviour of the braided composites could be made. As can be seen in Figure 4-4, the primary stage ended within the first 10 hours of the test and the secondary stage lasted until the test was over or until the sample fractured (in case of the $45^{o}$ braids loaded at 50% and 60% of failure load). Additionally, most samples did not exhibit a tertiary phase behaviour during the duration of the test.

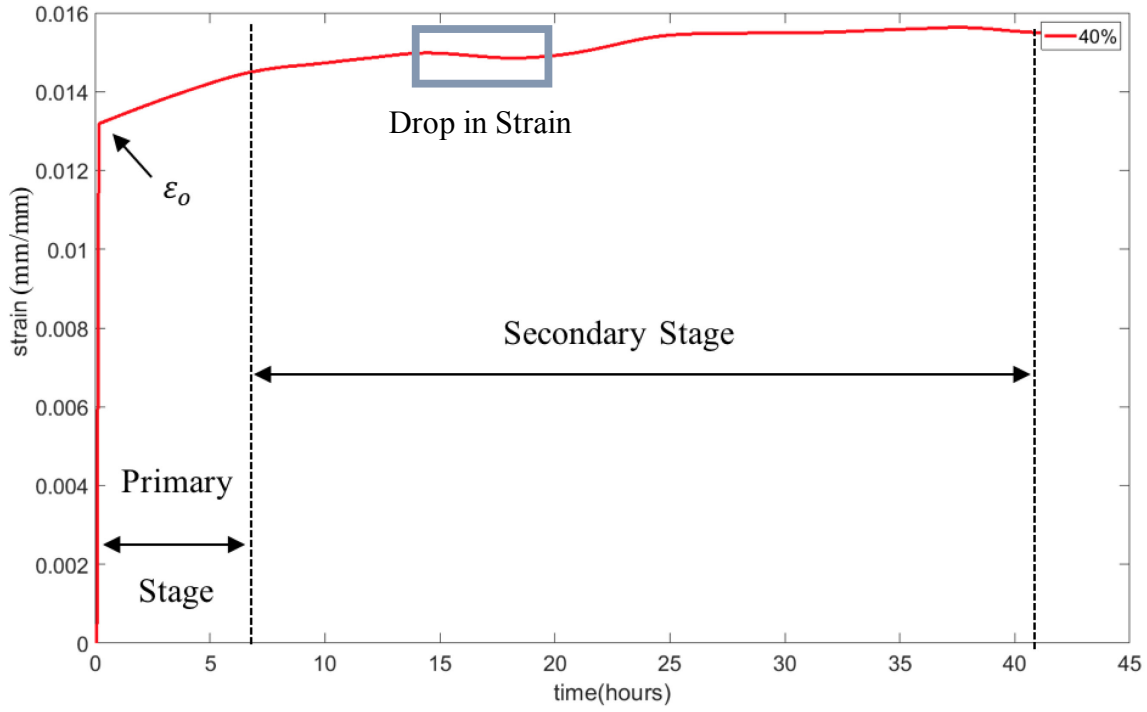


**Figure 4-4: Labelled creep curve showing the primary and secondary stages as well as the initial strain, $\varepsilon_o$, and the region where strain dropped.**

The sudden drop in strain is clearly shown in Figure 4-4 in the region of the graph surrounded by the blue box. This was the region that is illustrated by the sample images presented in Figure 4-2. Table 4-2 shows the strain values for the data points in the boxed region.

**Table 4-2: Time and Strain data points for data points in the boxed region of Figure 4-4**

| Time (hours) | Strain, $\varepsilon$ (mm/mm) | Difference in Strain, $\Delta\varepsilon$ (mm/mm) |
|---|---|---|
| 14.417 | 0.0149835 | -5.774E-08 |
| 14.500 | 0.014983 | -4.966E-07 |
| 14.583 | 0.0149821 | -9.046E-07 |
| 14.667 | 0.01498082 | -1.278E-06 |
| 14.750 | 0.01497921 | -1.616E-06 |
| 14.833 | 0.01497728 | -1.923E-06 |
| 14.917 | 0.01497508 | -2.204E-06 |
| 15.000 | 0.01497262 | -2.461E-06 |
| 15.083 | 0.01496992 | -2.7E-06 |
| 15.167 | 0.014967 | -2.921E-06 |
| 15.250 | 0.01496388 | -3.122E-06 |
| 15.333 | 0.01496057 | -3.301E-06 |
| 15.417 | 0.01495712 | -3.458E-06 |
| 15.500 | 0.01495352 | -3.593E-06 |
| 15.583 | 0.01494981 | -3.708E-06 |
| 15.667 | 0.01494601 | -3.807E-06 |
| 15.750 | 0.01494211 | -3.895E-06 |
| 15.833 | 0.01493814 | -3.974E-06 |
| 15.917 | 0.01493409 | -4.044E-06 |
| 16.000 | 0.01492999 | -4.106E-06 |
| 16.083 | 0.01492583 | -4.158E-06 |
| 16.167 | 0.01492163 | -4.199E-06 |
| 16.250 | 0.01491741 | -4.225E-06 |
| 16.333 | 0.01491317 | -4.237E-06 |
| 16.417 | 0.01490894 | -4.234E-06 |
| 16.500 | 0.01490472 | -4.215E-06 |
| 16.583 | 0.01490054 | -4.179E-06 |
| 16.667 | 0.01489642 | -4.124E-06 |
| 16.750 | 0.01489237 | -4.046E-06 |

The difference in strain column was used to identify the point in the data at which the strain began to decrease. Although the drop is initially quite small (-5.774E-08 mm/mm), it begins to increase. The virtual extensometer works by comparing all images to the first image. This would likely mean that for the images from which the data points in Table 4-2 were calculated seem to have a systematic error that caused the program to produce these unexplainable results. The sudden drop in strain was also seen in other samples tested. Studying the images also showed that the reason was due to the sensitivity of the virtual extensometer to lighting.

To compare the difference samples to each other, the plots for the different samples were produced on a single axis. This is shown in Figure 4-5. This included all three braid angles at the different percentages of failure loads tested. Not all samples tested in this work are included in this plot. Although more samples were tested as presented in the experiment matrix in Table 3-3, not all samples produced useable results. Due to changes in lighting or eccentric behaviour of the samples, the curves produced could not be averaged with the curves presented in Figure 4-5.

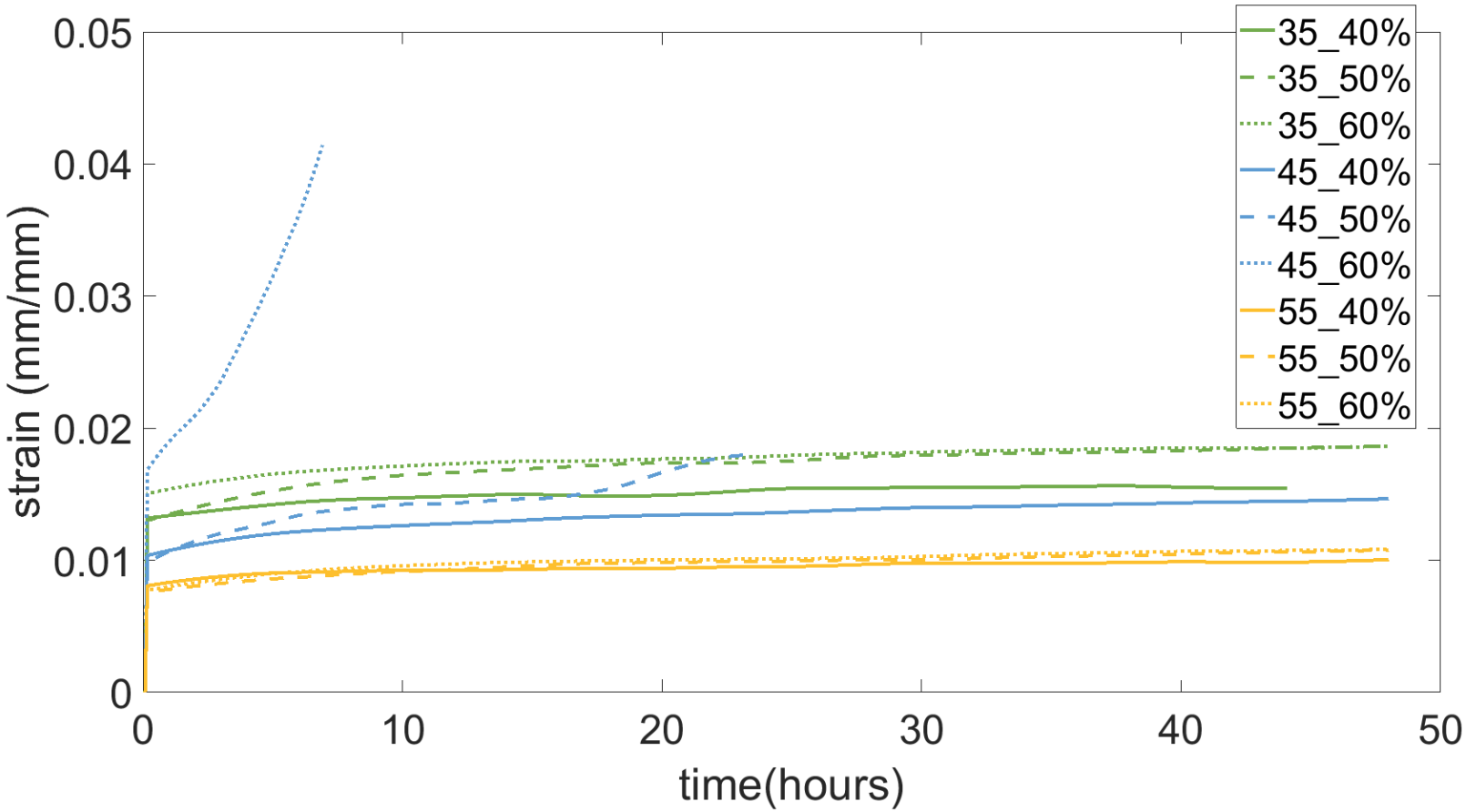


**Figure 4-5: All creep curves obtained for the different tubular braided composites**

From the plots in Figure 4-5, it can be concluded that the tubular braided composites mostly exhibit a typical creep curve behaviour. This is particularly clear for the $35^{o}$ braids and the $55^{o}$ braids. Plots clearly exhibit a primary stage during which the strain rate decreases. Following this, the samples quickly plateau to a steady creep rate as would be expected of a sample loaded to a sustained load. The plots also showed that the behaviour of the composites in creep was dependent on braid angle and percentage load.

## 4.5 Influence of Load on Creep Behaviour of braided composites

As mentioned earlier, three percentages of the failure load were tested for each of the three braid angles. These three percentages were selected to be a representative sample of the influence of the loading percentage. The strain vs time plots obtained for 35°, 45° and 55° braids are presented in Figure 4-6(a), (b) and (c) respectively.

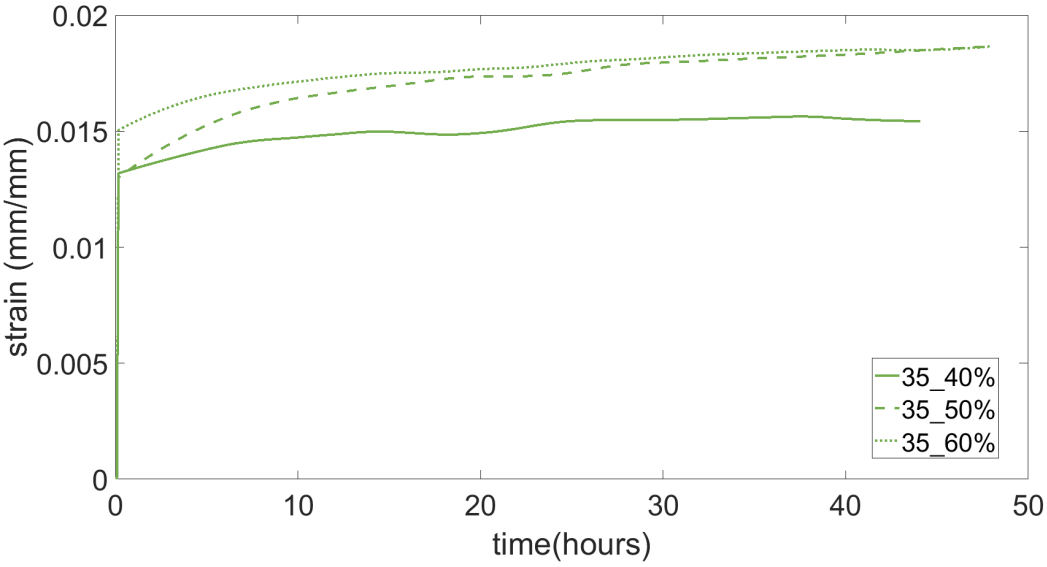
0.02
0.015
0.01
0.005
0
strain (mm/mm)
0
10
20
30
40
50
time(hours)
35_40%
35_50%
35_60%

(a)

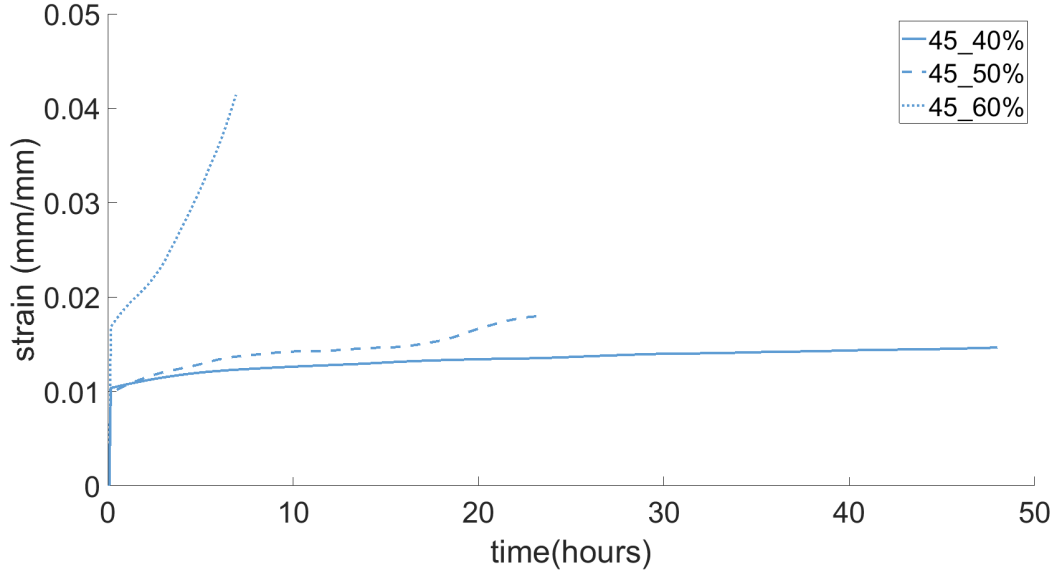
0.05
0.04
0.03
0.02
0.01
0
strain (mm/mm)
0
10
20
30
40
50
time(hours)
45_40%
45_50%
45_60%

(b)

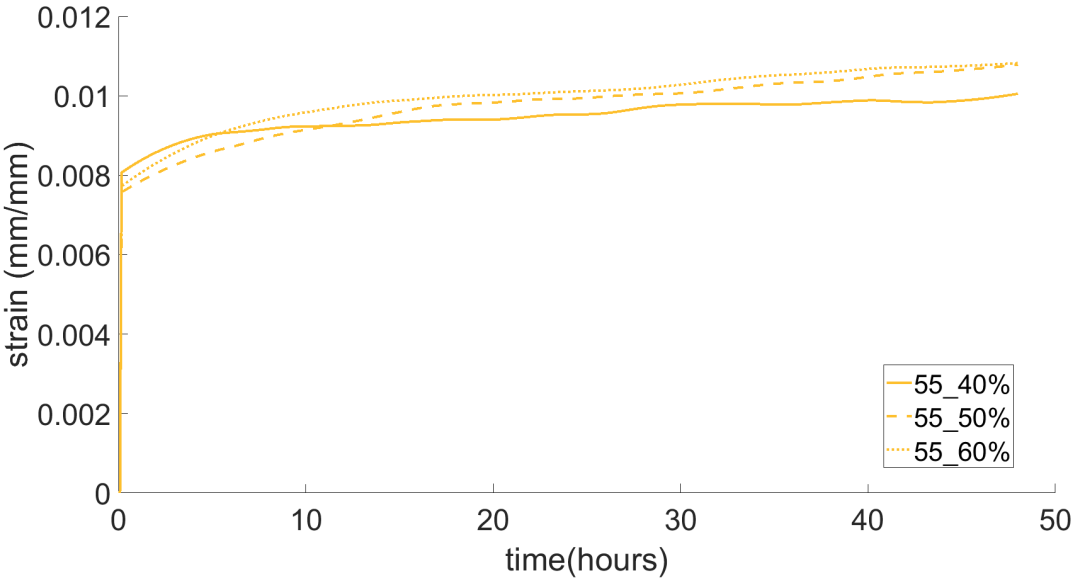


(c)

**Figure 4-6: Creep curves for (a) 35° (b) 45° and (c) 55° braids at different loading percentages**

It is important to analyze the influence of the load percentage on the creep behaviour of the braided composites. As can be seen in the graphs in Figure 4-6, the first observable trend is the increase in the strain range for the creep test as the load percentage is increased. When moving from 40% of the failure load to 50%, the level of strain the tubular braided composites experienced increased. This is to be expected of course, as the applied stress increases, the elongation experienced by the samples also increases, resulting in higher strain. This increase was also seen when load was increased from 50% to 60%. The increases in the strain experienced by the sample are quite clear from the plots for the $35^{o}$ and $55^{o}$ braids. For the $45^{o}$ braids, the behaviour of the braids did not follow the expected trend from the other two braid

angles. The values of the initial strain are presented in Table 4-3 along with the maximum expected initial strain values from previous work [1].

**Table 4-3: Initial strain values for the different samples at different percentages of failure load**

| Angle | Percentage of Failure Load (%) | Initial Strain, $\varepsilon_o$ (mm/mm) | Expected Initial Strain (mm/mm) |
|---|---|---|---|
| 35° | 40 | 0.0132 | 0.0096 |
| | 50 | 0.013 | 0.012 |
| | 60 | 0.015 | 0.0144 |
| 45° | 40 | 0.0104 | 0.007 |
| | 50 | 0.099 | 0.00875 |
| | 60 | 0.0168 | 0.0105 |
| 55° | 40 | 0.0081 | 0.0076 |
| | 50 | 0.0076 | 0.0095 |
| | 60 | 0.0077 | 0.0114 |

Although the plots in Figure 4-6 better show how increasing the load caused an resulted in an increase in the time-dependent strain of the braided samples, the initial strain values were not as clear. For the 35$^o$ braids, the initial strain is higher for the sample loaded to 60% of the failure load than the sample loaded to 40%. However, the 50% is lower than both. The same is noticed for the 45$^o$ braids. For the 55$^o$ braids, no trend is clear at all.

In the 35$^o$ and 55$^o$ braids, the samples reached the secondary stage of the creep curve and almost maintained the value of strain until the test was over. This can be seen from the straight-line segments at the end of the curves in Figure 4-6(a) and (c). For the 45$^o$ braids, the sample loaded to 40% of the failure load was able to maintain strain in the secondary stage of the creep test,

however, when loaded to 50%, the sample reached the secondary stage and after around 17-18 hours of testing, it entered the tertiary stage before fracturing. As for the 60%, the sample almost immediately entered the tertiary stage and fractured. Images for the behaviour of the 45$^{o}$ braids failing during the test are shown in Figure 4-7.

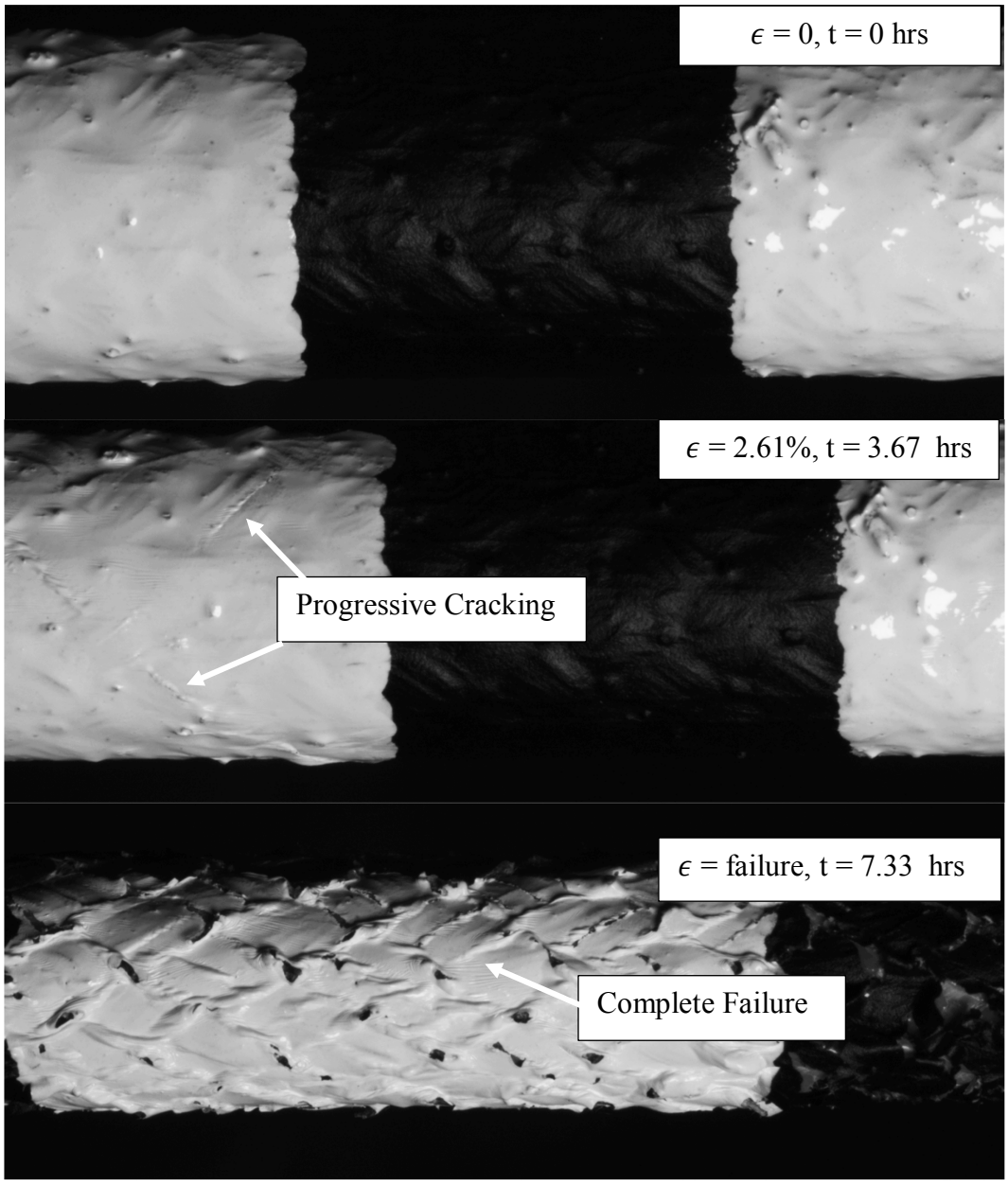


**Figure 4-7: Progressive Failure of 45° braids at 60% of failure load**

Close observation of the 45$^{o}$ braids at failure shows that the details of the failure mechanism. As the tension increased across the cross section, the resin-rich areas began to progressively fail, resulting in a necking-like behaviour of the braid composites. A close up of a failed 45$^{o}$ braid is shown in Figure 4-8 highlighting this failure.

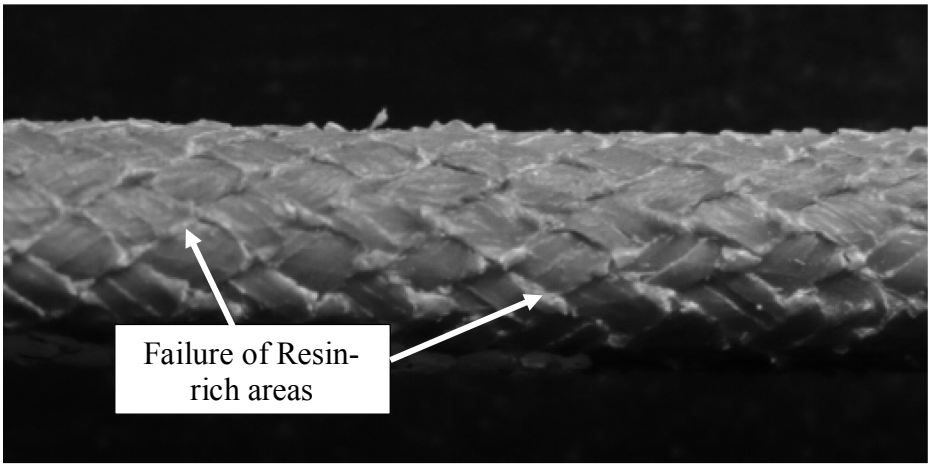


**Figure 4-8: Failure in 45° braids started in the resin-rich areas until the entire sample failed**

Another interesting point to highlight in the presented graphs is how the behaviour of the samples in the secondary stage currently seems to follow different paths that are not uniformly separated. For an isotropic, homogenous material such as steel, the behaviour shown in Figure 4-9 might be expected [2].

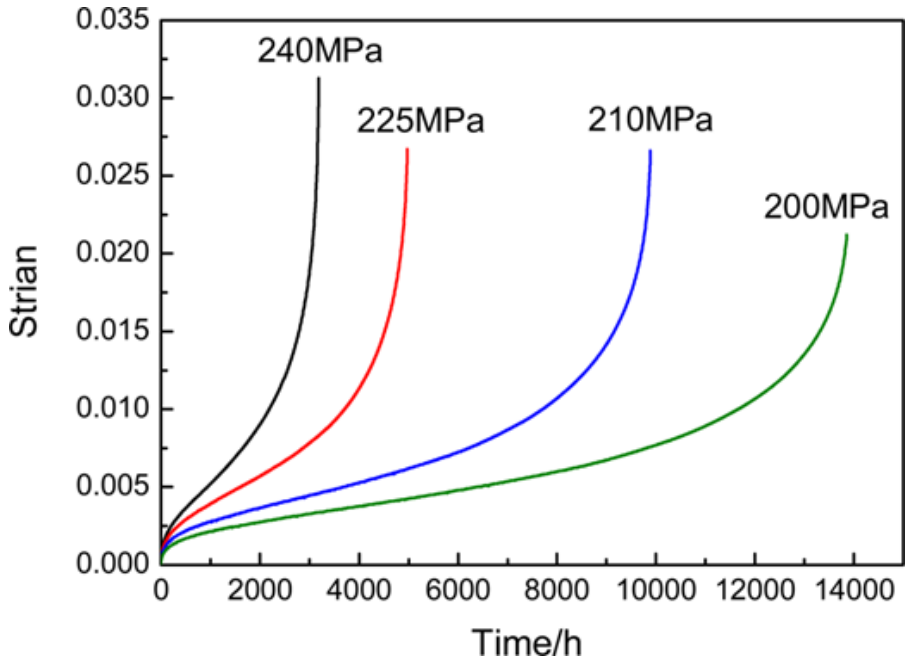


**Figure 4-9: Creep curves showing the influence of increasing stress on the creep curves of steel as adapted from [2]**

Since the initial strain values are more difficult to compare, the half-time strain values, $\varepsilon_{mid}$, were used instead. The half-time strain values were defined as the value of the strain at half the time of the total test (24 hours). If a sample failed before 24 hours has passed, a null value was reported. The half-strain values are plotted in Figure 4-10.

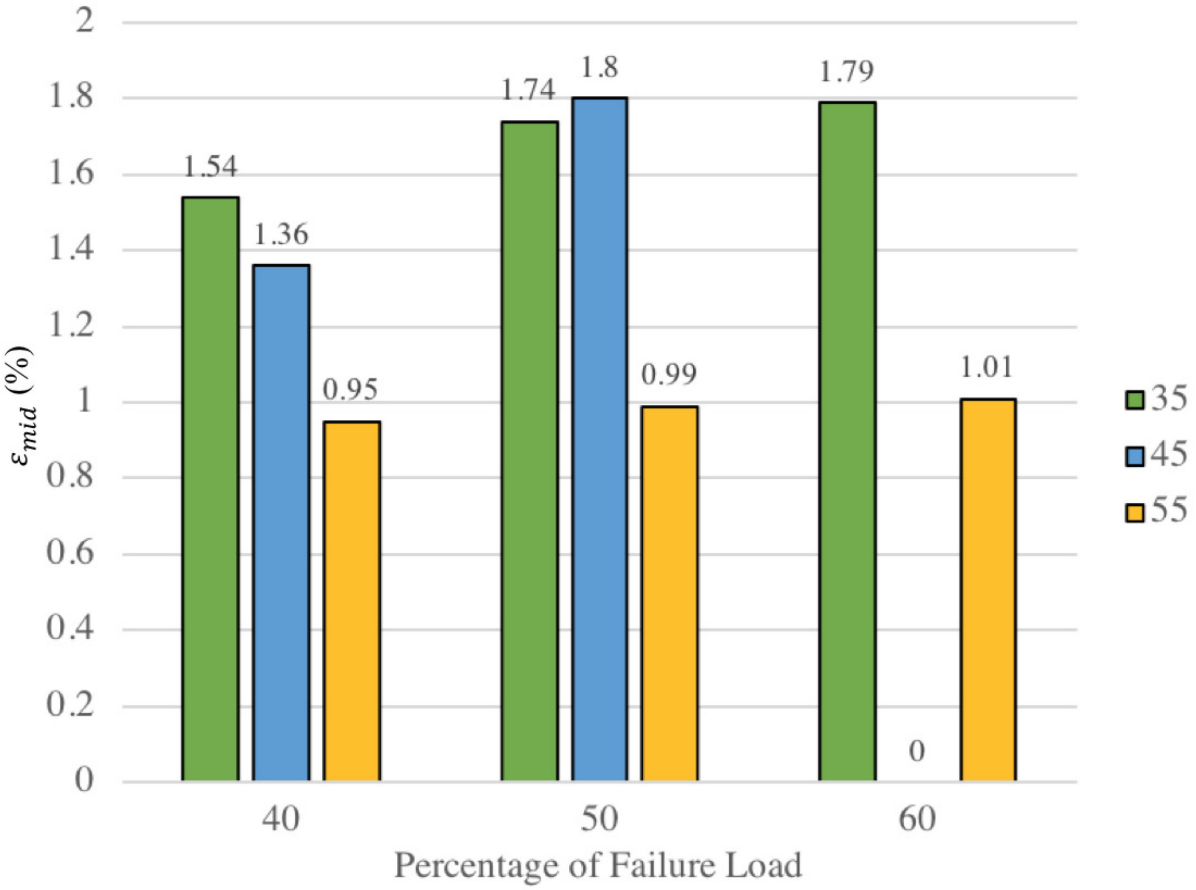


**Figure 4-10: Bar chart showing the different values for the mid-span strain for the different braid angles at different loading percentages.**

From Figure 4-10, it can be seen that for each of the braid angles, there is an upward sloping trend between the different percentages. As the percentage of the failure strain is increased, the strain increases. This conclusion seems to agree with what with expected, although quantifying the changes between the different loading percentages remains difficult. The null value for the $45^{o}$ braid at 60% of the failure load was due to the failure of the sample before reaching the 24 hour mark.

## 4.6 Endurance Limit Results

An important quantity to identify for analyzing the performance of the braids was the endurance limit. This represents the time after which a sample held at a constant load fails suddenly. The strain against the logarithmic of time curve for the 35° braid loaded at 40% of the fracture load is shown in Figure 4-11.

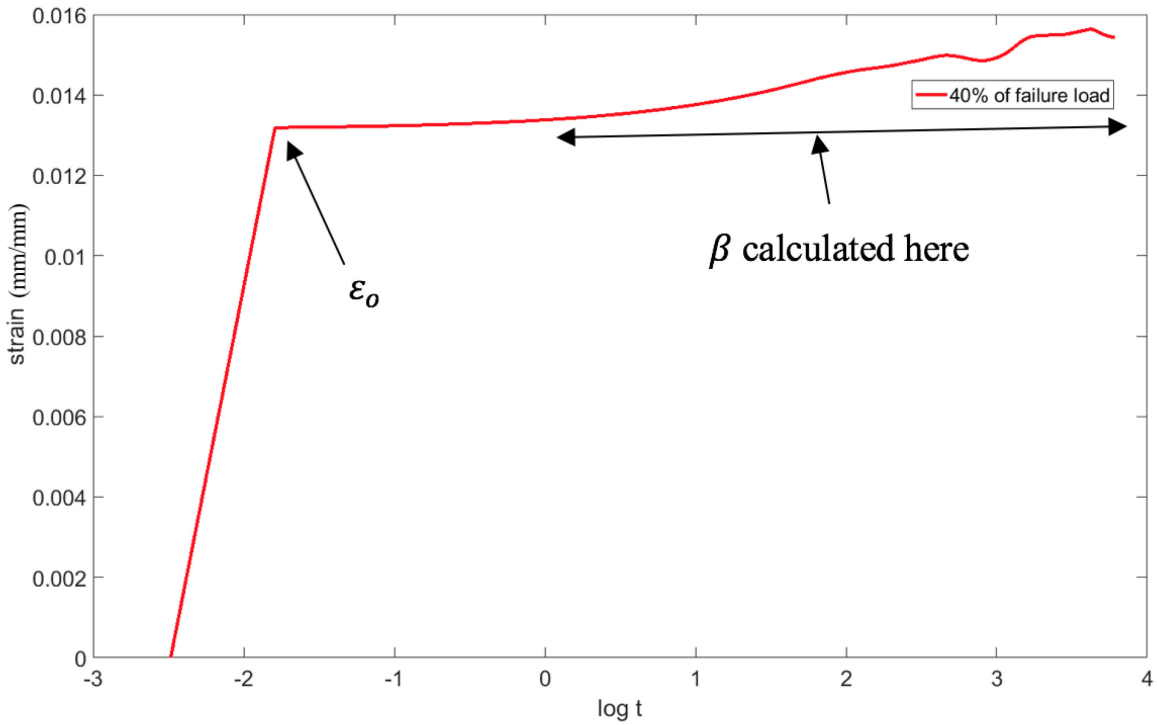


**Figure 4-11: A logarithmic creep curve for the 35° braids loaded at 40% of the fracture load with the region where $\beta$ was to be calculated**

Time values for the first 12 data points resulted in the negative log values on the x-axis of the plot Value of time for the data points collected within the first hour were less than 1 (in hours), resulting in negative values for the logarithmic function. Although ideally the isostress curve for

a creep test should be a straight line, experimental variation resulted in a different shape of the graph. However, there is clearly two stages in the graph after the onset of the initial strain. These represent the primary and secondary stages of creep. The region in which the strain decreased due to lighting can also be seen at the x-value of around 3. For calculations of the creep rate parameter, $\beta$, Table 4-4 shows the values of the logarithmic of time and strain difference used to define the secondary stage for the calculation of $\beta$. As mentioned in Chapter 3, this was defined as the point at which strain difference falls below $10^{-5}$. Following the calculation of the creep rate parameter, the endurance limit was calculated and output in years. The final value of the endurance limit for the 35° braids loaded at 40% of failure load was 15.1897 years.

**Table 4-4: Sample of the logarithm of time and strain values with values at which the secondary stage was defined are bolded**

| Log (t) | Strain (mm/mm) | Strain Difference (mm/mm) |
|---|---|---|
| 1.87180218 | 0.01446039 | 1.10267E-05 |
| 1.8845412 | 0.01447106 | 1.06775E-05 |
| 1.89711998 | 0.01448143 | 1.03689E-05 |
| **1.9095425** | **0.01449153** | **1.00934E-05** |
| **1.9218126** | **0.01450137** | **9.83933E-06** |
| 1.93393396 | 0.01451096 | 9.59617E-06 |
| 1.94591015 | 0.01452032 | 9.35833E-06 |
| 1.95774461 | 0.01452944 | 9.12204E-06 |
| 1.96944065 | 0.01453833 | 8.88364E-06 |

An endurance limit of 15.1897 years represents the time after which an ideal braid at angle 35° would fail if exposed to loads around 40% of the failure load. The calculation of $\beta$ for the sample shown in Figure 4-11 used 447 values of strain and time for the calculation. The results for the endurance limit calculations for the different samples are presented in Figure 4-12.

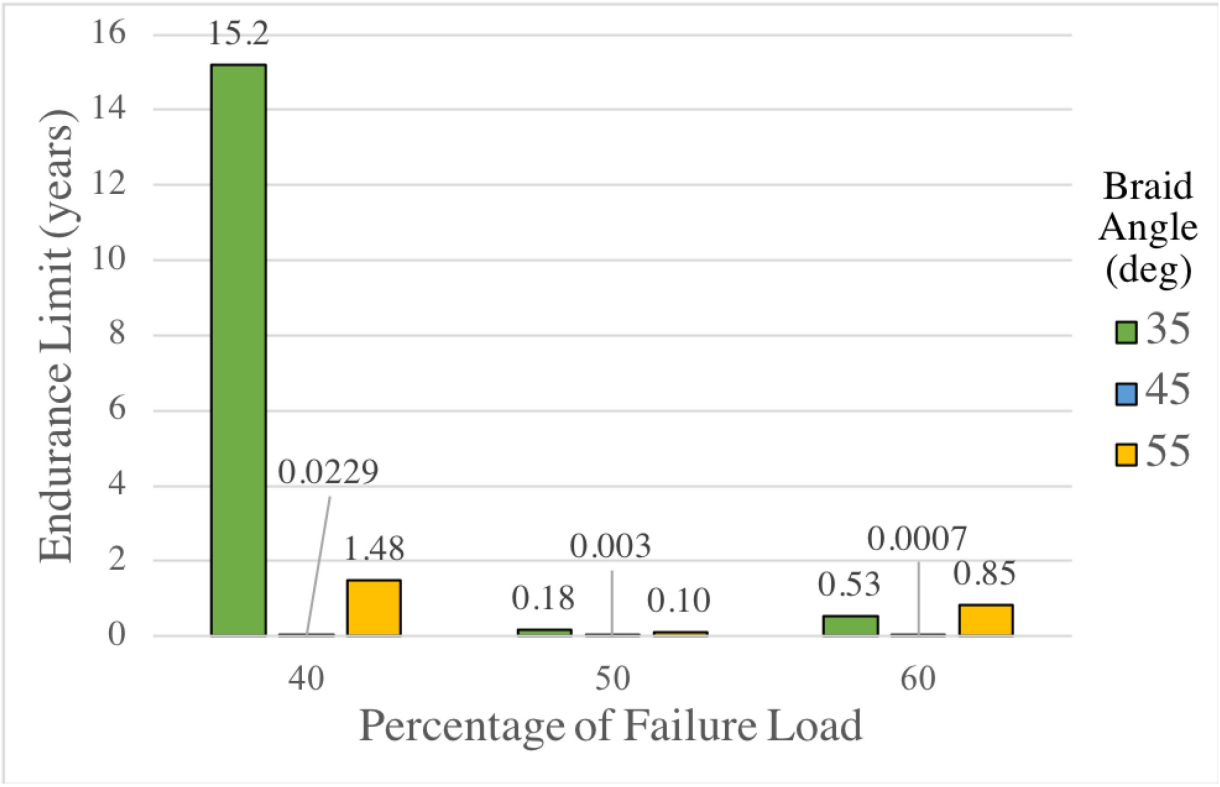


**Figure 4-12: Bar chart showing how the braid angle influences the endurance limit of the tubular braided composites.**

The resulting endurance limit values indicate that the hollow tubular composites in general do not last long when exposed to constant loads for a period of time. Although the 35° braids at 40% of the failure load had an endurance limit of around 15.2 years, the other tested samples did not exceed 1.48 years in the time to failure. The very small values of the 45° braids at 50% and 60%

of the failure load was due to the fact that they failed in the tests performed (within the 2 days allocated for testing).

## 4.7 Discussion

In order to advance the current products in the fiber reinforced polymer composite market, it was important to study Kevlar® composites which have been proposed as a possible alternative to steel in structural design [3]. This section presented the results of creep tests performed on tubular braided composites.

Using the strain data obtained from a virtual extensometer, the braided composites did exhibit a creep behaviour. The plots of the strain against the time had a distinct primary and secondary region with some samples having a tertiary phase as well. Although primary and secondary regions were clearly part of the creep curves for the $35^o$ braids and the $55^o$ braids, the behaviour of the $45^o$ braids was quite different, with samples tested at 50% and 60% of the failure load failing earlier than expected within the allocated time for testing. Other samples which were tested either confirmed these results, or produced results that could not be interpreted due to unexplainable eccentricities in the data.

Samples loaded at different percentages were expected to exhibit different strains, with higher stresses producing higher strains. Although the overall plots did show this, values for the initial strain, $\varepsilon_o$, did not show any apparent trend as presented in Table 4-3. The maximum difference between the expected and the actual initial strain values was 37.5% (for the $45^o$ braids at 60%). It is believed that the main reason was the difference in loading rate between the different tests. ASTM D7337 standards require that a sample being tested under creep be loaded within the first

five minutes of testing and that the load is maintained within ±1% of the failure load. No specifications on loading rate are highlighted in the standard [4]. Accordingly, the performed experimental procedure falls within the standard, but were not consistent because of the limitations of the equipment used for testing. It is important to note that a consistent loading rate can dramatically influence the linear behaviour of tubular braided composites as has been found in previous work by Melenka *et al.* [1].

Although the initial strain values did not seem to show any trends, analyzing the half-time strain, defined as the strain experienced by the sample at half of the time of the overall test showed a trend. Since the values of strain taken in the middle of the experiment were after the onset of the initial strain, these values were more representative of time-dependent creep strain. As shown in Figure 4-10, as the percentage load was increased the mid-strain values increased for all the braid angles. Comparing the $35^o$ degree braids to the $55^o$ braids, it can be seen that the mid-span strain is higher for the $35^o$ than the $55^o$ at 40%, 50% and 60% of the failure load. This is to be expected, as the load on a given sample is increased, the sample will experience more elongation per unit length due to the higher stress on the cross-sectional area.

Although the influence of the load on $\varepsilon_{mid}$ could be seen to follow a trend, this was less clear with the endurance limit. Endurance limit was important to report as it represented the life expectancy of the braids under the percentages of loads that they were exposed to. From the results however, for each of the $35^o$, $45^o$ and $55^o$ braids, finding a trend was very difficult. It is clear from the bar chart in Figure 4-12 though that at 40%, the endurance limit was noticeably higher than at 50% or 60% of the failure load. As the stress increases, the time to failure decreases, although this relationship is not linear. Although the endurance limit for the $35^o$ braids

at 40% of the failure load was above 15 years, the endurance limit was very low for the other samples, with none of the tested samples exceeding 1.5 years. In the scope of the intended application for these braided composites, the results show that using the $35^{o}$ braids to overwrap the core of the FRP composite rebar would result in better creep performance.

To calculate the endurance limit, the slope of the creep curves was averaged for values of strain difference less than $10^{-5}$. As can be seen in Figure 4-6, there are some points after the onset of the secondary stage of creep, where strain values decrease. This was considered a source of influence for the $\beta$ values, however, upon adjusting the graph to remove this drop and linearly interpolate between two values, the value of $\beta$ was found to be identical with no change in the endurance limit calculated for these values. It is important to note that strain calculations resulted in values of $\beta$ in the order of $10^{-4}$, with no changes happening in the final value of the endurance limit.

As presented in Table 4-1, although the $35^{o}$ and $55^{o}$ braids were relatively close to the theoretical braid angles, the $45^{o}$ braids showed the greatest deviation from the theoretical angle. This can only be attributed to errors in manufacturing. In the impregnation steps, yarns can easily shift out of position making the final sample angles after curing less than the theoretical. The manufacturing process was kept as consistent as possible between the different samples within the bounds of human error.

Another important source of errors is in the virtual extensometer software that was used. Strain values for this experimental work was in the range of 0.5-5% strain for all preformed tests (Figure 4-5). The resolution of the virtual extensometer was 0.000001 mm/mm. Despite the very high resolution, small changes in the lighting affected the results of the plotted creep curves. This

has not been documented in the work by Aldrich *et al.* Although the range of values for the creep tests were correct, the accuracy of using the virtual extensometer to measure creep strain could be considered a source of errors. The virtual extensometer, however, provided a simple non-contact method for directly measuring strain in the samples. Stereo Digital Image Correlation would be better for studying strain fields and out-of-plane strain. For this first study into creep behaviour of composites, using the virtual extensometer software was sufficient.

This work also attempted to identify how the braid angle influences the creep behaviour of the tubular braided composites. Braid angle is defined as the angle between the yarns of the braid and the longitudinal axis of the braid. A lower braid angle means that the braid is more aligned with the longitudinal axis. In axial tensile testing, a lower braid angle results in higher performance, in terms of lower strain to failure and in higher stiffness. At the lower braid angles, fibers contribute more to the overall behaviour of the composite. The fibers are more aligned with the axis of loading, allowing the fibers to dominate the braided composite's behaviour. Conversely, at higher braid angles, the fibers are aligned relatively transverse to the direction of loading. This results in a lower contribution of the fibers, and a higher contribution of the epoxy resin to the composites behaviour. The epoxy is significantly weaker than the fibers, which results in lower mechanical performance. This explanation of the behaviour of the composites matches the values of strains presented in Figure 4-5. Strain levels for the $35^{o}$ braids are higher than the $45^{o}$ and $55^{o}$ braids. Micromechanics of composites could also offer an explanation for the odd behaviour of the $45^{o}$ braids. $35^{o}$ braids show more influence of the fiber to the composite's behaviour and $55^{o}$ braids show more influence of the matrix phase to the composite's behaviour. At the angle in between them, the behaviour of the composite is

unpredictable. Neither phase can contribute more to the behaviour due to the geometry of the architecture. This could explain why at 50% and 60% of the failure load, the 45$^{o}$ braids tested failed. Such conclusions have been confirmed in previous work [1]. The creep results of the influence of braid angle indicate that in a structural application, where reinforcement is used to support the concrete in tension, a lower braid angle should be used in braided FRP composite rebars and 45$^{o}$ braids should be avoided.

Characterization of behaviour in testing for composite materials is known to be very difficult. Although the Kevlar® fibers have been studied in creep and shown to behave as expected for different loads applied, very few creep tests have been performed on the epoxy resin used in this work. Previous work by Ericksen showed that creep for 4617 epoxy was linear for several decades, but at larger stresses, the behaviour deviated from the logarithmic behaviour at shorter times. This work suggests that studying the creep of the epoxy used in this work could provide insight to the behaviour of the composites [5]. The majority of studies on the epoxy used in this work performed dynamic tests on the epoxy rather than sustained load tests.

From this work, an important step is made in studying the behaviour of braided Kevlar® composites in creep. For tension-bearing applications such as concrete reinforcement, braided composites at lower braid angles are recommended. At lower braid angles and lower percentage loads, the braided composites are less likely to fail earlier than the projected life of the composite.

## 4.8 References


[1] Garrett William Melenka and Jason P. Carey, "Experimental analysis of diamond and regular tubular braided composites using three-dimensional digital image correlation," *J. Compos. Mater.*, vol. 0, no. 0, pp. 1–21, 2017.

[2] J. Guo, F. Li, X. Zheng, H. Shi, and W. Meng, "An Accelerated Method for Creep Prediction From Short Term Stress Relaxation Tests," *Press. Vessel Technol*, vol. 138, no. 3, Feb. 2016.

[3] Marcus Ivey, "Towards the Development of Pseudoductile FRP Rebar," University of Alberta, 2015.

[4] ASTM, "Standard Test Method for Tensile Creep Rupture of Fiber Reinforced Polymer Matrix Composite Bars - D7337."

[5] R. H. Ericksen, "Room temperature creep of Kevlar® 49/epoxy composites," *Composites*, no. July 1976, pp. 189–194, 1976.

# CHAPTER 5 CONCLUSIONS, LIMITATIONS AND FUTURE WORK

## 5.1 Conclusions

Steel has traditionally been used to reinforce concrete structures. Fiber Reinforced Polymer (FRP) composites have been proposed as an alternative to steel in reinforced concrete [1]. Although glass fiber composite rebars are more commercially available, a new hybrid Kevlar® braided FRP composite rebar has been proposed as a promising alternative to steel [2]. Corrosion of steel in harsh environments severely affects the ability of steel to reinforce concrete. The proposed hybrid Kevlar® braided FRP composite rebar does not suffer from such severe corrosion and offers a strong competition with high specific strength and specific modulus [2]. To meet industry standard, the composite rebars must meet certain durability requirements, including creep strength. With no literature on the creep behaviour of Kevlar® braided composites in the literature, the objective of this research was to study the creep behaviour of Kevlar®-Epoxy tubular braided composites. This is an essential step in advancing the available market for FRP composite rebars.

To manufacture the Kevlar® reinforced tubular braided composites, the process used by Melenka *et al.* was followed [3]. Braided composites at three different braid angles ($35^o$, $45^o$ and $55^o$) were manufactured and tested at three different percentages of their fracture loads (40%, 50% and 60%). An experimental setup was devised to apply the creep loads according to ASTM standards [4]. To measure the strain, images were taken during the tests every five minutes. A virtual extensometer software developed by Aldrich *et al.* [5] calculated the strain from the

images by fitting an error function to the images and calculating how the samples deformed with respect to an initial unloaded sample image. The strain data was used to plot creep curves for the different samples at the different loading percentages.

The results showed the two-dimensional tubular braided composites showed a general creep behaviour; this had not been shown before in literature. All samples tested at 40% of the failure load showed this typical creep behaviour. The tubular braided composites would undergo a primary stage of strain stabilization and a secondary stage where the creep rate remained constant. The $45^{o}$ braids tested at 50% of the failure load exhibited a primary, secondary and tertiary stage before failure. As the percentage of failure load was increased, the strain levels experienced by the samples would increase. Unexpectedly, initial strain values showed no clear trend when studied. The strain at half the experimentation time, however, showed this increasing trend in strain when the loading percentage was increased. The relationship between load increments and increase in mid-span strain was not linear.

An important variable that was calculated from the data was the endurance limit, defined as the time after which a material held at sustained loads fails suddenly. $35^{o}$ braids were shown to have a higher endurance limit than the $45^{o}$ and $55^{o}$ braids. In each of the braid angles, samples tested at 40% of the failure load had a higher endurance limit than the samples tested at 50% and 60%. For the $45^{o}$ braids however, samples tested at 50% and 60% of the failure load failed prematurely after 23.8 hours and 7.3 hours respectively. Although the $35^{o}$ braids could sustain loads for over 15 years at 40% of the failure load, the other tested braids had a maximum endurance limit of around 1.5 years.

The influence of braid angle on the creep behaviour was also investigated in this work. The higher strain in the $35^o$ compared to the other braid angles can be explained by the nature of the tubular braided composites. At lower angles, fibers are aligned closer to the longitudinal axis. This allows for the fibers to have a more pronounced effect in the overall mechanical behaviour of the composite. For the higher angles, the influence of the fibers in the longitudinal direction becomes much less and consequently the resin assumes a bigger part in the overall mechanical performance of the composite. Compared to a braid angle of $55^o$, at $35^o$ the orientation of the fibers allows for higher strains to be achieved by the tubular braided composites. The results from the creep tests confirmed this.

Definitive trends in the strain and endurance limit values was difficult to see, however. An important conclusion that was made from this work is related to the performance of these braided composites in structural applications. In tension-bearing applications, the results of this work suggest that hybrid FRP braided composites should use braided overwraps at lower braid angles. Braided composites of these types would ultimately be more durable.

## 5.2 Limitations

There were a few limitations to the research done in this work. The manufacturing process proposed could have been more efficient. Using a batch production method to speed up manufacturing would help significantly and improving quality control on the current setup is likely to produce more accurate samples. The braided composite samples were not exactly at the theoretical braid angles tested in this work. Given the current method of hand impregnation of

the composites, this provides an explanation for the differences between manufacturing parameters and the final dimensions of the samples.

Another limitation in this work was related to the sole use of Kevlar® as the fiber material for the composites. Although no creep data is available in literature for Kevlar® braided composites, if these composites are to be considered in structural applications, it is important to note that using other fibers needs to be studied as well. This includes carbon and glass.

The limitations in testing for the creep behaviour included the inability to maintain a consistent loading rate between the different samples tested. Although this study conformed to the ASTM standards, differences in the loading rate affected the initial strain values. This also affected the results of the overall creep behaviour of the braided composites.

The limited sample size is another limitation of this work. Establishing clear trends with the samples used is very difficult. Pilot testing for the different samples took more time than anticipated and finalizing the experimental setup for the virtual extensometer took a number of trials with different samples. However, the displayed creep behaviour of the two-dimensional braided composites showed that further testing was unnecessary for this work. With no previous research done to study the creep behaviour of these composites, this was an important first step to understanding the general creep behaviour of these braided composites.

The virtual extensometer used to measure the strain in the data provided a good framework for this research in terms of characterizing the general behaviour of Kevlar® braided composites when exposed to constant loads for extended periods of time. The sensitivity of the method to lighting was problematic, however, and found to cause strain data to give illogical conclusions to

the behaviour of the composite. Correcting for this was found to have no influence on the endurance limit results.

## 5.3 Future Work

From the work undertaken, there are a number of avenues of future work and improvements. Looking, forward, using a more advanced technique such as Digital Image Correlation (DIC) would be excellent to study the strain fields created in the sample over the duration of the test. By studying these strain fields, a better understanding of the behaviour of the braided composites will be obtained. The development of strain in the sample over the duration of the test would provide valuable information for analyzing the behaviour of Kevlar® braided composites. This analysis could also be further extended to model the generic behaviour of Kevlar® braided composites when exposed to loads for extended periods of time.

The lack of research in studying the durability of two-dimensional braided Kevlar® composites offers a number of avenues for future work. The creep tests performed in this research only studied the behaviour of the braided composites at room temperature. In structural applications, the braids are likely to be exposed to harsher environments. Studying the creep behaviour of the braids at high and low temperatures and in moist environments would provide valuable information for using the hybrid FRP composites as reinforcement for concrete. An argument for the use of Kevlar® braided composites in structural applications can be made stronger if the different environmental conditions (temperature and pH) are varied in creep tests performed.

Kevlar® is known to be weakened by UV radiation and moisture. In structural application, the braided composites are very likely to be exposed to UV radiation and moisture, making these tests essential for supporting an argument for using FRP composite rebars in structural applications. Using lower braid angles (than the $35^{o}$ braids used in this work) to study the improvements in the endurance limit as well as using different epoxies with the Kevlar® fibers would give a more insight to the recommended geometry of braided composites if used in in FRP composite rebars.

Creep studies have also looked into the creep behaviour of the fibers and the epoxies individually. By doing this, inferences could be made on the overall behaviour of the composites. Performing similar creep tests on the Kevlar® fibers used and the epoxy used in these composites could be an important step in studying creep behaviour of braided composites.

Finally, no literature is known to be available on the creep failure mechanisms. Understanding how the braided composite fails when exposed to constant loads for long periods of time would be a crucial step in preventive mechanisms that could be applied to lengthen the functional life of the braided composites if used to reinforce concrete in hybrid FRP composite rebars.

## 5.4 References:


[1] ISIS Canada, "ISIS Educational Module 3: An Introduction to FRP-Reinforced Concrete," 2006.

[2] Marcus Ivey, "Towards the Development of Pseudoductile FRP Rebar," University of Alberta, 2015.

[3] Garrett William Melenka, "Analytical and Experimental Analysis of Tubular Braided Composites," University of Alberta, 2016.

[4] ASTM, "Standard Test Method for Tensile Creep Rupture of Fiber Reinforced Polymer Matrix Composite Bars - D7337."

[5] D. Aldrich, C. Ayranci, and D.S. Nobes, "OSM-Classic : An optical imaging technique for accurately determining strain," *SoftwareX*, no. 6, pp. 225–230.

# BIBLIOGRAPHY


N. Subramanian, "Introduction to Reinforced Concrete," in *Design of Concrete Reinforced Structures*, Oxford University Press, 2013, pp. 1–44.

D. D. L. Chung and X. Fu, "Effects of Corrosion on the Bond Between Concrete and Steel Rebar," *Cem. Concr. Res.*, vol. 27, no. 12, pp. 1811–1815, 1997.

B Vidya, D Manasa, and C Prasad, "Corrosion of steel in concrete with and without silica fume," *IUP J. Struct. Eng.*, pp. 16–25.

ISIS Canada, "ISIS Educational Module 2: An Introduction to FRP Composites for Construction," 2006.

ISIS Canada, "ISIS Educational Module 3: An Introduction to FRP-Reinforced Concrete," 2006.

Marcus Ivey, "Towards the Development of Pseudoductile FRP Rebar," University of Alberta, 2015.

ISIS Canada, "ISIS Educational Module 6: Application and Handling of FRP Reinforcements for Concrete," 2006.

ISIS Canada, "ISIS Educational Module 8: Durability of FRP Composites for Construction," 2006.

International Federation for Structural Concrete, "FRP Reinforcement in RC structures."

Garrett William Melenka and Jason P. Carey, "Experimental analysis of diamond and regular tubular braided composites using three-dimensional digital image correlation," *J. Compos. Mater.*, vol. 0, no. 0, pp. 1–21, 2017.

ACI Education Bulletin, "Reinforcement for Concrete— Materials and Applications."

P. Kumar Mehta and Paulo J.M. Monteiro, *Concrete Microstructure, Properties and Materials*, 4th ed. McGraw-Hill Education, 2001.

"Adaptive Components | Håvard Vasshaug." .

X. Gu, "Mechanical Properties of Concrete and Steel Reinforcement," in *Basic Principles of Concrete Structures,* Springer, 2016, pp. 21–58.

N. Subramanian, "Flexural Analysis and Design of Beams," in *Design of Concrete Reinforced Structures*, Oxford University Press, 2013, pp. 142–213.

T.J. MacGinley and B.S. Choo, Reinforced Concrete Design Theory and Examples, 2nd ed. .

P. Koutsoukos, D. Michalopoulos, and C. A. Apostolopoulos, "The Corrosion Effects on the Structural Integrity of Reinforcing Steel," *J. Mater. Eng. Perofrmance*, vol. 17, no. 4, pp. 506–516, 2008.

F. C. Campell, "Introduction to Composite Materials," in *Structural Composite Materials*, ASM International, 2010.

ISIS Canada, "An Introduction to FRP Composites for Construction."

ACI Committee 440, “Guide for the Design and Construction of Structural Concrete Reinforced with FRP Bars,” 2006.

V-ROD, “V-ROD HM.” .

TUFBAR, “TUFBAR Fiberglass Rebar (40 GPA).” .

Chris Burgoyne and Ioannis Balafas, “Why is FRP not a financial success?”

Frank Ko, “Braiding,” *ASM Handb.*, vol. 21, pp. 69–77.

Jason P. Carey, Handbook of Advances in Braided Composite Materials - Theory, Production, Testing and Applications. .

Frank K. Ko, Win Soomboonsong, and Harry G. Harris, “New Ductile Hybrid FRP Reinforcing Bar for Concrete Structures,” *J. Compos. Constr.*, pp. 28–37, 1998.

A. Nanni, C. Bakis, J. Terosky, and S. Koehler, “Self-monitoring, pseudo-ductile, hybrid FRP reinforcement rods for concrete applications,” *Compos. Sci. Technol.*, vol. 61, pp. 815–823, 2001.

Frank Ko, Andrew Head, and Christopher Pastore, *Handbook of Industrial Braiding*. Atkins and Pearce.

Jason Carey and Cagri Ayranci, “2D braided composites: A review for stiffness critical applications,” *Compos. Struct.*, vol. 85, pp. 43–58, 2008.

S. Pheonix, “Mechanical Response of a Tubular Braided Cable with an Elastic Core,” *Text. Res. J.*, vol. 48, no. 2, 1978.

L. Smith and S. Swanson, “Selection of Carbon Fiber 2D Braid Preform Parameters for Biaxial Loading,” *Compos. Des. Manuf. Cost Eff.*, vol. 48, pp. 33–44, 1994.

Garrett William Melenka, “Analytical and Experimental Analysis of Tubular Braided Composites,” University of Alberta, 2016.

M.S. Ahmadi, M.S. Johari, M. Sadighi, and M. Esfandeh, “An experimental study on mechanical properties of GFRP braid-pultruded composite rods,” *EXPRESS Polym. Lett.*, vol. 3, no. 9, pp. 560–568, 2009.

R. Fangueiro, G. Sousa, F. Soutinho, S. Jalali, and M. de Araujo, “Application of Braided Fibre Reinforced Composite Rods in Concrete Reinforcement,” *Mater. Sci. Forum*, vol. 514–516, pp. 1556–1560, 2006.

Young-Hwan Park, Young-Jun You, Jang-Ho Jay Kim, and Sung-Jae Kim, “Methods to enhance the guaranteed tensile strength of GFRP rebar to 900 MPa with general fiber volume fraction,” *Constr. Build. Mater.*, vol. 75, pp. 54–62, 2015.

Antonio Naani, Marcus Henneke, and Tadashi Okamoto, “Tensile properties of hybrid rods for concrete reinforcement,” *Constr. Build. Mater.*, vol. 8, no. 1, pp. 27–34, 1994.

Francesca Ceroni, Edoardo Cosenza, Manfredi Gaetano, and Marisa Pecce, “Durability issues of FRP rebars in reinforced concrete members,” *Cem. Concr. Compos.*, vol. 28, pp. 857–868, 2006.

Amnon Katz, "Bond to Concrete of FRP Rebars After Cyclic Loading," *J. Compos. Constr.*, vol. 4, no. 3, pp. 137–144, Aug. 2000.

Francesco Micelli and Antonio Naani, "Durability of FRP rods for concrete structures," *Durab. FRP Rods Concr. Struct.*, vol. 18, pp. 491–503, 2004.

M. Porter and B. Barnes, "Accelerated durability of FRP reinforcement for concrete structures," *Proc. 1st Int. Conf. Durab. Fiber Reinf. Polym. FRP Compos. Constr.*, vol. 98, pp. 191–202, 1998.

Gilbert Nkurunziza, Ahmed Debaiky, Patrice Cousin, and Brahim Benmokrane, "Durability of GFRP bars: A critical review of the literature," *Prog Struct Engng Mater*, vol. 7, pp. 194–209, 2005.

Rajan Sen, Gray Mullins, and Tom Salem, "Durability of E-glass/Vinylester Reinforcement in Alkaline Solutions," *ACI Struct. Jounal*, pp. 369–375, 2002.

Mina Dawood and Sami Rizkalla, "Environmental durability of a CFRP system for strengthening steel structures," *Constr. Build. Mater.*, vol. 24, no. 9, pp. 1682–1689, 2010.

Baolin Wan, Michael Petrou, and Kent Harries, "The Effect of the Presence of Water on the Durability of Bond between CFRP and Concrete," *J. Reinf. Plast. Compos.*, vol. 25, no. 8, pp. 875–890.

Mohamed A. Aboelseoud and John J. Myers, "Durability of Hybrid Composite Beam Bridges Subjected to Various Environmental Conditioning," *J. Compos. Constr.*, vol. 20, no. 6, 2016.

Shenghu Cao, Xin Wang, and Zhis WU, "Tensile Properties of CFRP and Hybrid FRP Composites at Elevated Temperatures," *J. Compos. Mater.*, vol. 43, no. 4, 2009.

Jitendra Tate, Ajit Kelkar, and John Whitcomb, "Effect of braid angle on fatigue performance of biaxial braided composites," *Int. J. Fatigue*, vol. 28, no. 10, pp. 1239–1247, 2006.

Jitendra Tate and Ajit Kelkar, "Stiffness degrafation model for biaxial braided composites under fatigue loading," *Compos. Part B Eng.*, vol. 39, no. 3, pp. 548–555, 2008.

John Montesano, Zouheir Fawaz, and Habiba Bougherara, "Use of infrared thermography to investigate the fatigue behavior of a carbon fiber reinforced polymer composite," *Compos. Struct.*, vol. 97, pp. 76–83, 2013.

International Federation for Structural Concrete, "FRP Reinforcement in RC structures."

Pericles Theocaris, "Viscoelastic Properties of Epoxy Resins Derived from Creep and Relaxation Tests at Different Temperatures," *Rhelogica Acta*, vol. 2, no. 2, pp. 92–96, 1962.

D. Katz, Y. Smooha, and A. I. Isayev, "Dynamic Properties of an unfilled and filled epoxy resin subjected to extensional creep," *J. Mater. Sci.*, vol. 15, no. 1980, pp. 1167–1174, 1980.

P. L. Walton and A. J. Majumdar, "Creep of Kevlar® 49 fibre and a Kevlar® 49-cement composite," *J. Mater. Sci.*, vol. 18, no. 1983, pp. 2939–2946, 1983.

R. H. Ericksen, "Room temperature creep of Kevlar® 49/epoxy composites," *Composites*, no. July 1976, pp. 189–194, 1976.

Morgan P. Hanson, “Effect of Temperature on Tensile and Creep Characteristics of PRD49 Fiber/Epoxy Composites,” NASA, Washington, D. C., 1972.

W. K. Goertzen and M. R. Kessler, “Creep Behaviour of carbon fiber/epoxy matrix composites,” *Mater. Sci. Eng.*, vol. A 421, no. 2006, pp. 217–225, 2006.

Xin Jing, Xiaoguang Yang, Duoqi Shi, and Hongwei Niu, “Tensile creep behavior of three-dimensional four-step braided SiC/SiC composite at elevated temperature,” *Ceram. Int.*, vol. 43, no. 9, pp. 6721–6729, 2017.

T. Yamaguichi, Y. Kato, T. Nishimura, and I. Uomoto, “Creep Rupture of FRP rods made of Aramid, Glass and Carbon Fibers.” Proceedings on the Third International Symposium on Non-metallic (FRP) Reinforcement for Concrete Structures, 1997.

CSA, “Canadian Highway Bridge Design Code,” 11th Edition, Jan. 2014.

Hexion Inc., “Technical Data Sheet (Epon Resin 826).” 2005.

“Epoxy Resin System for Pultrusion or Filament Winding.” Hexion, Jul-2007.

ASTM, “Standard Test Method for Tensile Creep Rupture of Fiber Reinforced Polymer Matrix Composite Bars - D7337.”

D. Aldrich, C. Ayranci, and D.S. Nobes, “OSM-Classic : An optical imaging technique for accurately determining strain,” *SoftwareX*, no. 6, pp. 225–230.

J. Guo, F. Li, X. Zheng, H. Shi, and W. Meng, “An Accelerated Method for Creep Prediction From Short Term Stress Relaxation Tests,” *Press. Vessel Technol*, vol. 138, no. 3, Feb. 2016.

# APPENDIX A: MATLAB® SCRIPTS

## A.1 Data Collection and Plotting Script

```
%open the data files for the collected strain data from the virtual
extensometer%

fidi = fopen('Strain.dat');
a    =    textscan(fidi,    '%f%f',    'HeaderLines',2,    'Delimiter','\n',
'CollectOutput',1);
fclose(fidi);
fidi = fopen('Strain2.dat');
b    =    textscan(fidi,    '%f%f',    'HeaderLines',2,    'Delimiter','\n',
'CollectOutput',1);
fclose(fidi);
fidi = fopen('Strain3.dat');
c    =    textscan(fidi,    '%f%f',    'HeaderLines',2,    'Delimiter','\n',
'CollectOutput',1);
fclose(fidi);
fidi = fopen('Strain4.dat');
d    =    textscan(fidi,    '%f%f',    'HeaderLines',2,    'Delimiter','\n',
'CollectOutput',1);
fclose(fidi);
fidi = fopen('Strain5.dat');
e    =    textscan(fidi,    '%f%f',    'HeaderLines',2,    'Delimiter','\n',
'CollectOutput',1);
fclose(fidi);
fidi = fopen('Strain6.dat');
f    =    textscan(fidi,    '%f%f',    'HeaderLines',2,    'Delimiter','\n',
'CollectOutput',1);
fclose(fidi);
fidi = fopen('Strain7.dat');
g    =    textscan(fidi,    '%f%f',    'HeaderLines',2,    'Delimiter','\n',
'CollectOutput',1);
fclose(fidi);
fidi = fopen('Strain8.dat');
h    =    textscan(fidi,    '%f%f',    'HeaderLines',2,    'Delimiter','\n',
'CollectOutput',1);
fclose(fidi);
fidi = fopen('Strain9.dat');
i    =    textscan(fidi,    '%f%f',    'HeaderLines',2,    'Delimiter','\n',
'CollectOutput',1);
fclose(fidi);

%convert the strain data collected from a cell structure to a matrix%

straindata1 = cell2mat(a);
straindata2 = cell2mat(b);
```

```
straindata3 = cell2mat(c);
straindata4 = cell2mat(d);
straindata5 = cell2mat(e);
straindata6 = cell2mat(f);
straindata7 = cell2mat(g);
straindata8 = cell2mat(h);
straindata9 = cell2mat(i);



%use the first column of the matrix to determine image numbers%

x1 = straindata1(:,1);
x2 = straindata2(:,1);
x3 = straindata3(:,1);
x4 = straindata4(:,1);
x5 = straindata5(1:282,1);
x6 = straindata6(1:83,1);
x7 = straindata7(:,1);
x8 = straindata8(:,1);
x9 = straindata9(1:576,1);

%convert image number to time values and calculate the logarithmic values for
the time values*

x1_hours = 5.*x1/60;
x1_logarithm = log(x1_hours);
x1_hours_plot = [2:529];
x2_hours = 5.*x2/60;
x2_logarithm = log(x2_hours);
x2_hours_plot = [2:576];
x3_hours = 5.*x3/60;
x3_logarithm = log(x3_hours);
x3_hours_plot = [2:576];
x4_hours = 5.*x4/60;
x4_logarithm = log(x4_hours);
x4_hours_plot = [2:576];
x5_hours = 5.*x5/60;
x5_logarithm = log(x5_hours);
x5_hours_plot = [2:282];
x6_hours = 5.*x6/60;
x6_logarithm = log(x6_hours);
x6_hours_plot = [2:83];
x7_hours = 5.*x7/60;
x7_logarithm = log(x7_hours);
x7_hours_plot = [2:576];
x8_hours = 5.*x8/60;
x8_logarithm = log(x8_hours);
x8_hours_plot = [2:576];
x9_hours = 5.*x9/60;
x9_logarithm = log(x9_hours);
x9_hours_plot = [2:576];
```

```
%use the second column of the matrix initially obtained for the strain values
for the different tests%

y1 = straindata1(2:529,2);
y2 = straindata2(2:576,2);
y3 = straindata3(2:576,2);
y4 = straindata4(2:576,2);
y5 = straindata5(2:282,2);
y6 = straindata6(2:83,2);
y7 = straindata7(2:576,2);
y8 = straindata8(2:576,2);
y9 = straindata9(2:576,2);

%use a moving mean with 10 points and a rloess smoothing function to remove
outliers in data%

straindata1meaned = movmean(y1,10);
straindata1meaned = smooth(x1_hours_plot,straindata1meaned,0.2,'rloess');
straindata1meanedplot = [0 ; straindata1meaned];
straindata2meaned = movmean(y2,10);
straindata2meaned = smooth(x2_hours_plot,straindata2meaned,0.2,'rloess');
straindata2meanedplot = [0 ; straindata2meaned];
straindata3meaned = movmean(y3,10);
straindata3meaned = smooth(x3_hours_plot,straindata3meaned,0.2,'rloess');
straindata3meanedplot = [0 ; straindata3meaned];
straindata4meaned = movmean(y4,10);
straindata4meaned = smooth(x4_hours_plot,straindata4meaned,0.2,'rloess');
straindata4meanedplot = [0 ; straindata4meaned];
straindata5meaned = movmean(y5,10);
straindata5meaned = smooth(x5_hours_plot,straindata5meaned,0.2,'rloess');
straindata5meanedplot = [0 ; straindata5meaned];
straindata6meaned = movmean(y6,10);
straindata6meaned = smooth(x6_hours_plot,straindata6meaned,0.2,'rloess');
straindata6meanedplot = [0 ; straindata6meaned];
straindata7meaned = movmean(y7,10);
straindata7meaned = smooth(x7_hours_plot,straindata7meaned,0.2,'rloess');
straindata7meanedplot = [0 ; straindata7meaned];
straindata8meaned = movmean(y8,10);
straindata8meaned = smooth(x8_hours_plot,straindata8meaned,0.2,'rloess');
straindata8meanedplot = [0 ; straindata8meaned];
straindata9meaned = movmean(y9,10);
straindata9meaned = smooth(x9_hours_plot,straindata9meaned,0.2,'rloess');
straindata9meanedplot = [0 ; straindata9meaned];

%plot the different curves using the smoothed data%

plot(x1_hours,straindata1meanedplot,'LineWidth',3)
hold on
plot(x2_hours,straindata2meanedplot,'LineWidth',3)
```

```
plot(x3_hours,straindata3meanedplot,'LineWidth',3)
plot(x4_hours,straindata4meanedplot,'LineWidth',3)
plot(x5_hours,straindata5meanedplot,'LineWidth',3)
plot(x6_hours,straindata6meanedplot,'LineWidth',3)
plot(x7_hours,straindata7meanedplot,'LineWidth',3)
plot(x8_hours,straindata8meanedplot,'LineWidth',3)
plot(x9_hours,straindata9meanedplot,'LineWidth',3)

%plot properties settings%

y_axis=ylabel('strain (mm/mm)');
x_axis=xlabel('time(hours)');
leg=legend('35_40%','35_50%','35_60%','45_40%','45_50%','45_60%','55_40%','55
_50%','55_60%')
set(leg, 'Interpreter','none')
set(gca,'fontsize',20)
```

## A.2 Endurance Limit Calculation Script

```
%open the data files for the collected strain data from the virtual
extensometer%

fidi = fopen('Strain.dat');
a    =    textscan(fidi,    '%f%f',    'HeaderLines',2,    'Delimiter','\n',
'CollectOutput',1);
fclose(fidi);

%convert the strain data collected from a cell structure to a matrix%

straindata1 = cell2mat(a);

%use the first column of the matrix to determine image numbers%

x1 = straindata1(:,1);

%convert image number to time values and calculate the logarithmic values for
the time values*

x1_hours = 5.*x1/60;
x1_logarithm = log(x1_hours);
x1_hours_plot = [2:529];

%set value of the failure strain for the particular braid angle%

failure_strain=0.024;
```

```
%use the second column of the matrix initially obtained for the strain values
for the different tests%

y1 = straindata1(2:529,2);

%use a moving mean with 10 points and a rloess smoothing function to remove
outliers in data%

straindata1meaned = movmean(y1,10);
straindata1meaned = smooth(x1_hours_plot,straindata1meaned,0.2,'rloess');
straindata1meanedplot = [0 ; straindata1meaned];

%plot isostress curve for the sample%

plot(x1_logarithm,straindata1meanedplot,'LineWidth',3,'Color','r')

%calculate values of the differences to use to calculate the strain%

straindifference=abs(diff(straindata1meanedplot));
timedifference=abs(diff(x1_logarithm));
slope=[straindifference timedifference];
i=1;

%loop to check at which point the values of the difference fall below the set
error%

while (i<528)
    if (straindifference(i)<(1*10^-5))
        i_slope=i;
        break
    else
        i=i+1;
    end
end

%initialization of slope calculation%

pointsforslope=528-i_slope;
slope_total=0;

%loop to average the values of the slope for all points after the point
calculated by previous loop%

while (i_slope<528)
    slope_total=slope_total+slope(i_slope, 1)/slope(i_slope, 2);
    i_slope=i_slope+1;
end

%calculate the value of beta from the slope and work out endurance limit%
```

```
beta= slope_total/pointsforslope;
endurance_limit=exp((failure_strain-straindata1meanedplot(2))/beta)/(24*365)
```

## A.3 OSM Virtual Extensometer Code as adapted from Aldrich et al.

```
%+--------------------------------------------------------------------------+
%|                                                                          |
%| FILENAME : OSM_Suite_m                                  VERSION : B.1.2  |
%|                                                                          |
%| TITLE : OSM Software Suite                        AUTHOR : Daniel Aldrich |
%|                                                                          |
%+--------------------------------------------------------------------------+
%|                                                                          |
%| DEPENDENT FILES :                                                        |
%|       > OSM_Suite_fig                                                    |
%|       > OSM_Classic_m                                                    |
%|       > OSM_Classic_fig                                                  |
%|       > Video_Converter_m                                                |
%|       > Video_Converter_fig                                              |
%|                                                                          |
%| DESCRIPTION :                                                            |
%|       This program is designed to be the main screen for the OSM         |
%|        Software Package.                                                 |
%|                                                                          |
%| PUBLIC FUNCTIONS :                                                       |
%|       <none>                                                             |
%|                                                                          |
%| NOTES :                                                                  |
%|       <none>                                                             |
%|                                                                          |
%| COPYRIGHT :                                                              |
%|       Copyright (c) 2015 Daniel Aldrich                                  |
%{
%|       Permission is hereby granted, free of charge, to any person        |
%|       obtaining a copy of this software and associated documentation     |
%|       files (the "Software"), to deal in the Software without            |
%|       restriction, including without limitation the rights to use,       |
%|       copy, modify, merge, publish, distribute, sublicense, and/or       |
%|       sell copies of the Software, and to permit persons to whom the     |
%|       Software is furnished to do so, subject to the following           |
%|       conditions:                                                        |
%|                                                                          |
%|       The above copyright notice and this permission notice shall be     |
%|       included in all copies or substantial portions of the Software.    |
%|                                                                          |
%|       THE SOFTWARE IS PROVIDED "AS IS", WITHOUT WARRANTY OF ANY KIND,    |
%|       EXPRESS OR IMPLIED, INCLUDING BUT NOT LIMITED TO THE WARRANTIES    |
%|       OF MERCHANTABILITY, FITNESS FOR A PARTICULAR PURPOSE AND           |
%|       NONINFRINGEMENT. IN NO EVENT SHALL THE AUTHORS OR COPYRIGHT        |
%|       HOLDERS BE LIABLE FOR ANY CLAIM, DAMAGES OR OTHER LIABILITY,       |
```

```
%|       WHETHER IN AN ACTION OF CONTRACT, TORT OR OTHERWISE, ARISING     |
%|       FROM, OUT OF OR IN CONNECTION WITH THE SOFTWARE OR THE USE OR    |
%|       OTHER DEALINGS IN THE SOFTWARE.                                  |
%}
%|                                                                        |
%| CHANGES :                                                              |
%|       B.1.1 23/10/2015 DA Addition of OSM: Classic and Video Converter |
%|       A.0.1 16/10/2015 DA Creation of Main Menu for the Suite          |
%|                                                                        |
%+------------------------------------------------------------------------+

function varargout = OSM_Suite(varargin)
% Last Modified by GUIDE v2.5 21-Oct-2015 19:02:45

% Begin initialization code - DO NOT EDIT
gui_Singleton = 1;
gui_State = struct('gui_Name',       mfilename, ...
                   'gui_Singleton',  gui_Singleton, ...
                   'gui_OpeningFcn', @OSM_Suite_OpeningFcn, ...
                   'gui_OutputFcn',  @OSM_Suite_OutputFcn, ...
                   'gui_LayoutFcn',  [] , ...
                   'gui_Callback',   []);
if nargin && ischar(varargin{1})
    gui_State.gui_Callback = str2func(varargin{1});
end

if nargout
    [varargout{1:nargout}] = gui_mainfcn(gui_State, varargin{:});
else
    gui_mainfcn(gui_State, varargin{:});
end
% End initialization code - DO NOT EDIT

function OSM_Suite_OpeningFcn(hObject, eventdata, handles, varargin)
handles.output = hObject;

folderCheck()

guidata(hObject, handles);

function varargout = OSM_Suite_OutputFcn(hObject, eventdata, handles)
varargout{1} = handles.output;

function mainMenu_DeleteFcn(hObject, eventdata, handles)
delete(handles.mainMenu)

function osmClassic_Callback(hObject, eventdata, handles)
mainMenu_DeleteFcn(hObject, eventdata, handles)
cd(fullfile(cd(),'bin','OSM_Classic'))
run('OSM_Classic.m')
```

```
function osmTwoD_Callback(hObject, eventdata, handles)

function gigeImaq_Callback(hObject, eventdata, handles)

function xCorrelation_Callback(hObject, eventdata, handles)

function videoConversion_Callback(hObject, eventdata, handles)
mainMenu_DeleteFcn(hObject, eventdata, handles)
cd(fullfile(cd(),'bin','Video_Converter'))
run('Video_Converter.m')

function quit_Callback(hObject, eventdata, handles)
mainMenu_DeleteFcn(hObject,eventdata,handles)

function[] = folderCheck()
if exist('Input','dir')~=7
    mkdir('Input')
    cd('Input')
    mkdir('Classic')
    mkdir('2Dimesional')
    mkdir('Correlation')
    mkdir('Videos')
    mkdir('Other')
    cd('..')
else
    cd('Input')
    if exist('Classic','dir')~=7
        mkdir('Classic')
    end
    if exist('2Dimensional','dir')~=7
        mkdir('2Dimensional')
    end
    if exist('Correlation','dir')~=7
        mkdir('Correlation')
    end
    if exist('Videos','dir')~=7
        mkdir('Videos')
    end
    if exist('Other','dir')~=7
        mkdir('Other')
    end
    cd('..')
end
if exist('Output','dir')~=7
    mkdir('Output')
    cd('Output')
    mkdir('Classic')
    mkdir('2Dimesional')
    mkdir('Correlation')
    mkdir('Other')
    cd('..')
else
```

```
    cd('Output')
    if exist('Classic','dir')~=7
        mkdir('Classic')
    end
    if exist('2Dimensional','dir')~=7
        mkdir('2Dimensional')
    end
    if exist('Correlation','dir')~=7
        mkdir('Correlation')
    end
    if exist('Other','dir')~=7
        mkdir('Other')
    end
    cd('..')
end
```